CONFOCAL MICROSCOPY ANALYSIS OF THE ROLES OF INTRACELLULAR pH IN THE REGULATION OF POLARISED GROWTH OF *Dryopteris* PROTONEMATA

Volume 2

Richard M. Parton

Doctor of Philosophy
University of Edinburgh
1996

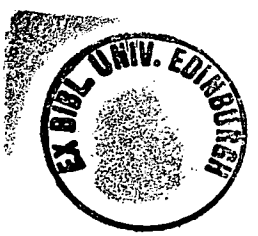

This thesis is dedicated to my Parents and to all those fern gametophytes who selflessly gave up their lives for Science.

"The researches of many commentators have already thrown much darkness on this subject, and it is probable that, if they continue, we shall soon know nothing at all about it"

Mark Twain

"Once you have eliminated the impossible, what ever is left, however improbable, must be correct."

Captain Spock,
(Star Trek VI)

VOLUME-2 FIGURES

Chapter 1 Figures
Fig. 1 - Components of polarity and polarised growth
Fig. 2 - Generalised signal transduction pathway components
Fig. 3 - Proton movements around growing tips
Fig. 4 - Fluorescent dyes used for intracellular ion concentration measurement
Fig. 5 - The fern life cycle
Fig. 6 - Developmental stages of a typical fern gametophyte

Chapter 2 Figures
Fig. 7 - Gametophyte culture treatments
Fig. 8 - Perfused thin-layer chamber
Fig. 9 - Handling of liquid-cultured protonemata
Fig. 10 - Ester-loading of cells with dye
Fig. 11 - Microinjection of protonemal filaments
Fig. 12 - Procedure for ionophoretic microinjection of fern protonemata
Fig. 13 - Scanhead layout and light-path of the Bio-Rad MRC-600 CLSM
Fig. 14 - Layout of the CLSM
Fig. 15 - CLSM settings for physiological imaging
Fig. 16 - Ratio processing procedure
Fig. 17 - Calibrated pseudocolour look-up table (LUT) for ratio images.

Chapter 3 Figures
Fig. 18 - Developmental stages of *Dryopteris affinis* gametophytes
Fig. 19 - Time-course of gametophyte development
Fig. 20 - Typical protonemal apical-cell structure
Fig. 21 - Protonemal apical cell tip forms
Fig. 22 - Apical cell "swelling" response
Fig. 23 - Phototropic reorientation of apical growth
Fig. 24 - Typical rhizoid apical structure
Fig. 25 - Rhizoid tip forms
Fig. 26 - Apical extension of rhizoids
Fig. 27 - Secondary rhizoid
Fig. 28 - Stressed cells
Fig. 29 - Recovery of rhizoids after stress
Fig. 30 - Staining of apical structures with fluorescent dyes
Fig. 31 - Distribution of endoplasmic reticulum in chlorocyte cells
Fig. 32 - Distribution of mitochondria in apical chlorocytes
Fig. 33 - Distribution of mitochondria in a rhizoid

Chapter 4 Figures
Fig. 34 - Microinjection of fern protonemata with fluorescent dyes
Fig. 35 - Low pH loading of fern protonemata with cSNARF-1 free-acid
Fig. 36 - Ester-loading of fern protonemata with cSNARF-1 AM
Fig. 37 - cSNARF-1 imaging and chloroplast autofluorescence
Fig. 38 - Ester-loading of rhizoids with cSNARF-1 AM
Fig. 39 - Subcellular localisation of cSNARF-1 in rhizoids after AM ester-loading
Fig. 40. - Rhizoid viability after cSNARF-1 AM ester-loading and confocal imaging
Fig. 41 - Confocal optical sectioning

VOLUME-2 FIGURES

Chapter 5 Figures

Fig. 42 - pH response curve of cSNARF-1 free-acid *in vitro*
Fig. 43 - Calibration curves for the pH response of cSNARF-1 free-acid *in vitro*
Fig. 44 - Effects of environmental conditions on the pH response of cSNARF-1 free-acid tested *in vitro*
Fig. 45 - Calibration of the pH response of cSNARF-1 free-acid *in situ*
Fig. 46 - Random "noise" levels in confocal fluorescence and ratio images
Fig. 47 - The influence of fluorescence image pixel intensity on observed ratio value
Fig. 48 - Estimation of the spatial resolution and precision of pH measurement for cSNARF-1 ratio images
Fig. 49 - Dissection of physiological cSNARF-1 fluorescence confocal images and their corresponding ratios
Fig. 50 - Methods of extraction of numerical data from physiological images
Fig. 51 - Sampling cSNARF-1 confocal ratio images with a linear median transect
Fig. 52 - Image thresholding to eliminate low signal and vacuolar signal contributions from ratio images
Fig. 53 - Ratio image of a vegetative hypha of *Neurospora crassa* loaded with cSNARF-1 10 kDa dextran-conjugate
Fig. 54 - cSNARF-1 dual emission ratio image misalignment artefact
Fig. 55 - Confocal and non-confocal imaging of cSNARF-1 in a rhizoid of *D. affinis*
Fig. 56 - cSNARF-1 confocal ratio imaging at different depths within a rhizoid

Chapter 6 Figures

Fig. 57 - Typical cSNARF-1 confocal ratio images of growing *D. affinis* rhizoids
Fig. 58 - Cytoplasmic pH in fern gametophyte rhizoids
Fig. 59 - recovery of rhizoids after intracellular pH manipulation using cell permeant weak acids and bases
Fig. 60 - Effects of extracellular buffering at pH 5.6 and 6.0 on *D. affinis* rhizoids
Fig. 61 - Effects of extracellular buffering at pH 7.0 on *D. affinis* rhizoids
Fig. 62 - Effects of extracellular buffering at pH 8.0 on *D. affinis* rhizoids
Fig. 63 - Possible positions of pH gradients in a tip-growing cell

Abbreviations

General:

DIC	differential interference contrast (microscopy)
ER	endoplasmic reticulum
EM	electron microscopy
h	hour(s)
kDa	kilodalton
λ	wavelength
MF	actin microfilaments
min.	minute(s)
MT	microtubules
n	number (of samples or replicates)
PC	personal computer
pH_c	cytoplasmic pH (cytosolic pH specified separately)
pH_i	internal pH
pH_o	external pH
pKa	pH at which an acid is present in its protonated and unprotonated forms in equal concentrations
sec.	second(s)
s.d.	standard deviation
s.e.m	standard error
TLC	thin-layer chamber
UV	ultra-violet
VDU	video display unit
V/V	volume by volume
W/V	weight by volume

Continued over

Abbreviations

Chemicals:

-AM	acetoxymethyl (ester group)
BCECF	2`,7`-bis-(2-carboxyethyl)-5- (and-6)- carbxyfluorescein
cAMP	cyclic adenosine monophosphate
$DiOC_6$	3,3`-dihexyloxacarbocyanine iodide
$DiOC_7$	3,3`-diheptyloxacarbocyanine iodide
DMSO	dimethylsulphoxide
CFDA	5-(and-6)-carboxyfluorescein diacetate
DNP	2,4-dinitrophenol
EtOH	ethanol
Fluo-3	1-(2-amino-5-(2,7-dichloro-6-hydroxy-3-oxo-3H-xanthen-9-yl)-2-(2′-amino-5′-methylphenoxy)-ethane-N,N,N′,N′-tetraacetic acid.
Fura-2	1-[2-(5-carboxyoxazol-2-yl)-6-aminobenzofuran-5-oxy]-2-(2′-amino-5′-methylphenoxy)-ethane-N,N,N′,N′-tetraacetic acid.
HEPES	N-(2-hydroxyethyl)- piperazine-N`-2-ethanesulphonic acid
Indo-1	1-[2-amino-5-(6-carboxyindol-2-yl-phenoxyl]-2-(2′-amino-5′-methylphenoxy)-ethane-N,N,N′,N′-tetraacetic acid.
IP_3	phosphatidylinositoltrisphosphate
LYCH	Lucifer Yellow CH, [6-amino-2,3-dihydro-1,3-dioxo-2 hydrazinocarboxylamino--1H-benz [d,e] isoquinaline-5,8-disulfonic acid]
MES	2-(N-morpholino) ethanesulphonic acid
NMR	nuclear magnetic resonance
Rhod-123	rhodamine 123
SDS	sodium dodecyl sulfate
cSNARF-1	5-(and-6)-carboxy-seminapthorhodafluor-1
TRIS	2-Amino-2-hydroxymethyl-1,3-propanediol

Continued over

Abbreviations

Imaging Terminology:

Acc	accumulation filter
BL	black level
CA	confocal aperture
CCD	charge-coupled device
COMOS	confocal mouse operated software
K	Kalman filtering
CLSM	laser scanning confocal microscope
LUT	look-up table
MPL	Command line software
ND	neutral density filter
PMT	photomultiplier tube
SOM	keyboard operated confocal software
TCSM	Time-course and ratiometric software
WORM	write-once-read-many

Figure labelling:

Ac	apical cell
AC	apical cytoplasm
Bc	basal cell
Ch	chloroplast
CW	cell wall
C	cytoplasm
ER	endoplasmic reticulum
M	mitochondrion
N	nucleus
P	plastid
PM	plasma-membrane
T	vacuole membrane or tonoplast
V	vacuole

Chapter 1

Fig. 1: Components of polarity and polarised growth. The flow diagram presents a simplistic representation of the steps proposed to be involved in polarised cellular responses to environmental stimuli.

The three phases: "Initiation", "Fixation" and "Reorientation" and their component steps have been defined on the basis of experimental manipulations performed on many different cell types (see Table 1 and references therein). For more general discussions see: Poovaiah & Reddy (1993); Kropf (1992); and Nick & Furuya (1992). The scheme shown is, of necessity, very simplified and reflects the general experimental design employed whereby a single experimental variable or stimulus is employed and the pathway to a particular response is characterised. "Initiation" refers to the transient events in the perception and transduction of a stimulus by the cell (this is described further in Chapter 1;,Fig. 2). "Fixation" marks a phase when the cell becomes more committed to a particular response. Here the "Fixation" stage incorporates the final morphological expression of response such as cell division, synthesis of new cell wall or cytological organisation. The "Reorientation" phase is an attempt to take into account the ability of cells to modify their polarity or, alternatively, to depolarise and re-establish a new polar organisation in response to further stimuli.

Fig. 1: Components of polarity and polarised growth

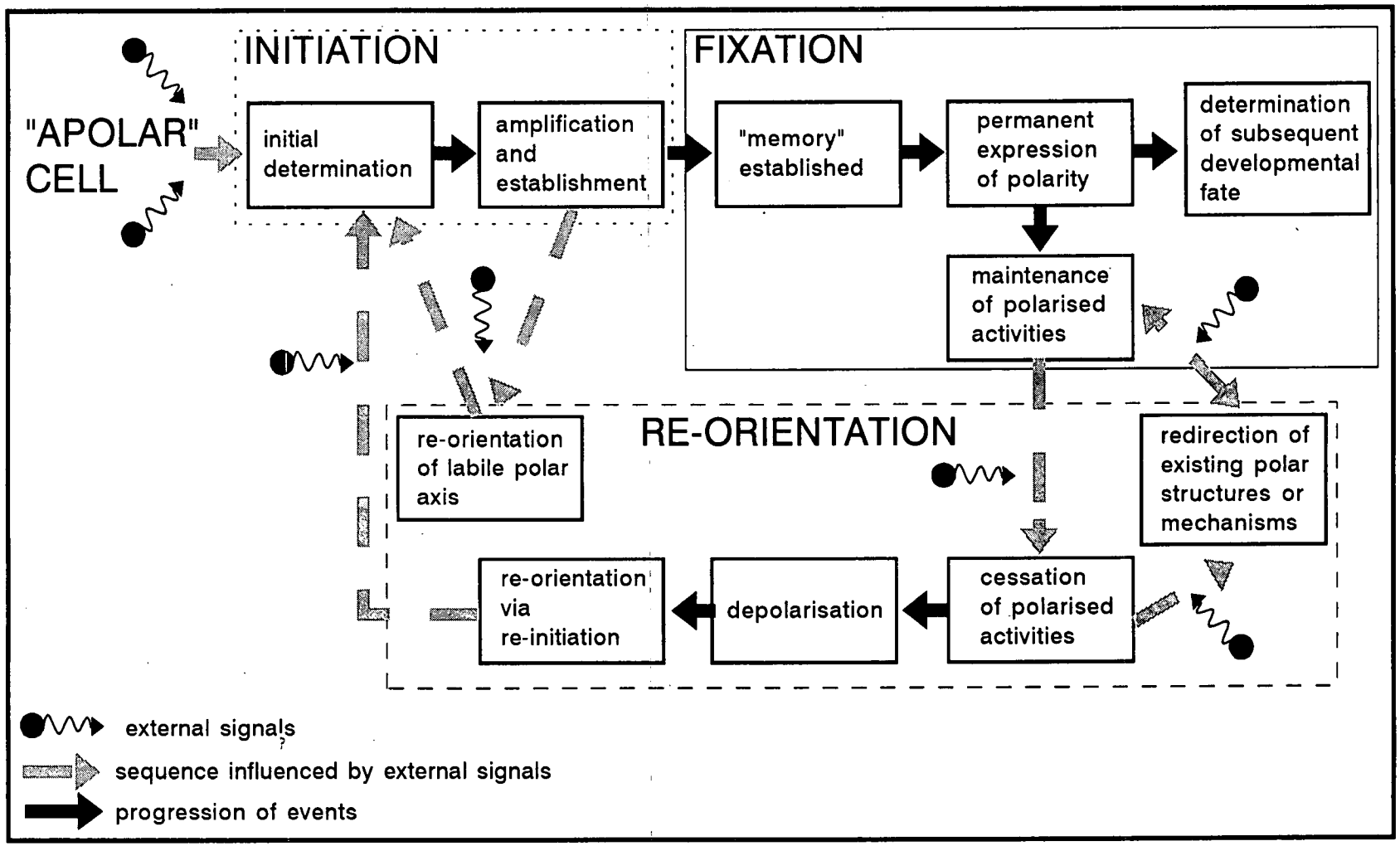

Fig. 2: Generalised signal transduction pathway components. The key components involved in the transduction of a signal between external stimulus and intracellular response are shown. The basic concepts of such signalling pathways were defined for Ca^{2+} mediated signalling in animal cells (Cheung, 1982). It has since been discovered that many features are conserved between animal and plant cells (Brownlee, 1994). Other ionic species such as protons potentially have second messenger roles (Guern *et al.*, 1991).

Fig. 2: Generalised signal transduction pathway components

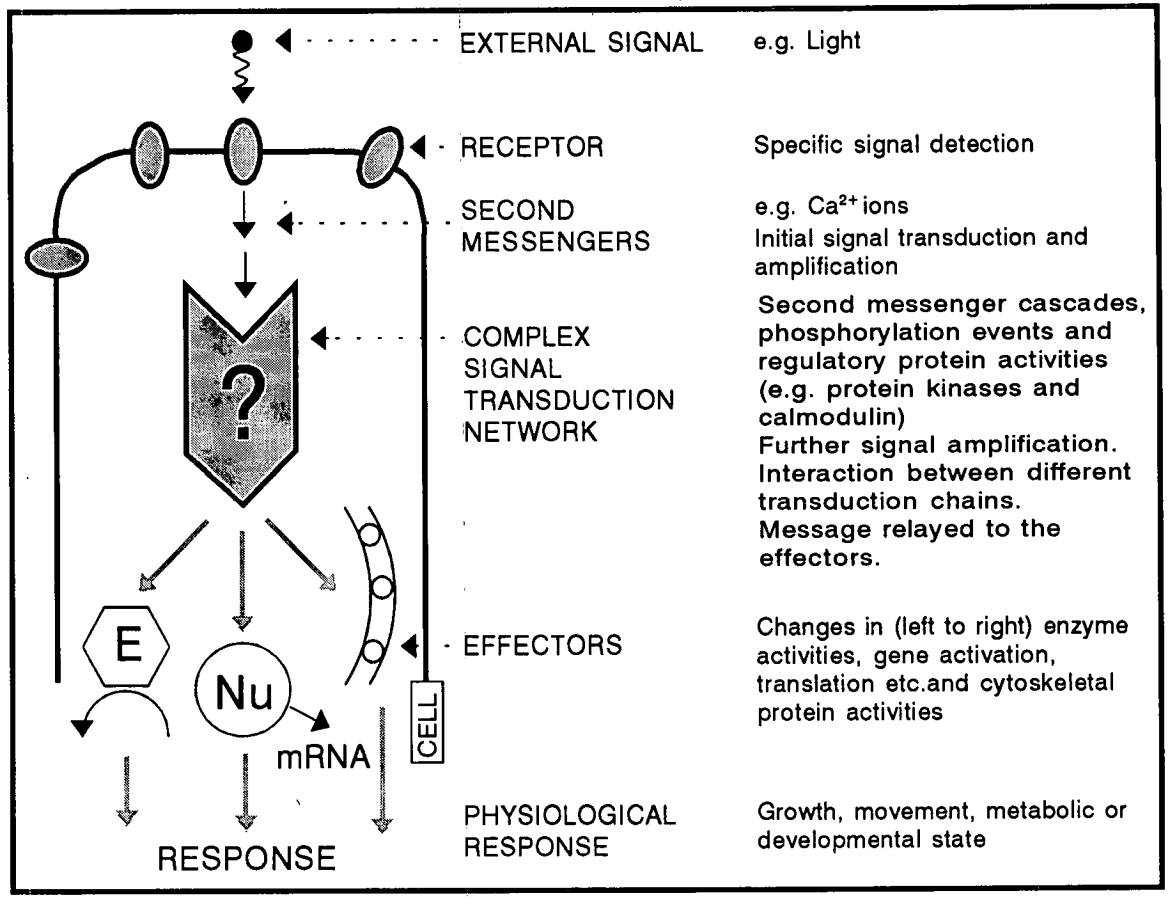

Fig. 3: Proton movements around growing tips. Individual diagrams were modified from figures in Gibbon & Kropf (1991) and Gow (1989). The arrows indicate movement of protons, or proton equivalents, between the cell (symplast) and external medium. (The apoplast may also have a role but this is difficult to investigate.) These models are based on measurements of extracellular pH profiles, proton translocating membrane activities and membrane potential measurements (Gow, 1989). Such models have been used to make inferences about intracellular pH and in attempts to explain the results of intracellular pH measurements (Prebble *et al.*, 1995; Gibbon & Kropf, 1994; Harald & Caldwell, 1990).

Fig. 3: Proton movements around growing tips

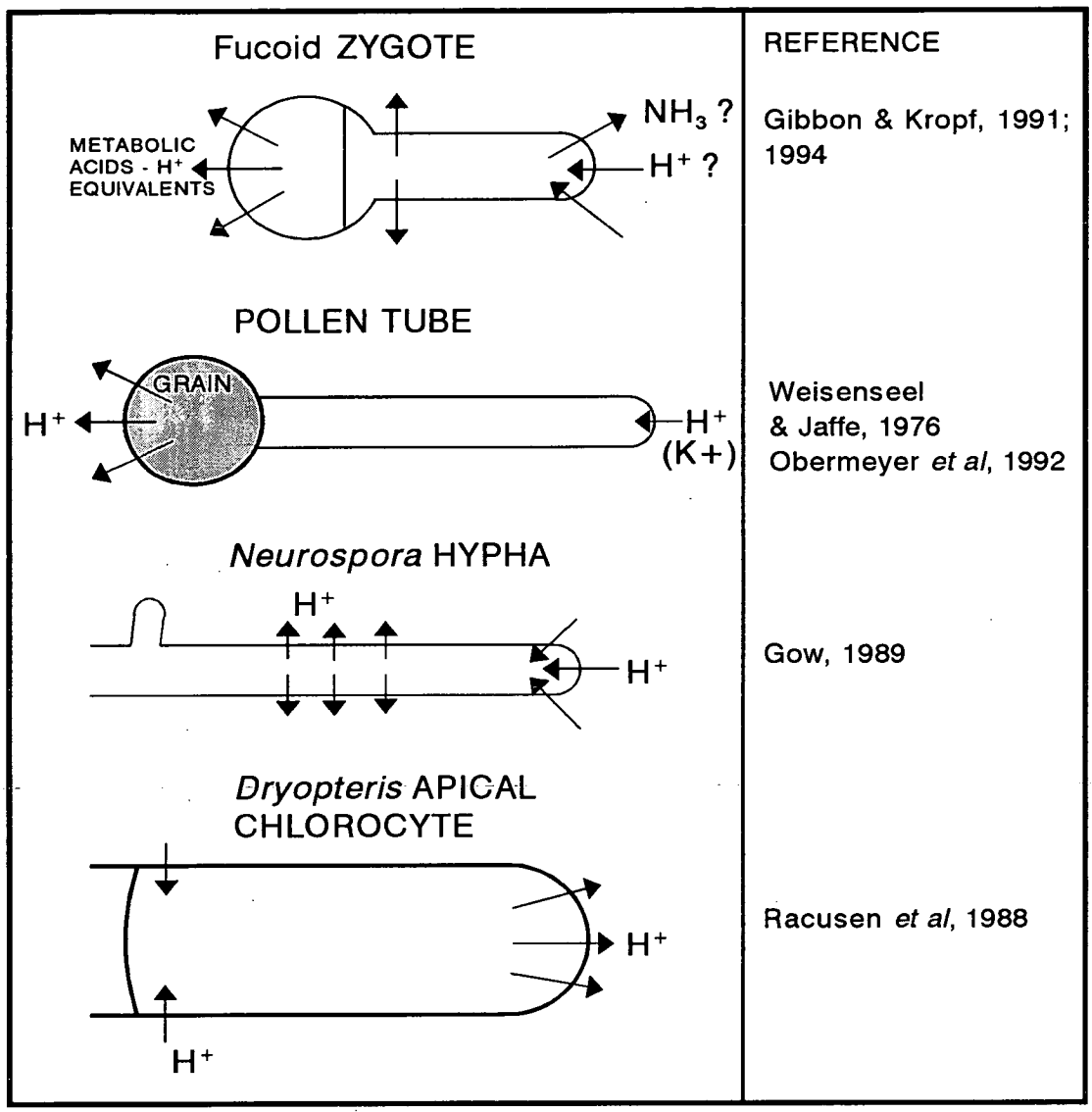

Fig. 4: Fluorescent dyes used for intracellular ion concentration measurement. Spectra were reproduced in modified form from Haugland (1992). (A) Emission spectrum of a "ratioable" (dual emission) ion sensitive dye: pH sensitive cSNARF-1 excited at 514 nm. The fluorescence of the protonated (acid) and deprotonated (basic) forms of the dye differ in their emission spectra; the former peaking at 580 nm, the latter at 640 nm. A ratio of the fluorescence peaks of the two forms of the dye (generally recorded within the ranges marked by the dashed lines) is proportional to pH but independent of the dye concentration. Excitation ratioable dyes, such as the pH sensitive BCECF, are examined in a similar manner: excitation is performed at two different wavelengths sequentially and two corresponding fluorescence intensity recordings are made (over the same emission range) and subsequently ratioed. (B) Emission spectrum of a single wavelength ion sensitive dye: Ca^{2+} sensitive Calcium Green-1 excited at 488 nm. Emission intensity, peaking between 510 and 560 nm, is directly proportional to the free calcium ion concentration (roughly over the range 0.01 - 1 μM). Estimates of absolute values for [ion] can only be made if the concentration of dye is taken into account.

Fig. 4 : Fluorescent dyes used for intracellular ion concentration measurement

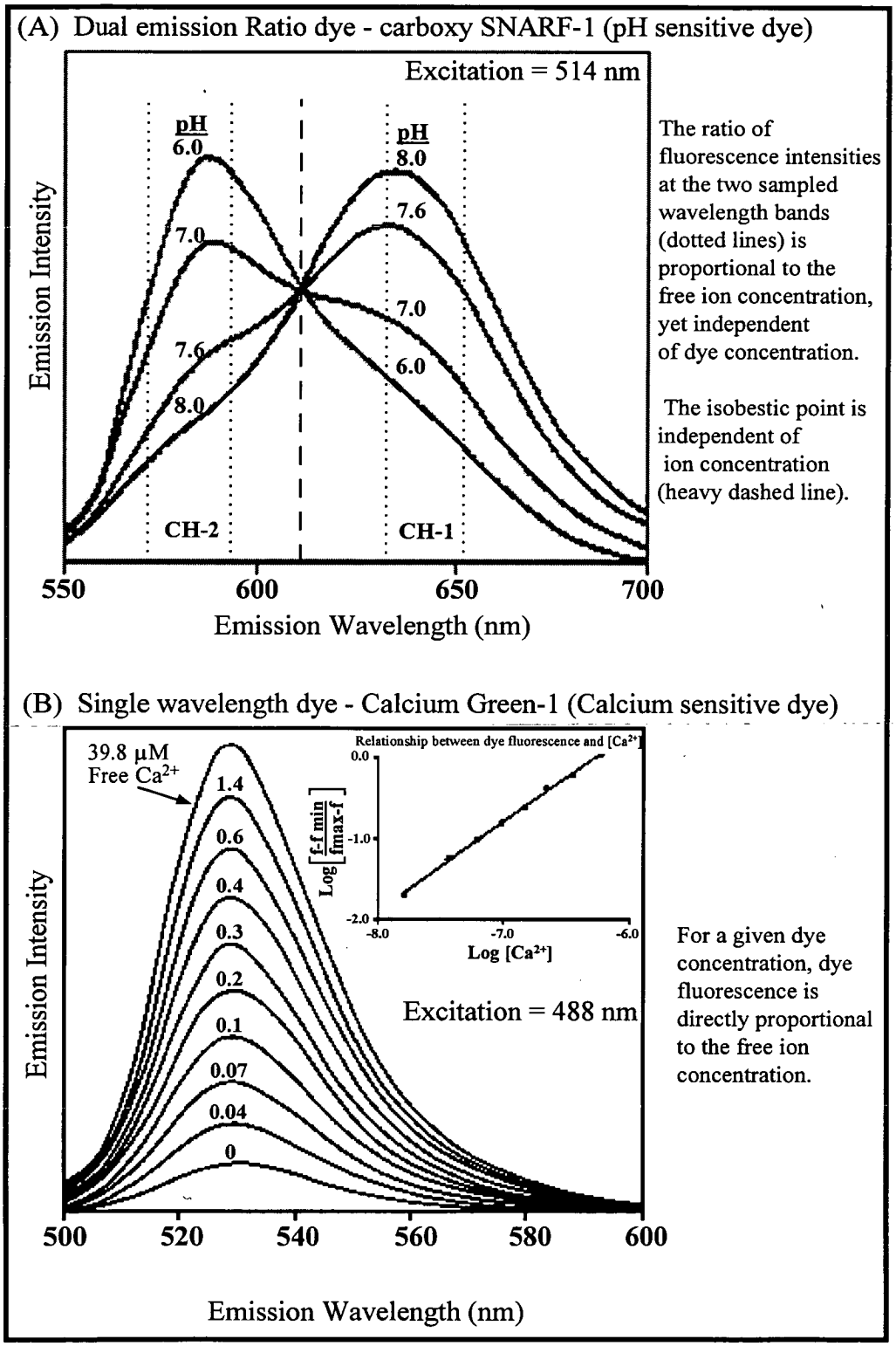

Graphs were adapted from Haugland (1992)

Fig. 5: The fern life cycle. (A) The typical alternation of the asexual sporophyte and sexual gametophyte generations of a fern. The value (n) represents the chromosomal complement of the "haploid" gametophytes. Actual ploidy levels vary considerably. (B) An example of a naturally occurring variation, resulting in asexual reproduction, in which sporophyte cells arise directly from gametophyte tissue (apogamy). The same ploidy is maintained throughout the cycle by an incomplete mitosis during spore formation by the sporophyte (diplospory). This reproductive cycle was the only form exhibited by the fern (*Dryopteris affinis* - characterised by Dyer (1979)) which provided much of the experimental material for the research described in this thesis.

Fig. 5: The fern life cycle

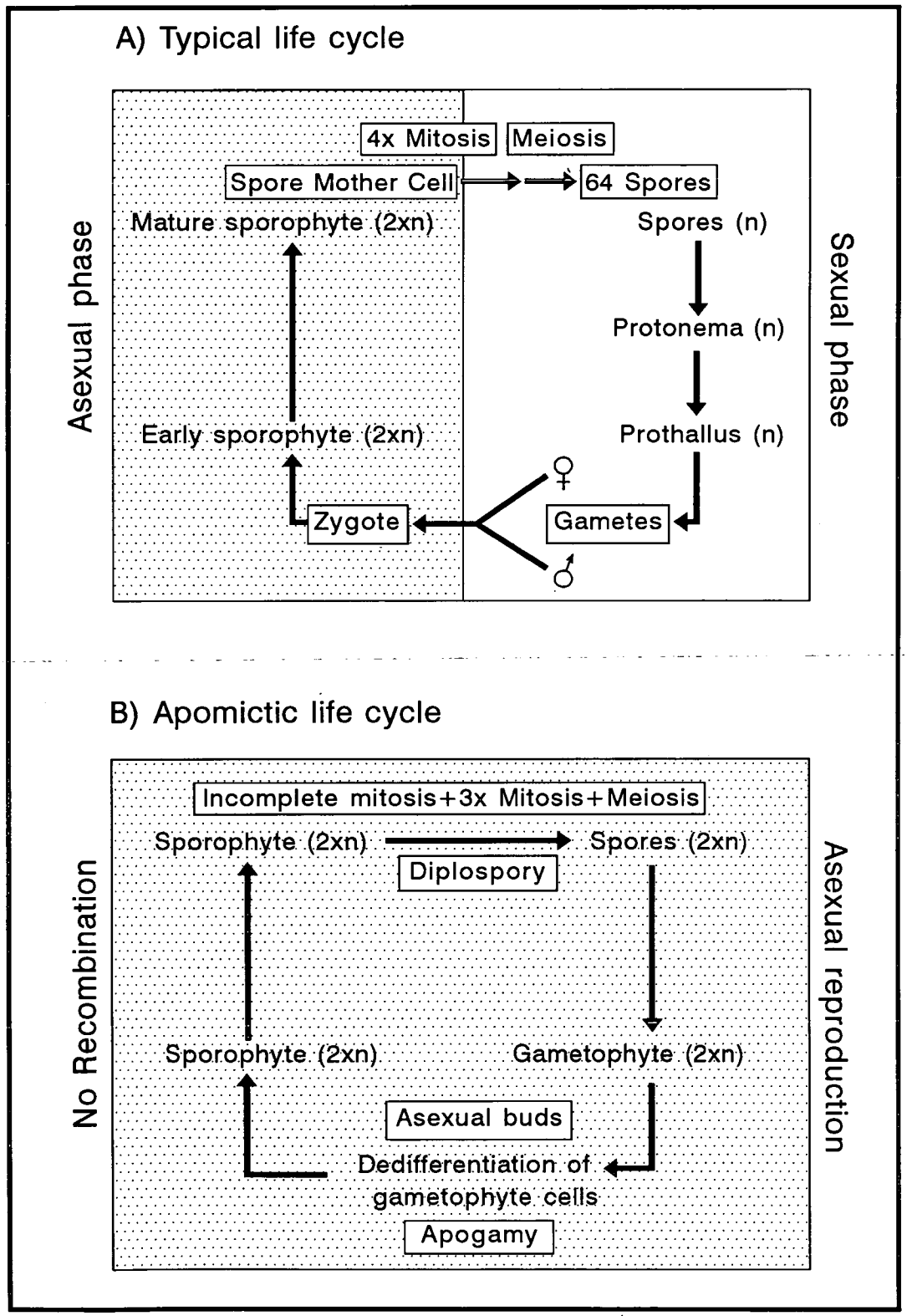

Fig. 6: Developmental stages of a typical fern gametophyte. Spores germinate under appropriate conditions, often requiring low intensity light or red light to trigger germination. The subsequent stages of protonemal development, transition and development of the mature prothallus bearing sexual reproductive structures are very dependent upon illumination conditions (Dyer, 1979; Raghavan, 1990). Here development under two extremes of illumination conditions is illustrated. The low white light intensity or red-light path (dark arrows) exhibits a prolonged protonemal stage which may result in filaments many cells long and never proceed to prothallus formation. Although prothallus development has been recorded under red and green illumination conditions (Grill, 1987; 1990; 1993), white or blue light is generally required for full development of reproductive structures. The higher white light intensity or blue light path (grey arrows) exhibits a greatly reduced filamentous stage and rapid transition to prothallus development. Clear differences in the shape of individual cells can be seen under the different illumination conditions.

Fig.6: Developmental stages of a typical fern gametophyte

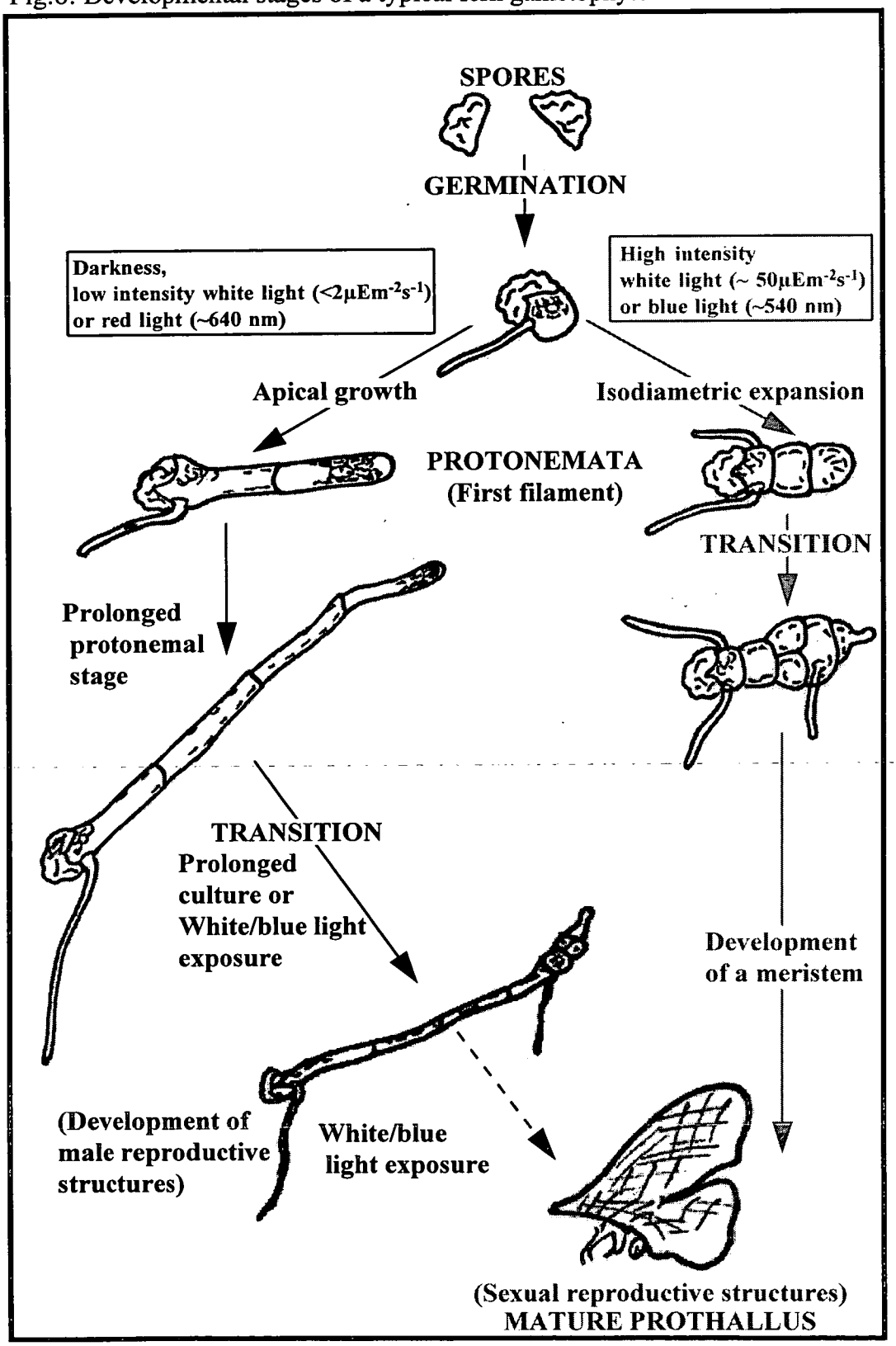

Chapter 2

Fig. 7: Gametophyte culture treatments. The flow diagram shows the steps involved in the culture of gametophytes from spores to either the primary rhizoid or early protonemal filament stages. The "pre-treatments" are a series of steps designed to reduce both fungal and bacterial contamination of the culture. Both contaminants are present in the initial spore stock. "Culture" relates to the growth of material to the desired stage for experimentation. Culture conditions and procedures for individual steps are described in more detail in the main text.

Fig. 7: Gametophyte culture treatments

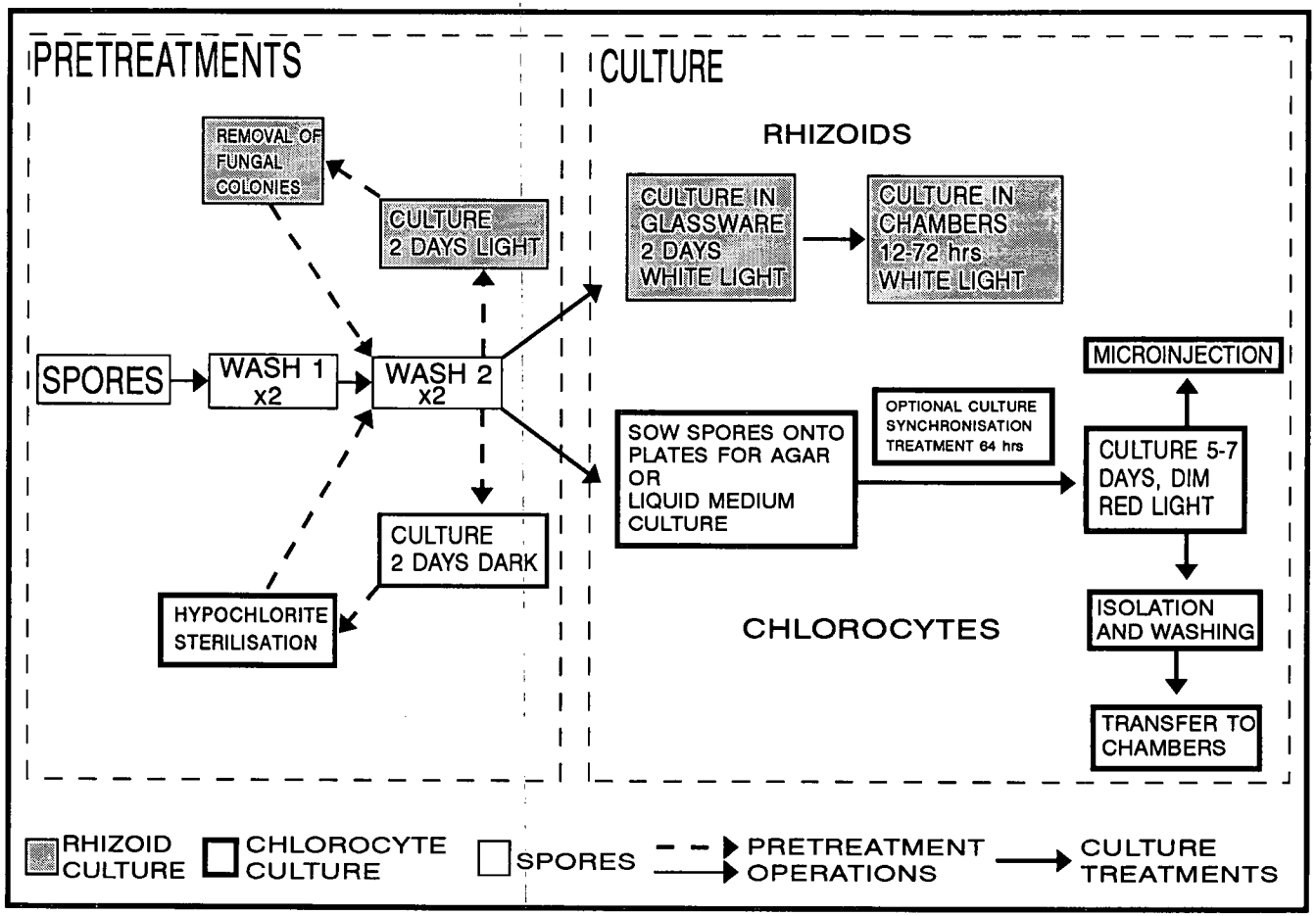

Fig. 8: Perfused thin-layer chamber. Layout of the thin-layer chamber showing both its component parts and fully assembled as in use. Descriptions of components can be found in Section 2.1.2. The thin-layer chamber provided a means by which individual gametophytes could be examined on the microscope while still allowing access to the bathing medium. The design minimised the physical disturbance to gametophytes during alteration of the bathing medium. Changes to the medium composition of the upper compartment eventually reached the medium immediately surrounding gametophytes (in the lower compartment) by diffusion through the separating mesh. Such chambers allowed normal growth of gametophytes for periods of over two weeks. Rhizoids intended for confocal analysis were cultured in the chamber from the germinated spore stage. This avoided the need for damaging isolation procedures.

Fig. 9: Handling of liquid-cultured protonemata. The equipment and manipulations for the handling of liquid cultured protonemata, prior to examination or experimental treatment, are described. The basic steps are as follows:

Step 1). Floating gametophytes are transferred, using a nylon mesh scoop, from the culture plate to a wetting medium containing 0.004% Tween-20. The gametophytes are swirled gently to encourage "wetting".

Step 2). Submerged ("wetted") gametophytes are transferred to a filter-tube using a wide tipped (~ 5 mm) glass Pasteur pipette. At this stage filaments are concentrated in a small volume.

Step 3). The filter-tube allows the medium surrounding the gametophytes to be exchanged. The bathing medium is never completely removed in order to reduce physical damage. Several medium exchanges are used to "clean up" a culture or to remove excess dye after loading cells.

Step 4). Transfer of washed gametophytes to a slide for examination. Coverslips were never placed directly onto a gametophyte suspension but supported either by silicone grease or a rubber gasket.

Fig. 8: Perfused thin-layer chamber

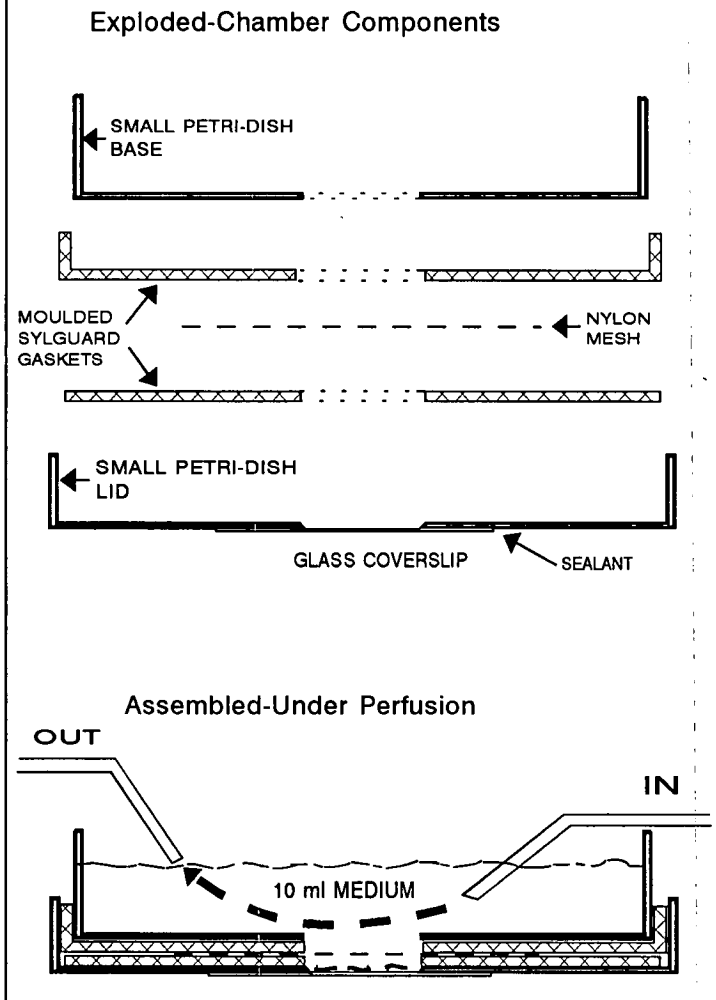

Fig. 9: Handling of liquid-cultured protonemata

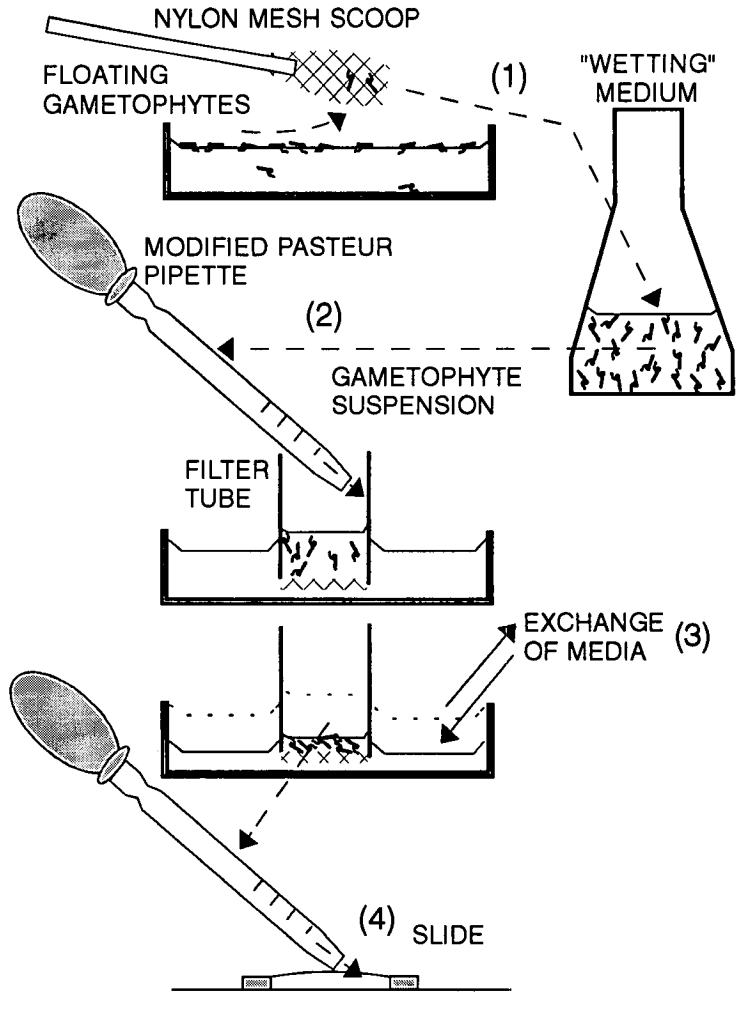

Fig. 10: Ester-loading of cells with dye

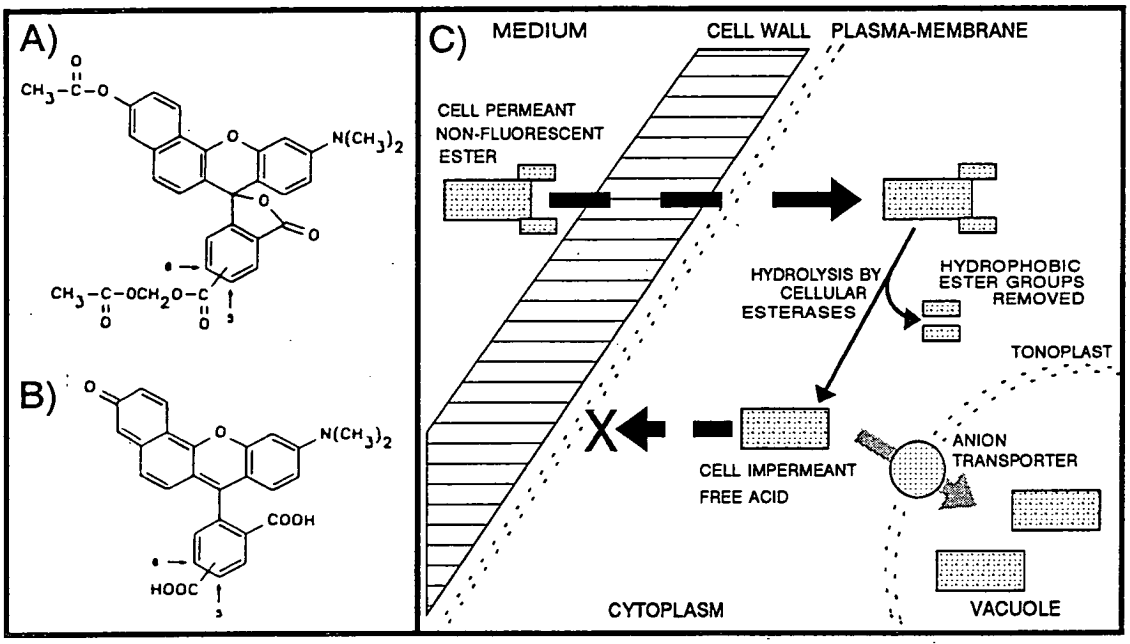

(A and B) Structures of the cell permeant, non-fluorescent cSNARF-1 AM ester and the fluorescent, cell impermeant cSNARF-1 free acid, respectively. Structures were taken from Haugland (1992). (C) The processes by which cells accumulate dye through ester-loading.

Fig. 11: Microinjection of protonemal filaments. Layout of the microscope stage (inverted microscope) during ionophoretic microinjection of a protonemal filament. See Section 2.1.2 for a description of the equipment. A chamber was used which allowed an agar block with adherent protonemata to be held down under perfusion with liquid medium. A holding pipette was used to steady individual protonemal filaments for injection. A similar set-up was employed for pressure microinjection.

Fig. 11: Microinjection of protonemal filaments

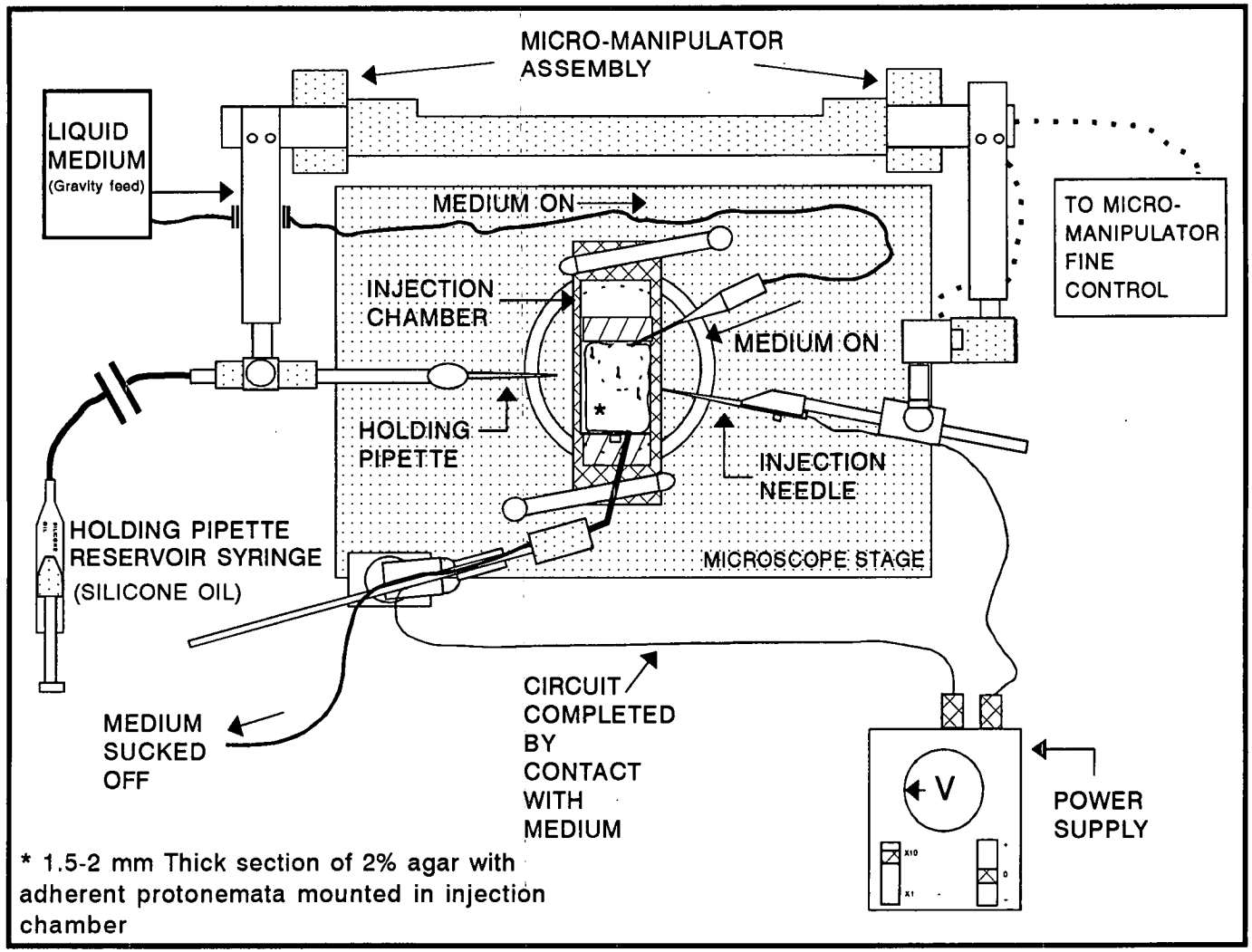

Fig. 12: Procedure for ionophoretic microinjection of fern protonemata. Flow diagram describing the procedure used for ionophoretic microinjection of protonemal filaments.

Fig.12: Procedure for ionophoretic microinjection of fern protonemata

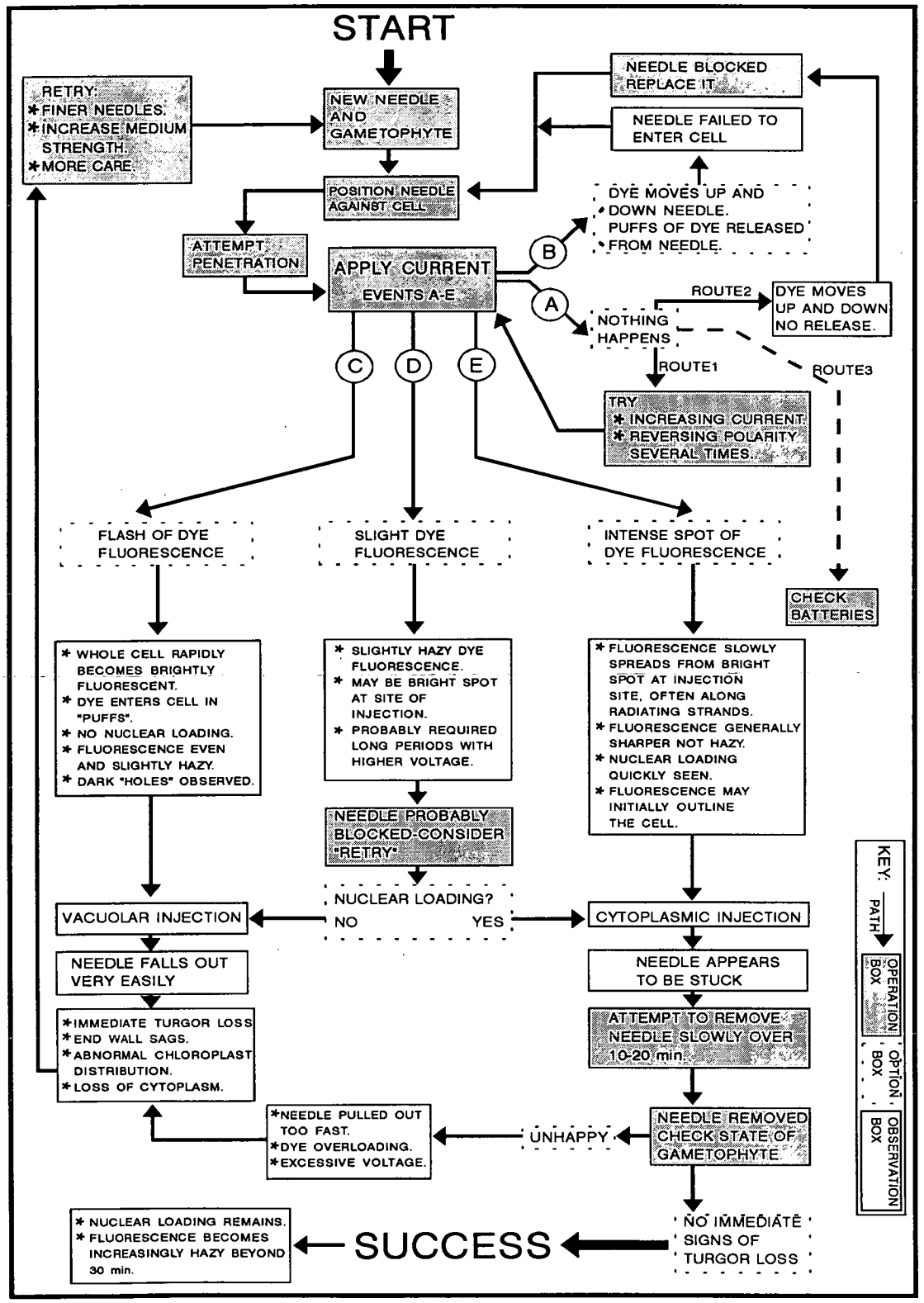

Fig. 13: Scanhead layout and light-path of the Bio-Rad MRC-600 CLSM. The excitation and emission light-paths for the Bio-Rad MRC-600 CLSM are shown. Note the positions of the filter sets which control the excitation illumination, separate the emission signals from reflected light, and divide the emission signal between the two photomultipliers. The different filter combinations used are listed in Table 3. The "folded" emission beam arrangement allows a genuine confocal pinhole to be replaced with a variable diameter confocal aperture (labelled pinhole here), see Pawley (1995).

Fig. 13: Scanhead layout and light-path of the Bio-Rad MRC-600 CLSM

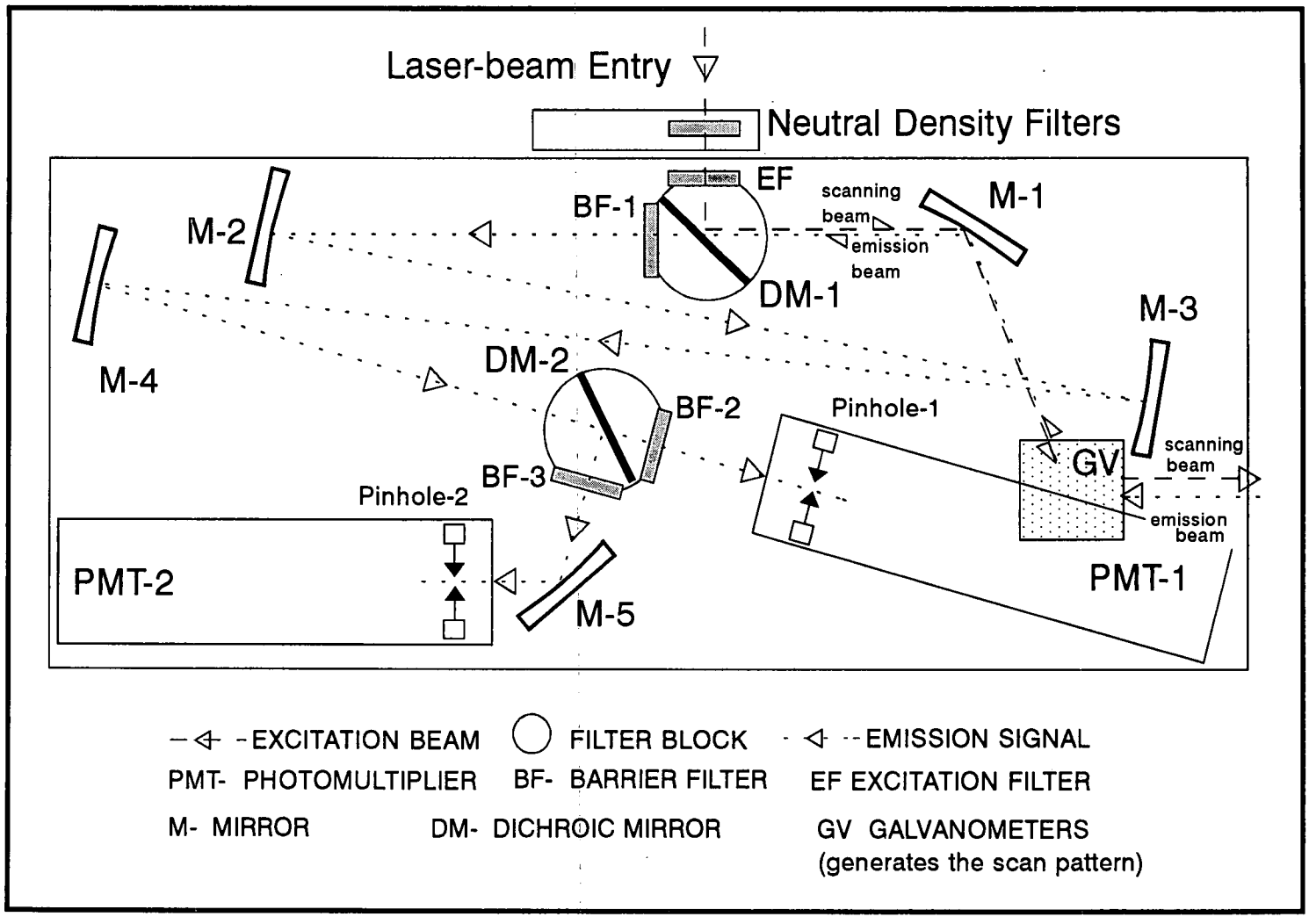

Fig. 14: layout of the CLSM

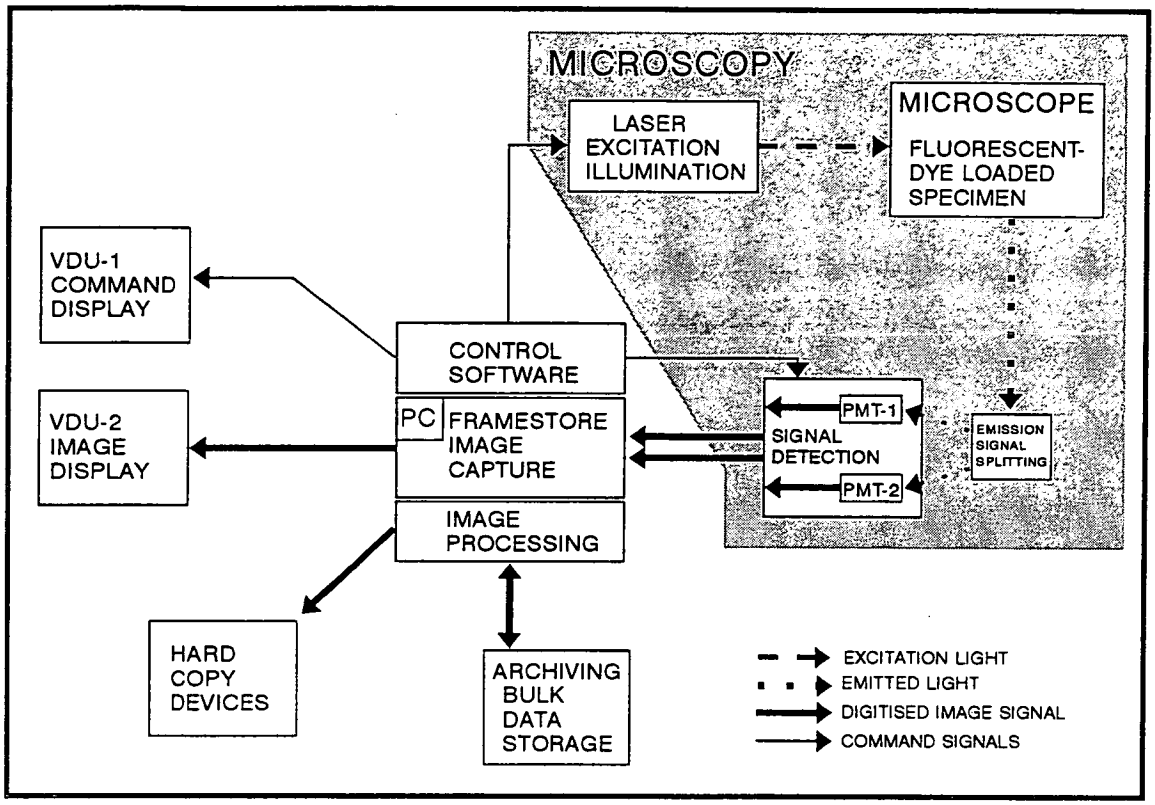

The diagram shows the layout of the CLSM and its peripheral equipment; individual items are listed in Section 2.1.4. The fluorescent sample on the microscope stage is excited by a beam of light from a laser source. The beam is scanned across the sample in a raster pattern and the light emissions, produced by the dye, at each point, pass back along the same optical path as the laser beam and are detected by the PMT's (see Fig. 13). At the PMT the signal is amplified and converted to a digital output. The digitised signal from a PMT is passed to the framestore of the computer where signal strength is converted to pixel intensity for each sample point and the image is generated. The computer, fitted with a framestore, scan-generator card and appropriate image handling software, controls and functions in both image capture and subsequent image processing. Video display units (VDU screens) allow access to the program commands and viewing of collected images.

Fig. 15: CLSM settings for physiological imaging. Diagram of the options and compromises in imaging settings which must be made in order to achieve the best quality physiologically relevant images with the CLSM. Imaging settings are discussed in the main text and listed in Table 4.

Fig. 15: CLSM settings for physiological imaging

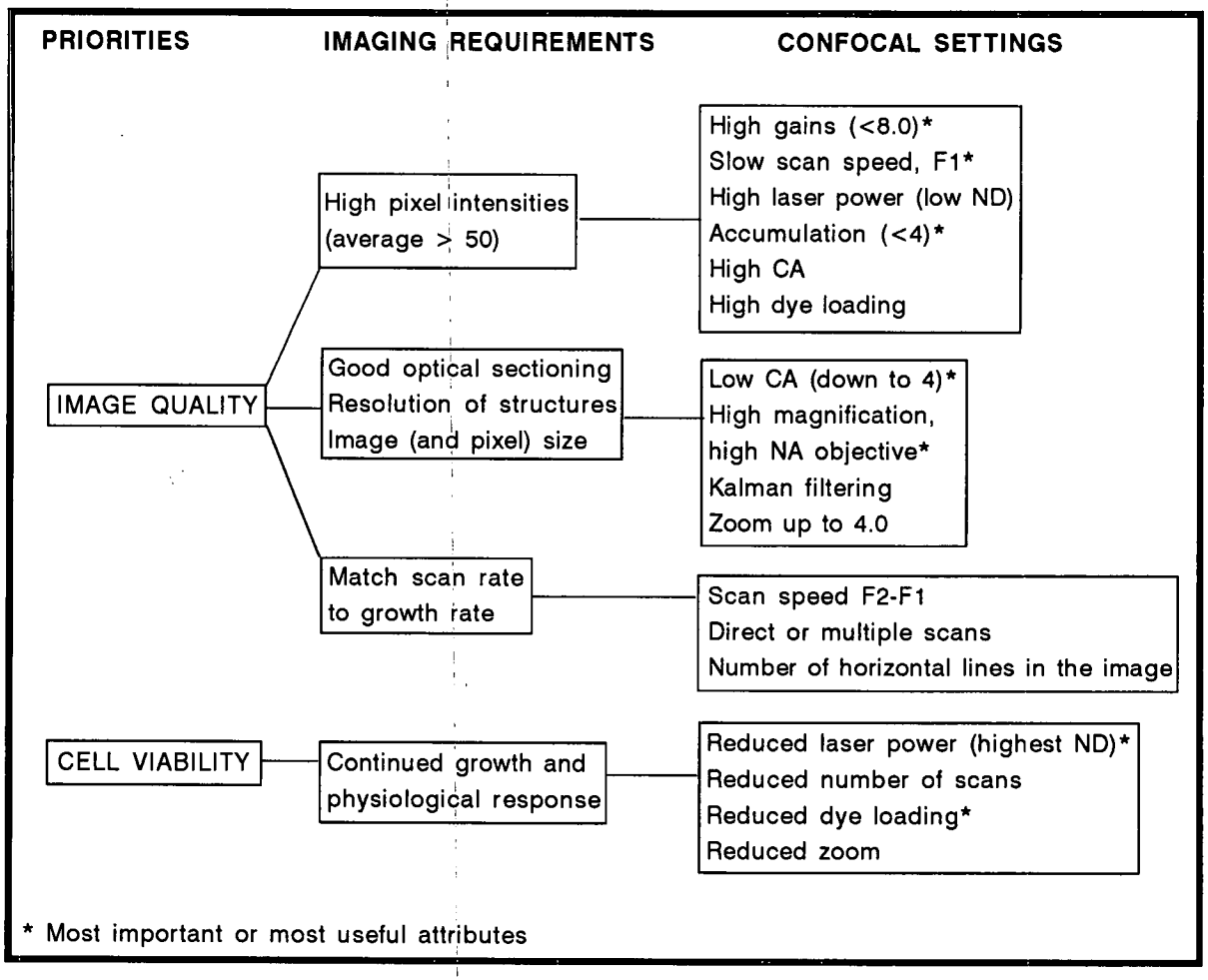

Fig. 16: Ratio processing procedure. The flow diagram shows different stages in the ratio processing of pairs of dual channel fluorescence images. Here cSNARF-1 images are shown.

1) The background or "dark image" was generally collected immediately after the fluorescence image (see main text). This dark image, which consisted of PMT signal in the absence of light (electronic "noise"), was subtracted directly from the fluorescence signal.

2) Thresholding eliminates (sets to 0) all pixels below a certain level. Thresholding was used to eliminate autofluorescence and noise from outside the specimen. Low threshold values were used (<15) to avoid degrading genuine fluorescence signal.

3) Ratioing involved pixel-by-pixel division of one fluorescence image into the other by the computer. The resulting ratio values (generally between 0 and 4) were re-scaled for display as 0 - 255 grey level pixel values in the ratio image (see Fig. 17; the relationship between grey scale pixel values and the ratio value is given in figure legends where appropriate). 0 - 255 grey scale ratio images were pseudocoloured according to a colour look up table (see Fig. 17). A median 3 x 3 filter was subsequently applied to ratio images to reduce the level of random noise. Any misalignment in the fluorescence image pair (which generally became apparent only after ratioing) was corrected by shifting one fluorescence image relative to the other and re-ratioing (not shown).

4) Numerical analysis was generally performed on ratio images (see Chapter 5). Areas of low fluorescence signal or high autofluorescence in the fluorescence image were avoided when sampling the corresponding ratio.

5) Independent calibration experiments were used to relate ratio value (pixel intensity) to actual [ion]. Calibration was performed after physiological image capture using the same confocal settings and imaging parameters.

Fig. 16: Ratio processing procedure

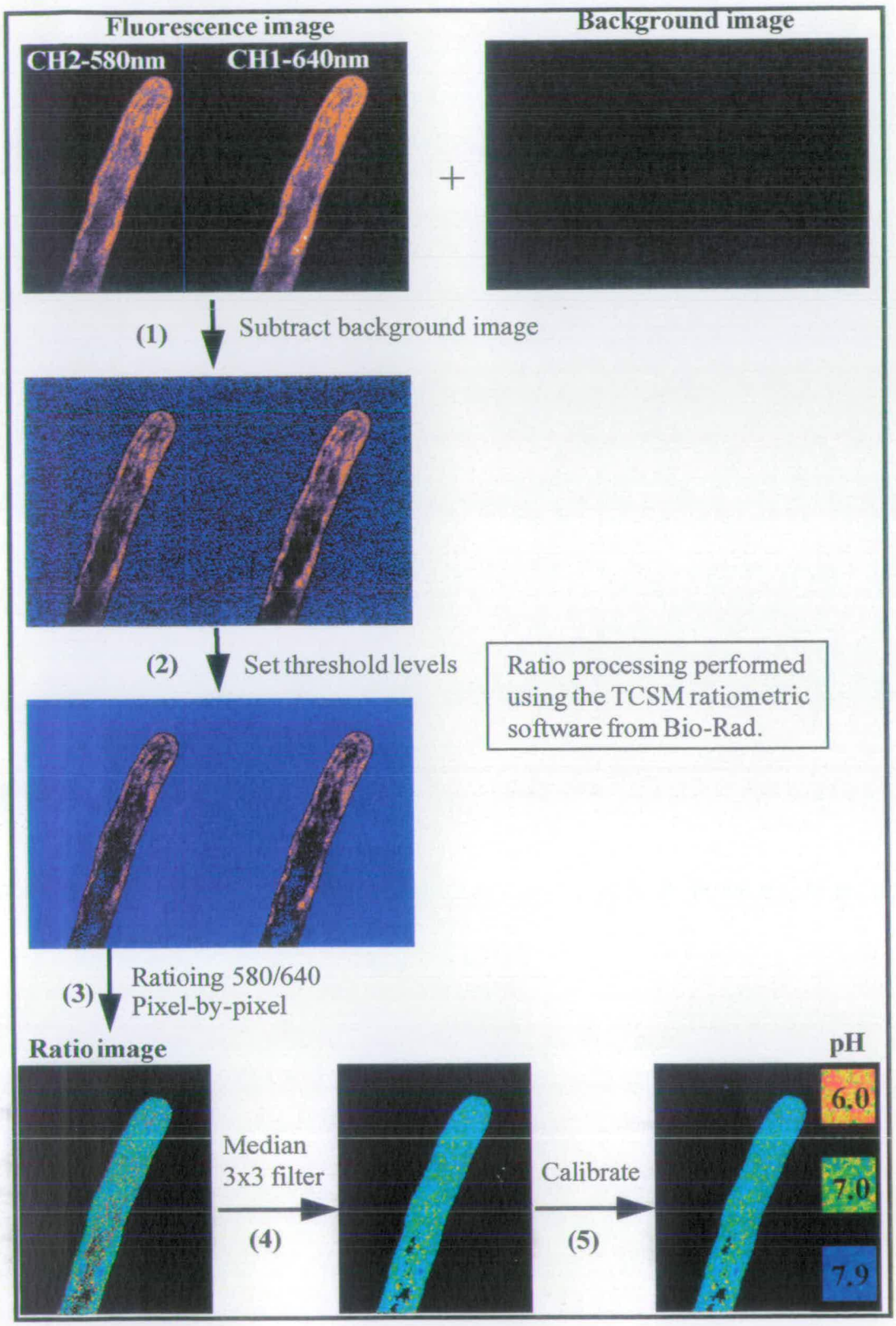

Fig. 17: Calibrated pseudocolour look-up table (LUT) for ratio images. The relationship between ratio value, the pixel intensity in a ratio image and their relationship to *in vitro* calibration data is shown. Each of the 256 pixel intensities corresponds to a ratio value, here the range 0 - 255 corresponds to ratios of 0 - 2 (generally ratio ranges from 0 to between 2 and 4 were used). The ratio value (or pixel intensity) determined from a calibration image for a given pH can be seen to lie over a range rather than a single value because of the variation between individual pixels (note the *in vitro* calibration images). The [ion] value for a region within an image should, therefore, be given within defined confidence limits based on the level of between-pixel random variation. In this respect a pseudocolour LUT wedge is misleading in suggesting that a single colour in an image represents a particular [ion], and worse, that each individual pixel reports actual [ion]. Because of the inherent variation of individual pixels only average pixel values (averaged over time or over an area) should be considered when estimating [ion]. This is discussed in Chapter 5.

Fig. 17: Calibrated pseudocolour look-up table (LUT) for ratio images

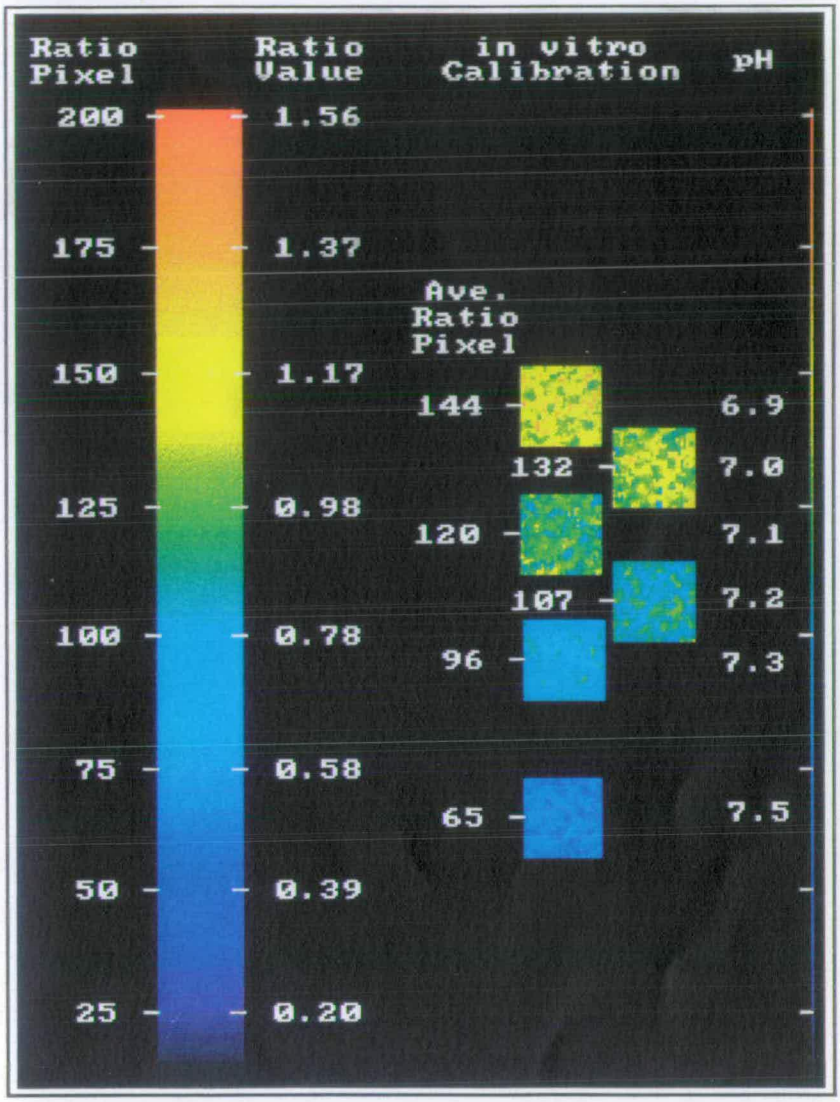

Chapter 3

Fig. 18: Developmental stages of *Dryopteris affinis* gametophytes. (A-I) Development of liquid cultured fern gametophytes. Tracings were taken from photographic negatives. Rhizoids are indicated with an arrowhead. (A, B and C) Tracings of: a dry spore; imbibed swollen spore; and germinated spore with emergent rhizoid, respectively. There was little or no difference between red and white light cultured spores up to this stage, 5 days after sowing the spores. (D, E and F) Tracings of gametophytes cultured in white light (50 - 200 $\mu\in m^{-2}s^{-1}$) for 6 days, 11 days and 14 days, respectively. Note the large diameter, roughly isodiametric, chlorocyte cells, with well developed chloroplasts. Rhizoids were well developed and occur in increasing numbers with increasing time in culture. (G, H and I) Tracings of gametophytes cultured in red light (2 - 5 $\mu\in m^{-2}s^{-1}$) after 6 days, 8 days and 13 days, respectively. Chlorocytes were narrow and elongate, with poorly developed chloroplasts. The rate of cell division was low and only a single rhizoid developed, which was often narrow and slow growing. Scale bar = 100 μm.

Fig. 19: Time-course of gametophyte development. The events of gametophyte development for culture under white light (50 - 200 $\mu\in m^{-2}s^{-1}$) and red light (2 - 5 $\mu\in m^{-2}s^{-1}$) are compared. Refer to Fig. 18 for examples of the growth stages and Chapter 1; Fig. 6 for the developmental path of a typical gametophyte.

Fig. 18: Developmental stages of *Dryopteris affinis* gametophytes

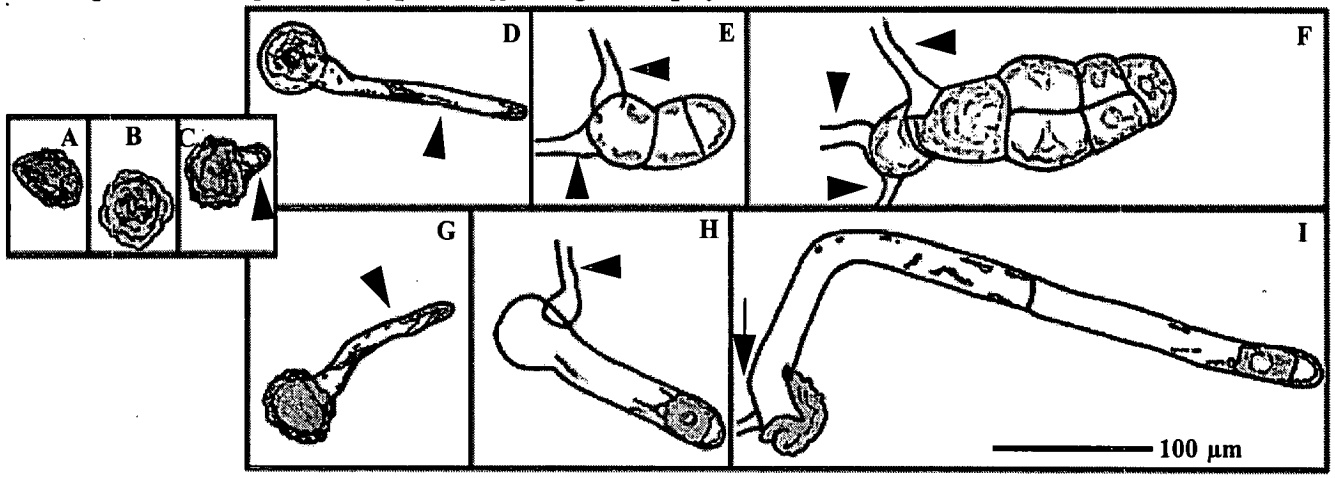

Fig. 19: Time -course of gametophyte development

Culture Time (days)	0 - 2	2 - 4	4 - 6	6 - 8	8 - 0	10 - 12	12 - 14
	Darkness	Continuous light: 2 - 5 $\mu Em^{-2}s^{-1}$ Red or 50 - 200 $\mu Em^{-2}s^{-1}$ White					
Events in white light		Spores become rounded	Spore rupture Rhizoid emergence and early elongation	Rhizoid elongation Primary chlorocyte swelling	Rhizoid elongation Secondary rhizoids Chlorocyte division		Multiple cells, reorientation division Secondary rhizoids
Cells	spore cell		1 + rhizoid	1 - 2 + rhizoid	2 - 3 + multiple rhizoids		3 - 4 + rhizoids
Events in red light		Spores become rounded	Spore rupture Rhizoid emergence and early elongation	Rhizoid elongation Primary chlorocyte emergence/elongation	Primary rhizoid deterioration Primary chlorocyte elongation and division		Multiple cell elongate filament
Cells	Spore cell		1 + rhizoid		1 - 2 + rhizoid		2 - 3 + rhizoid
	Imbibed spores		**Germination**	**Rhizoid development Chlorocyte development**	**Protonemal development**		**Prothallus Protonema**

Fig. 20: Typical protonemal apical-cell structure. (A) DIC image (x40 oil immersion objective) of a typical red light-cultured apical chlorocyte (10 days culture). (B) Interpretative diagram highlighting key structural features of a typical apical chlorocyte. Scale bar = 20 μm. Individual features are discussed in the main text. N = nucleus; C = cytoplasm; V = vacuole; Ch = chloroplast.

Fig. 20: Typical protonemal apical-cell structure

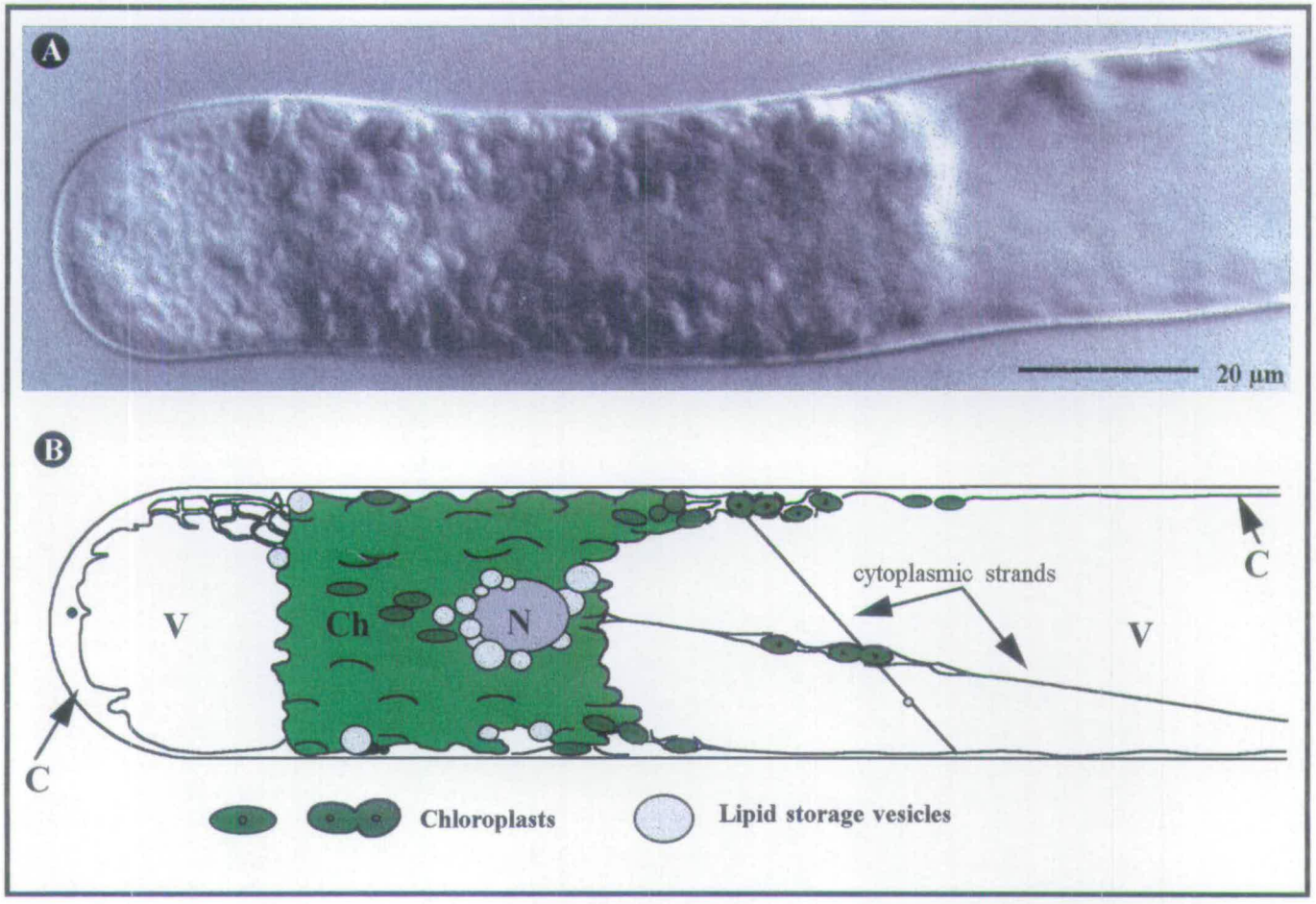

Fig. 21: Protonemal apical cell tip forms. (A-G) DIC images of typical apical chlorocytes cultured in liquid medium under red light (2 - 5 $\mu\in m^{-2}s^{-1}$). (A-D) Examples of *Dryopteris* apical chlorocytes referred to as the "vacuolated", "tubule filled" and "chloroplast filled" forms, respectively. (E and F) Examples of "thinning apical cytoplasm" forms believed to be associated with cell division (see Section 3.4.2 of the main text and Table 2). (G) A typical apical chlorocyte of *Adiantum capillus-veneris* included for comparison; note the smaller dimensions and chloroplast packed apical region. Scale bar = 20 μm.

Fig. 21: Protonemal apical cell tip forms

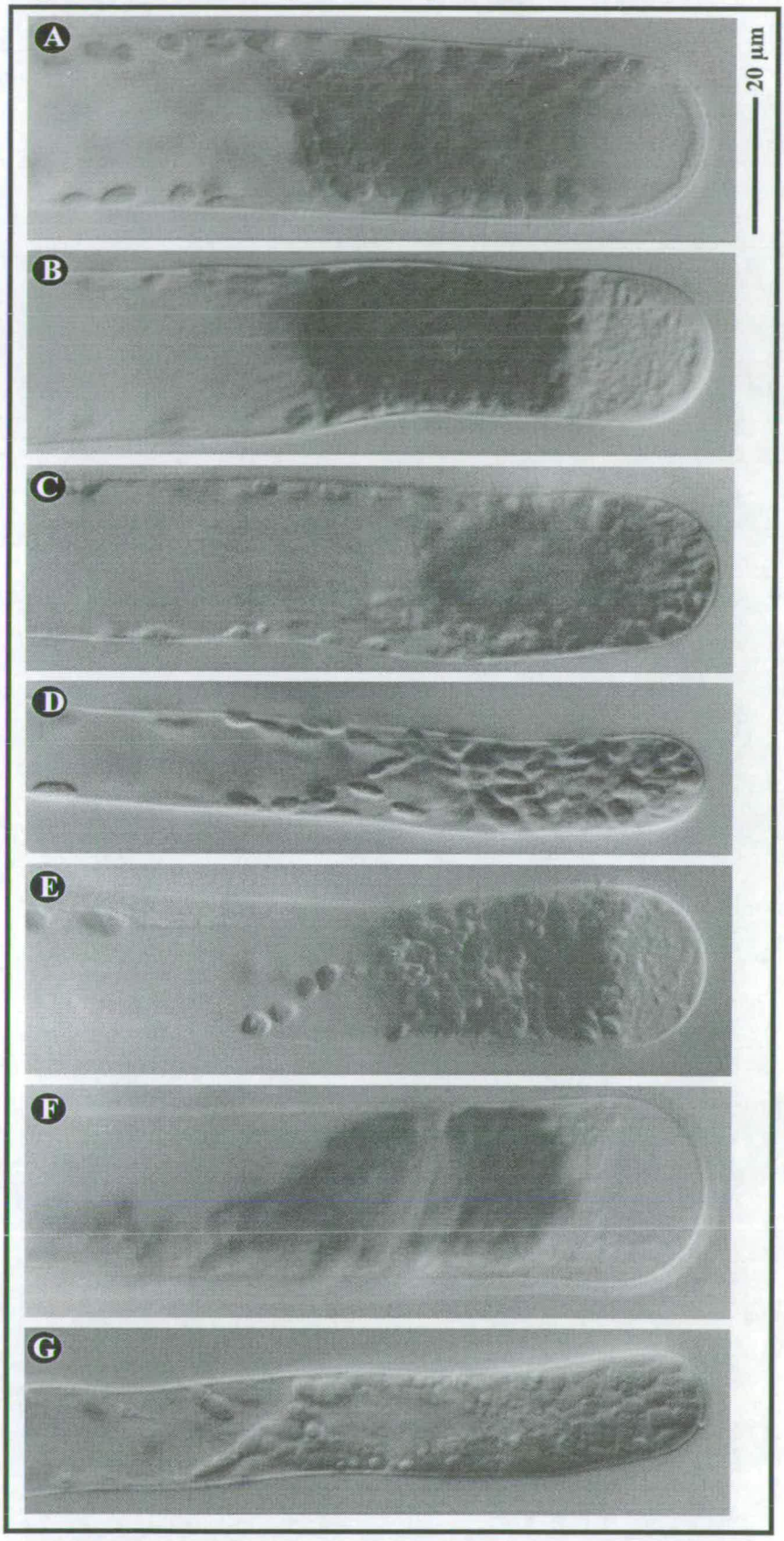

Fig. 22: Apical cell "swelling" response. (A and B) Graphs showing the changes in the proportions of different tip forms, within populations of protonemata, during white light-induced photomorphogenesis. Gametophytes cultured in liquid medium under red light for 12 days were exposed to white light at 50 $\mu\in m^{-2}s^{-1}$. Samples were removed at intervals for scoring. Averages of three independent repeat experiments were plotted, at least 3x200 protonemata were examined at each time point. (A) Apical chlorocyte swelling response (as defined in the main text, Section 3.5.1). General observations on the extent of "swelling" are indicated (i-iii). (B) Changes in the relative numbers of the other tip forms within a population (as defined in Chapter 3; Table 2): "vacuolated"; "tubule filled" and "green". Only chloroplast filled tips which were not swollen were scored as "Green". (C and D) Time-course of the apical chlorocyte "swelling" response in high intensity white light (150 $\mu\in m^{-2}s^{-1}$) at 21°C. (Ci and Di) Typical vacuolated tip forms of a protonema cultured under red light (2 - 5 $\mu\in m^{-2}s^{-1}$). (C and D ii-iv) Cessation of apical extension and increase in lateral expansion after white light irradiation: (ii) - 6 h; (iii) - 15 h; (iv) - 40 h. The exclusion of chloroplasts from the extreme apex during swelling (ii and iii) is not completely typical (E is a more typical example) and was probably a result of the intense illumination and possible heating effects experienced during prolonged examination under the microscope. Chloroplasts did eventually move into the tip (iv). Note the apical division after initial swelling which produced a roughly isodiametric apical cell (Div). Scale bar = 20 μm.

Fig. 22: Apical cell "swelling" response

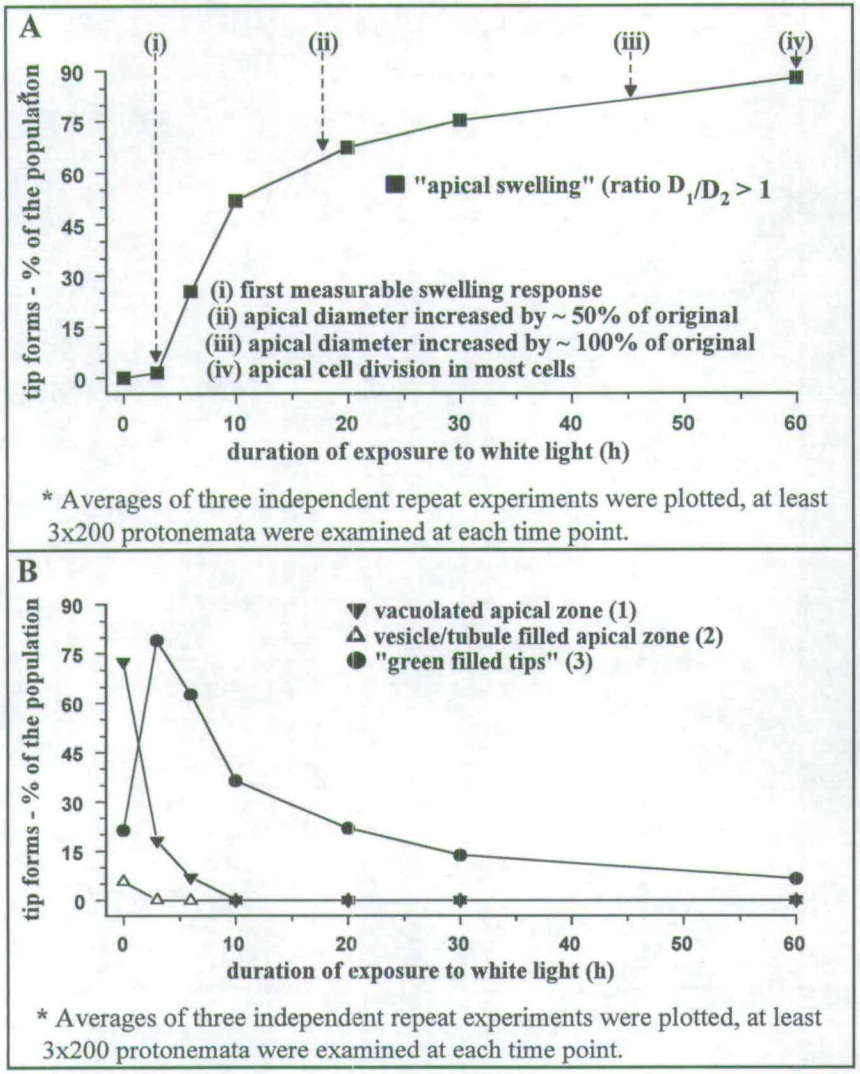

Fig. 23: Phototropic reorientation of apical growth

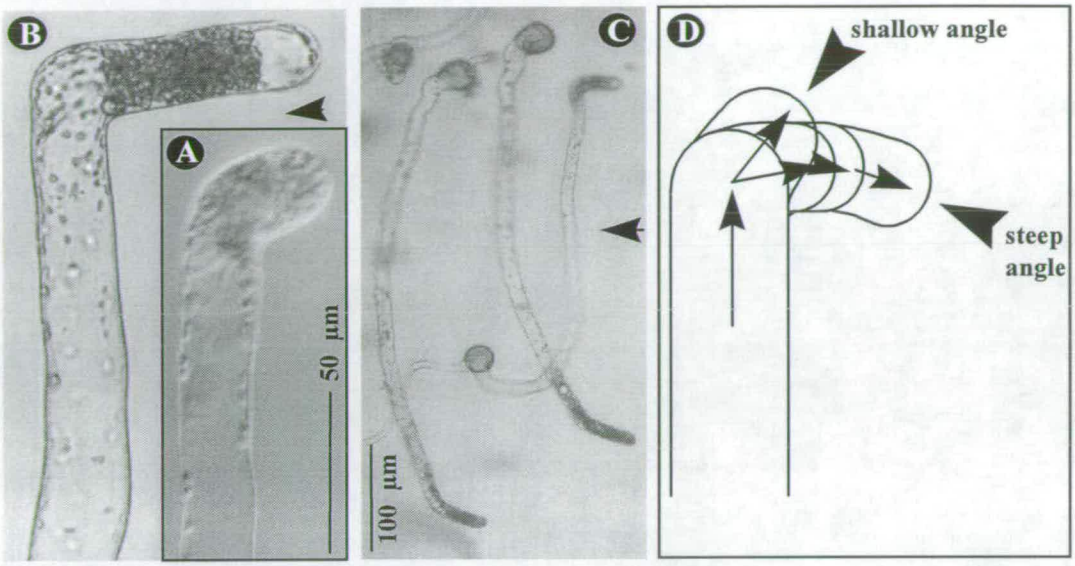

Examples of phototropic reorientation of growth in *Dryopteris* (A and B) and *Adiantum* (C) apical chlorocytes. Red light-grown protonemata were isolated under dim red light and irradiated laterally with red light (4 $\mu Em^{-2}s^{-1}$) in a specially modified thin-layer chamber. Examination on the microscope was only performed under green "safe-light" illumination (Kadota & Furuya, 1977). After redistribution of chloroplasts into the apex and repositioning of the nucleus closer to the extreme tip (Fig. 21C), reorientation proceeded as a lopsided swelling. (A) was after 6 h. (B) Vacuolated tips reformed once growth was established in the new orientation - this was after 18 h. In *Adiantum*, where the new direction of irradiation was at 90° or greater to the initial growth orientation, then reorientation took place in stages each involving partial reorientation of less than 90°. This is illustrated in the interpretative diagram (D). Scale bars = 50 µm for (A and B) and 100 µm for (C).

Fig. 24: Typical rhizoid apical structure. (A) DIC image (x100 oil immersion objective) of a typical liquid cultured rhizoid (7 days after sowing). (B) Corresponding interpretative diagram highlighting key structural features. Scale bar = 15 μm. Individual features are discussed in the main text. AC = apical cytoplasm; C = cytoplasm; N = nucleus; CW = cell wall.

Fig. 24: Typical rhizoid apical structure

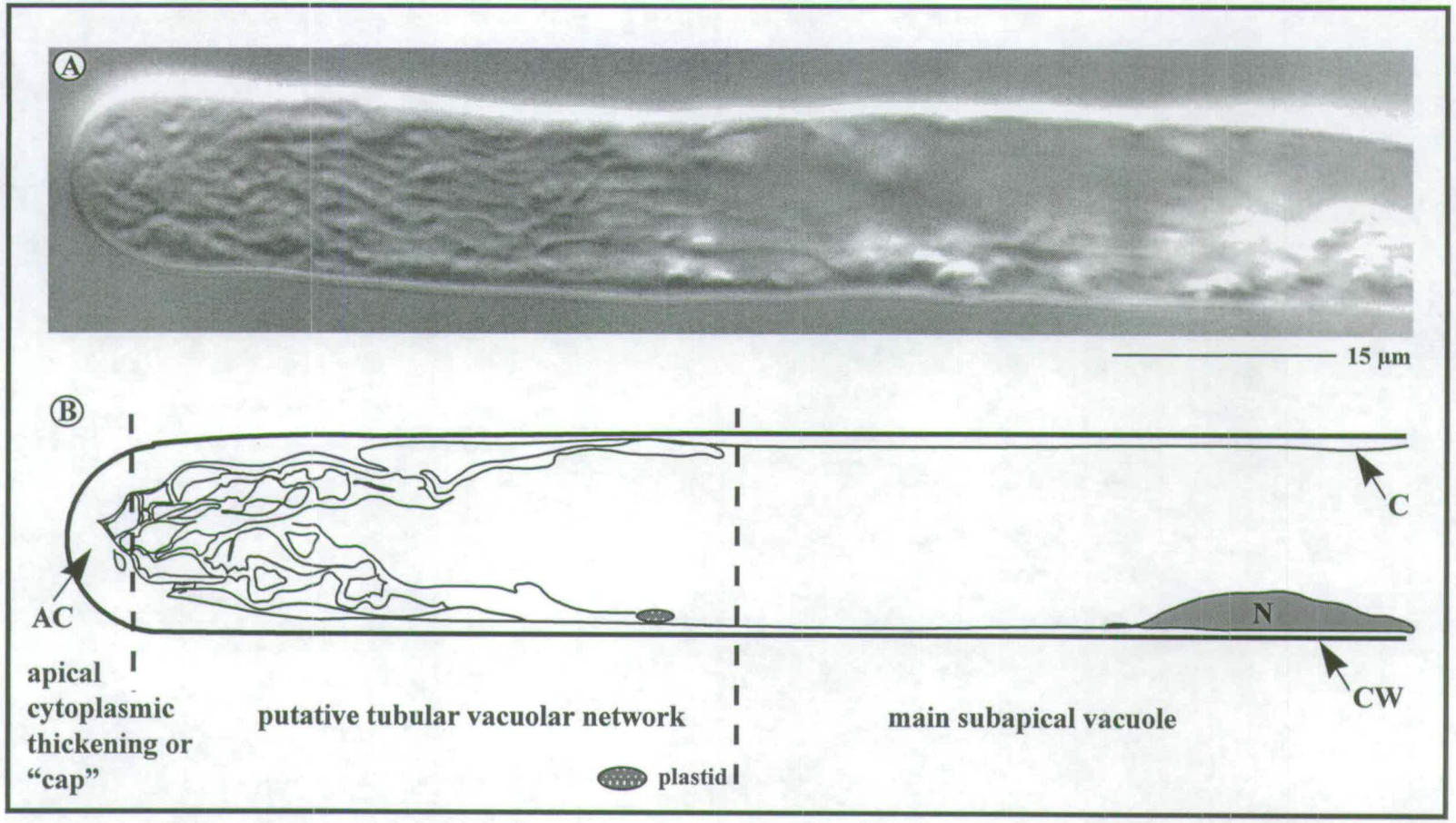

Fig. 25: Rhizoid tip forms

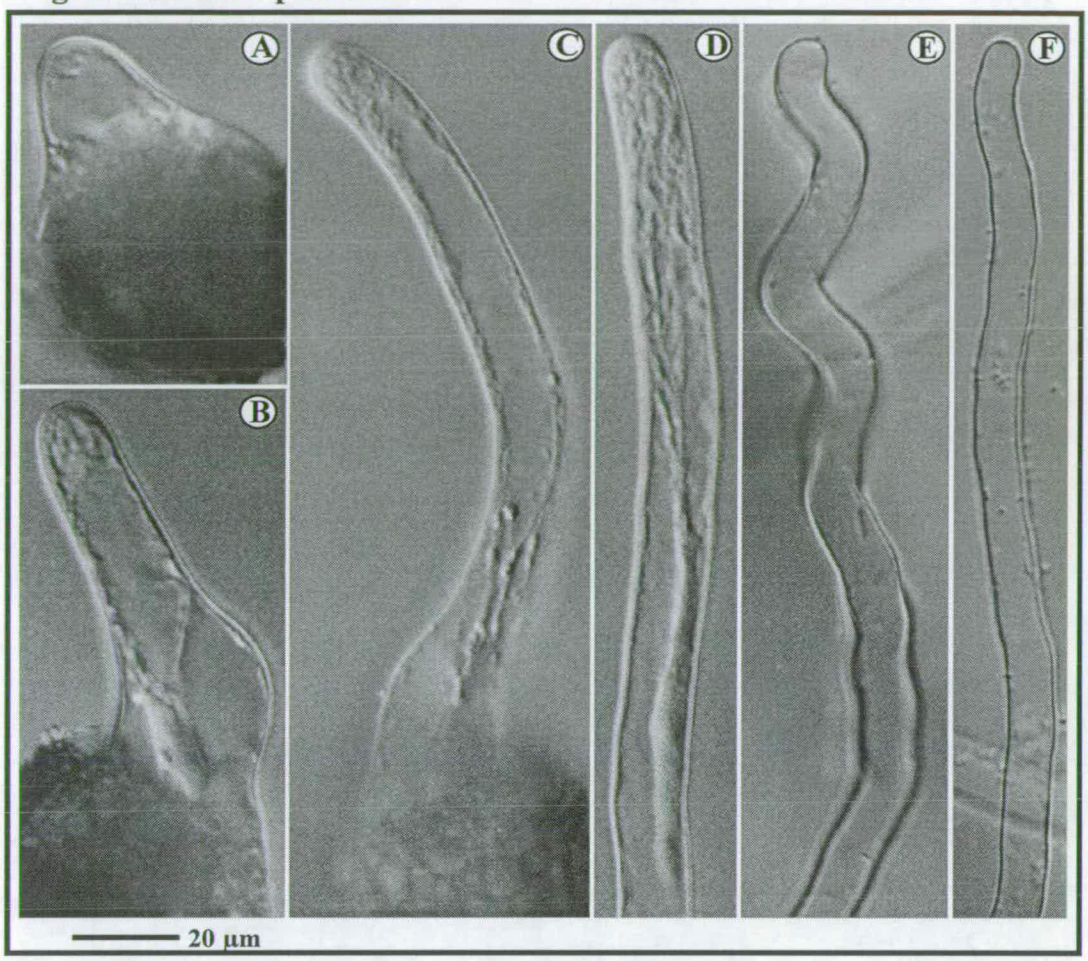

(A-F) DIC, x40 objective, images of typical *Dryopteris* rhizoids cultured in liquid medium under white light (50 $\mu Em^{-2}s^{-1}$) for 4 - 14 days. (A) Initial rhizoid emergence; 3 - 5 days old. (B) Early elongation stage; 4 - 6 days old. (C) Early elongation stage ~ 100 µm long; the main experimental material. (D) Later elongation stage; 6 - 14 days in culture and up to 2 - 3 mm in length. (E) Terminally differentiated, full grown rhizoids after longer than 14 days culture; up to 3 mm long. Note the development of the apical cytoplasmic structure with age (A-D) and its eventual deterioration in full grown rhizoids (E-F). Scale bar = 20 µm.

Fig. 26: Apical extension of rhizoids. Growth time-course for an individual rhizoid in a thin-layer chamber on the microscope stage. (Ai-vi) Images taken at 15 min. intervals using the transmission detector of the CLSM. The position of the nucleus is marked with an arrow. (B) A set of images, similar to (A), overlaid to highlight extension at the apex. Such image sets were used to determine individual growth rates - see Chapter 3; Table 3 and Chapter 4; Table 3. Scale bar = 20 μm.

Fig. 26: Apical extension of rhizoids

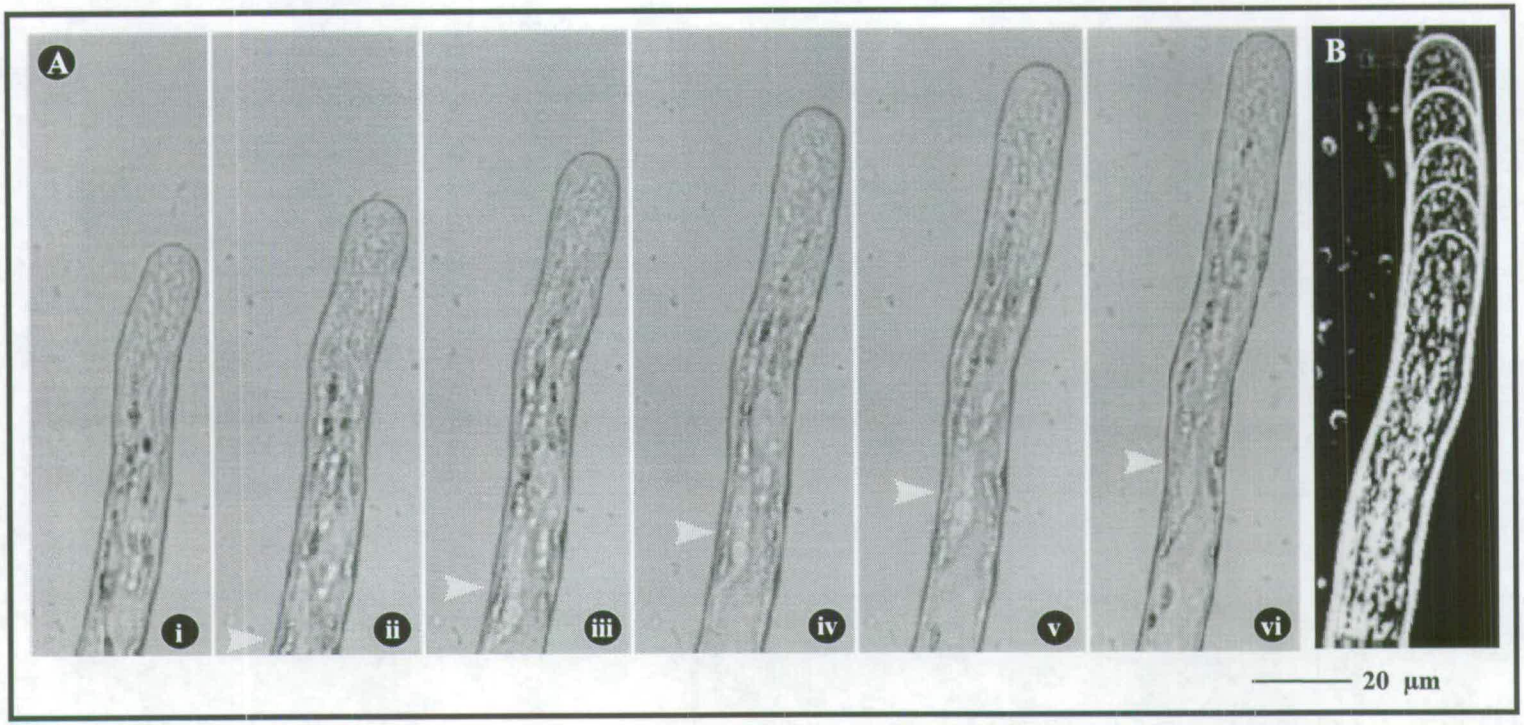

Fig. 27: Secondary rhizoid

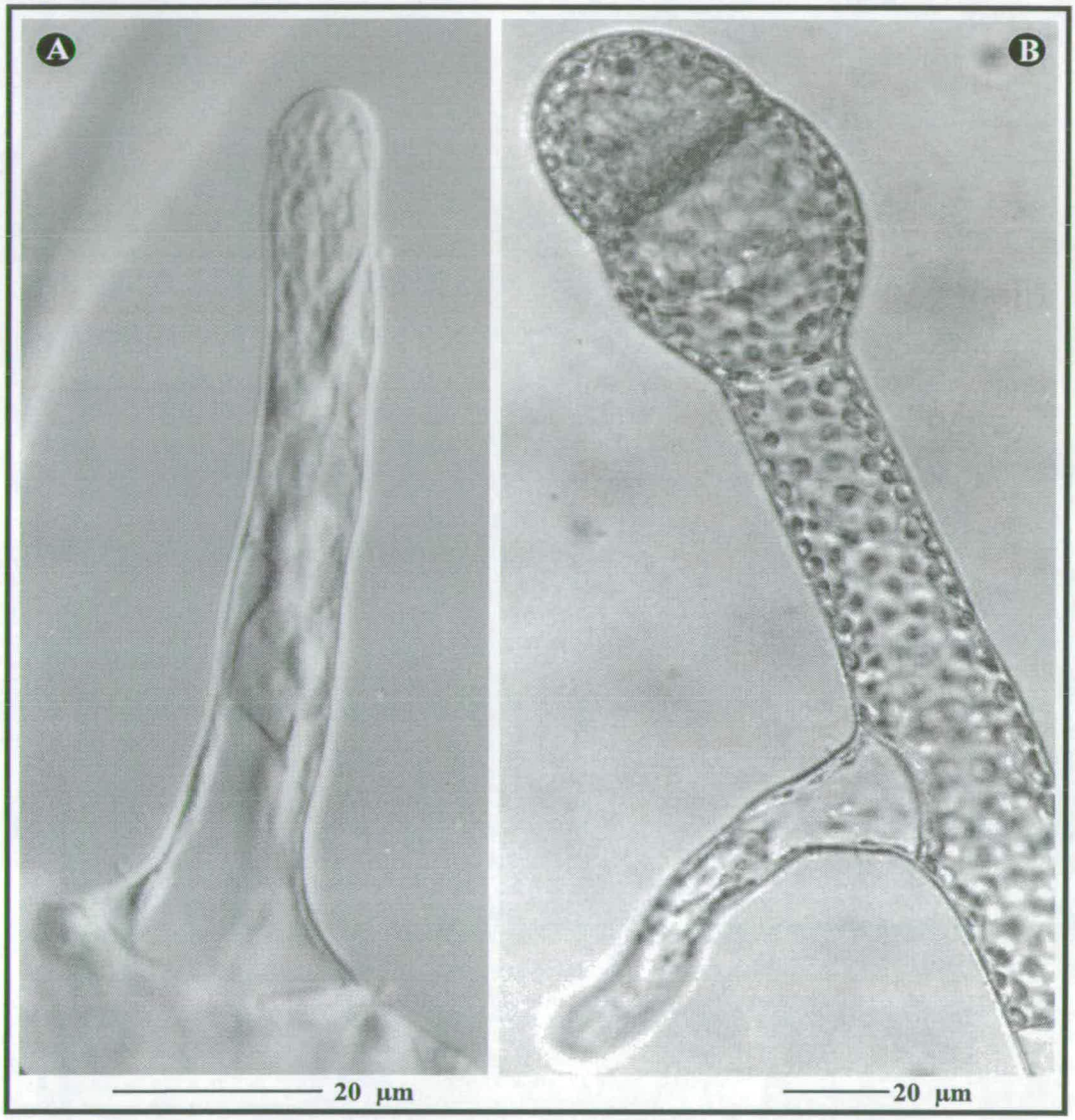

(A and B) Examples of secondary rhizoids produced on the subapical chlorocyte 6 days after initial exposure of a red light grown protonema to white light. (A) DIC x100 oil immersion objective. (B) DIC x40 oil immersion objective. Scale bars = 20 µm.

Fig. 28: Stressed cells. (A-D) Examples of apical chlorocytes exhibiting signs of stress. (A) Abnormal development of a protonema, note the orientation of the cell wall separating the apical and subapical chlorocytes (arrowheads) and the evacuated apex of the apical chlorocyte. (B) Mechanically stressed apical chlorocyte - note the evacuated apical region and rounded appearance of chloroplasts. (C) An individual cell stressed by prolonged examination under the microscope. Redistribution of the apical cytoplasm can be seen. Chloroplasts also appeared more rounded than normal. (D) Typical chemically stressed individual (in this case 100 μM verapamil) the apex was evacuated and the chloroplasts were rounded and clumped together (inset). (E-J) Apical regions of rhizoids showing signs of stress. (E i-iii) Sequence of images of a rhizoid showing the redistribution of apical cytoplasm as a result of stress from the intense illumination of the microscope lamp. Ei-Eiii were taken before treatment; after 1 h; and after 3 h, respectively. (F) Swelling response of a rhizoid due to an unknown contaminant in the culture medium. (G-J) The effects of mechanical stress; note the deterioration of the apical cytoplasmic distribution in each case. (J) A ruptured individual; the cytoplasm has extruded from the tip. See Table 7 and Section 3.9 of the main text. Scale bars = 20 μm (A-D); 5 μm (D) insert; and 10 μm (E-J).

Fig. 28: Stressed cells

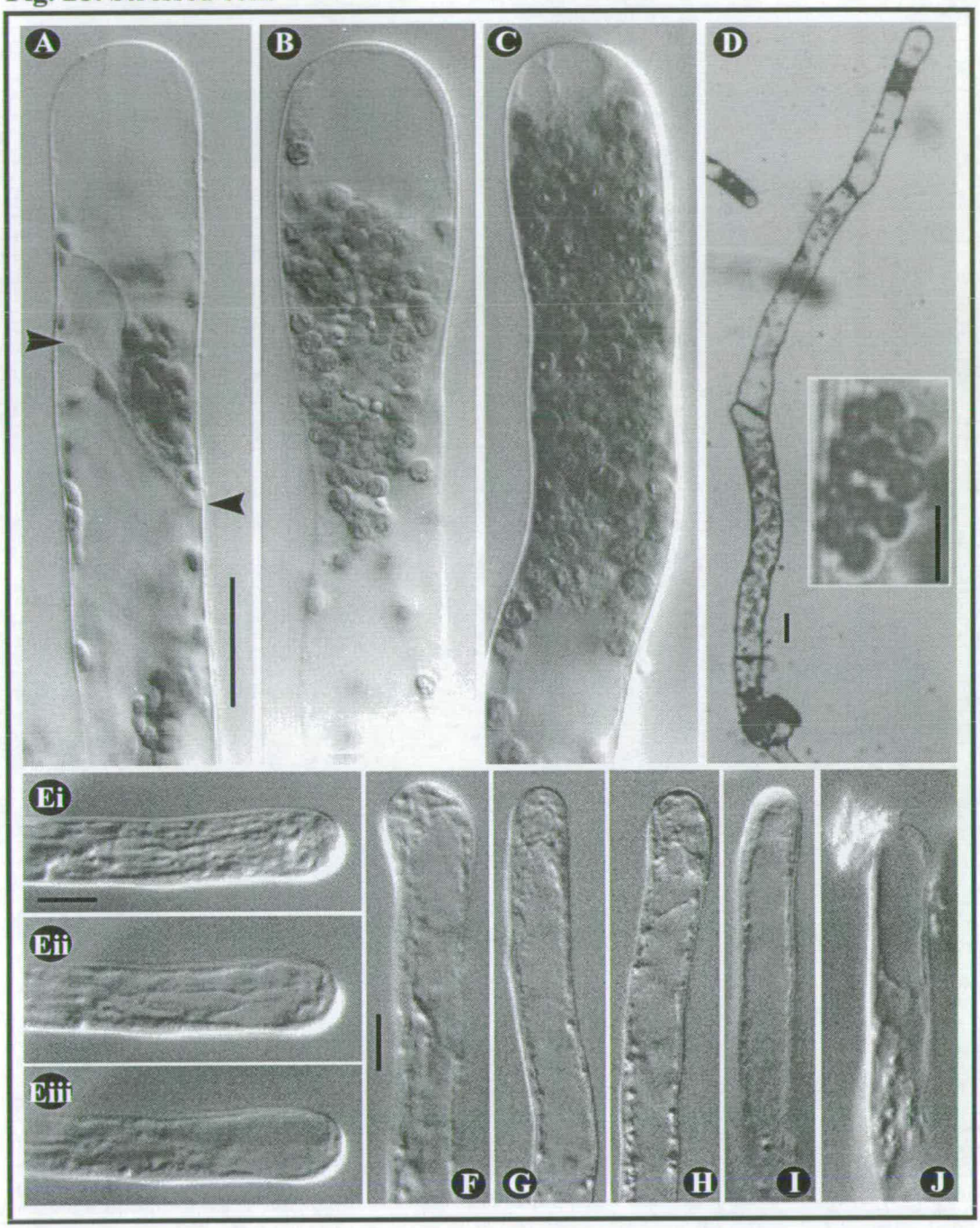

Fig. 29: Recovery of rhizoids after stress

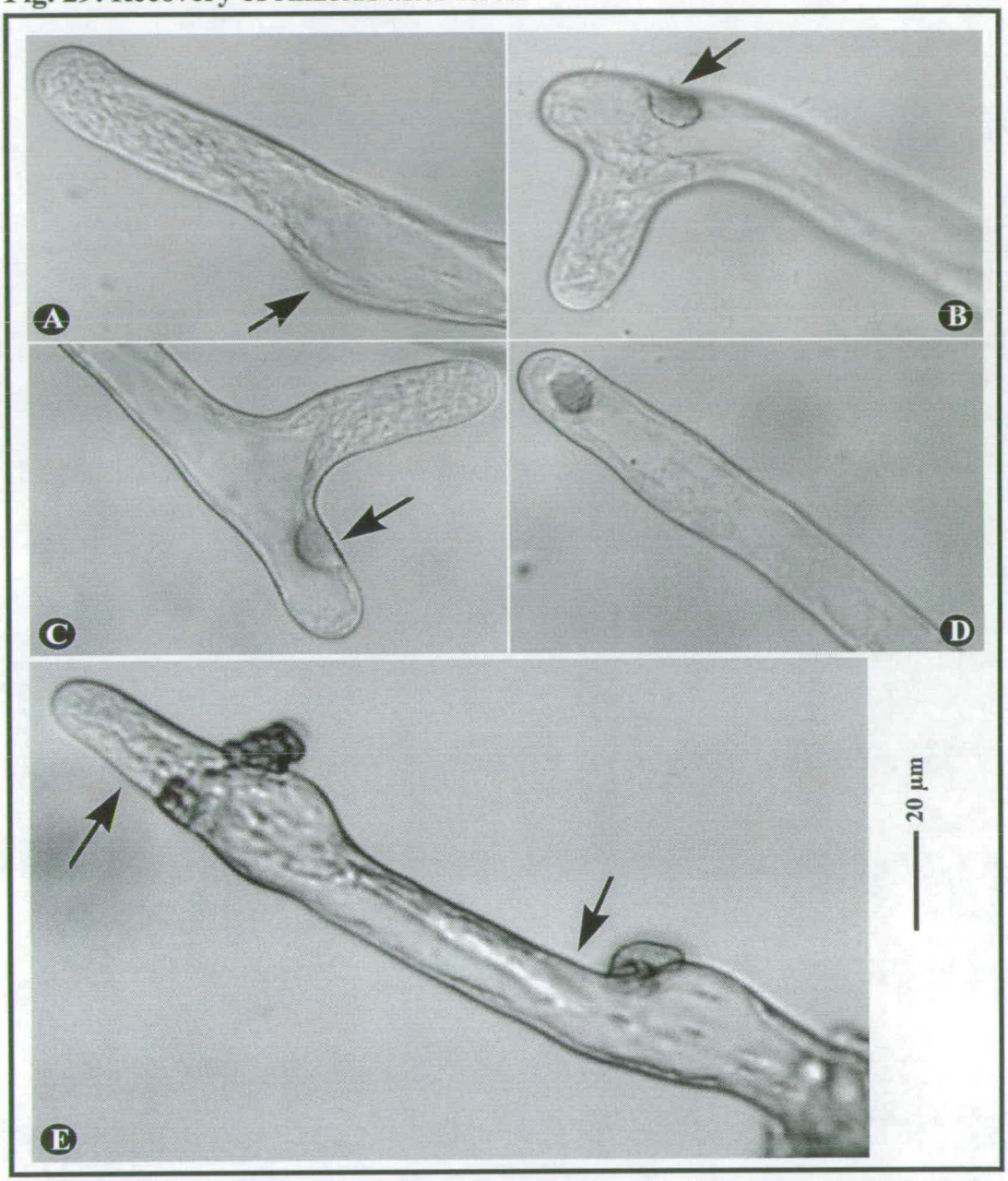

(A-D) Rhizoid tip regeneration 24 h after disruption of the apical structure as a result of mechanical stress, caused by isolation methods described in Chapter 2; Section 2.2.7.1. (A) Slight disturbance of growth (arrow). (B and C) Wound response (arrows), evacuation of cytoplasm from the original tips and regeneration of new tip structures. (D) Failure to regenerate a new tip structure and resume apical growth. (E) Chemically stressed rhizoid showing multiple attempts at recovery (arrows). Scale bar = 20 µm.

Fig. 30 (A-D): Staining of apical structures with fluorescent dyes. (A) General staining of the protonemal apical cell with $DiOC_6$. Chloroplast autofluorescence was not detected on the gain settings used. (Ai) Bright-field. (B) Confocal fluorescence images of Nile red staining of an apical chlorocyte. In addition to staining membrane the stain associates with lipid storage which fluoresce brightly. Chloroplast autofluorescence was not detected on the gain settings used. (Bi) Bright-field. (C and D) Confocal fluorescence images of LYCH staining of a protonema. (C) External LYCH excluded from the cell (chloroplast autofluorescence is too weak to detect with the gains necessitated by the high external LYCH concentration. (D) LYCH binding to the cell wall (only chloroplast autofluorescence is visible within the cell - compare D with the location of chloroplasts in the bright field image Di). (Ci and Di) Bright-field images. Scale bars = 20 μm (A and B); 25 μm for (C) and 50 μm for (D).

Fig. 30 (E): Staining of apical structures with fluorescent dyes. (E) Confocal fluorescence images of Nile red staining of a rhizoid tip. (Ei) Bright-field. The arrow marks the position of an autofluorescent plastid. Scale bar = 20 μm).

Fig. 30 (A-D): Staining of apical structures with fluorescent dyes

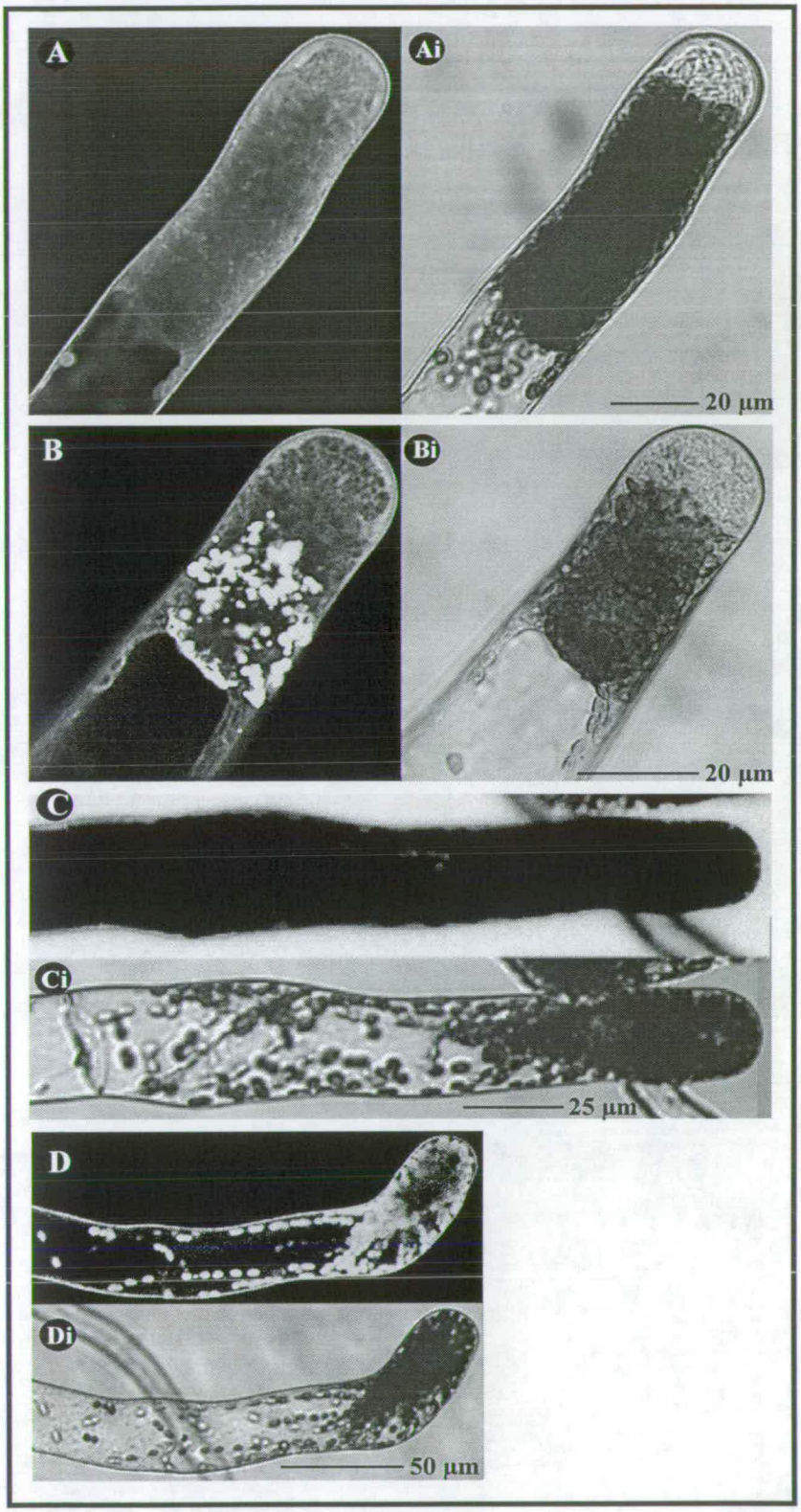

Fig. 30 (E): Staining of apical structures with fluorescent dyes

Fig. 31: Distribution of endoplasmic reticulum in chlorocyte cells. (A-C) Confocal fluorescence images of $DiOC_6$ stained chlorocyte cells showing the distribution of the peripheral endoplasmic reticulum. Imaging settings on the CLSM were: x40 dry (NA 0.95) objective; zoom 2.5; CA settings 4-8; Kalman filter n = 3 - 7; F2 (see Chapter 2; Tables 2 and 4). The fluorescence images shown are maximum projections of 5-10 optical sections taken at 1 μm focus steps. Chloroplast autofluorescence is just visible. (Ai-Ci) Corresponding bright-field images collected with the transmission detector. In the apical cell (A, B and corresponding bright-field images) the chloroplasts (arrows) can be seen to obscure imaging of the ER, which appears to lie underneath. ER could not be visualised at the extreme apex which stained very brightly. Behind the apex, the ER can be seen as a network of hexagonal tubules with areas of plate-like structure. In subapical cells (C) the network of hexagonal ER tubules is even more obvious. The network of tubules appears to be tighter towards the apical end of both apical and subapical chlorocytes. In A-C some staining of mitochondria (small bright dots) can be seen (refer to Fig. 32B). Scale bar = 20 μm.

Fig. 32: Distribution of mitochondria in apical chlorocytes. (A and B) Confocal fluorescence imaging of Rhodamine-123 and $DiOC_6$ stained chlorocyte cells, respectively, to reveal the distribution of mitochondria. CLSM: x40 (NA 0.95) dry objective; zoom 2.5; CA setting 4; Kalman filter n = 2-5; F2 (see Chapter 2, Table 2). Displayed fluorescence images are projections of 15 - 25 optical sections taken at 1.5 µm focus steps. Chloroplasts autofluorescence is just visible. (Ai and Bi) Corresponding bright-field images collected with the transmission detector. Scale bar = 20 µm.

Fig. 32: Distribution of mitochondria in apical chlorocyte

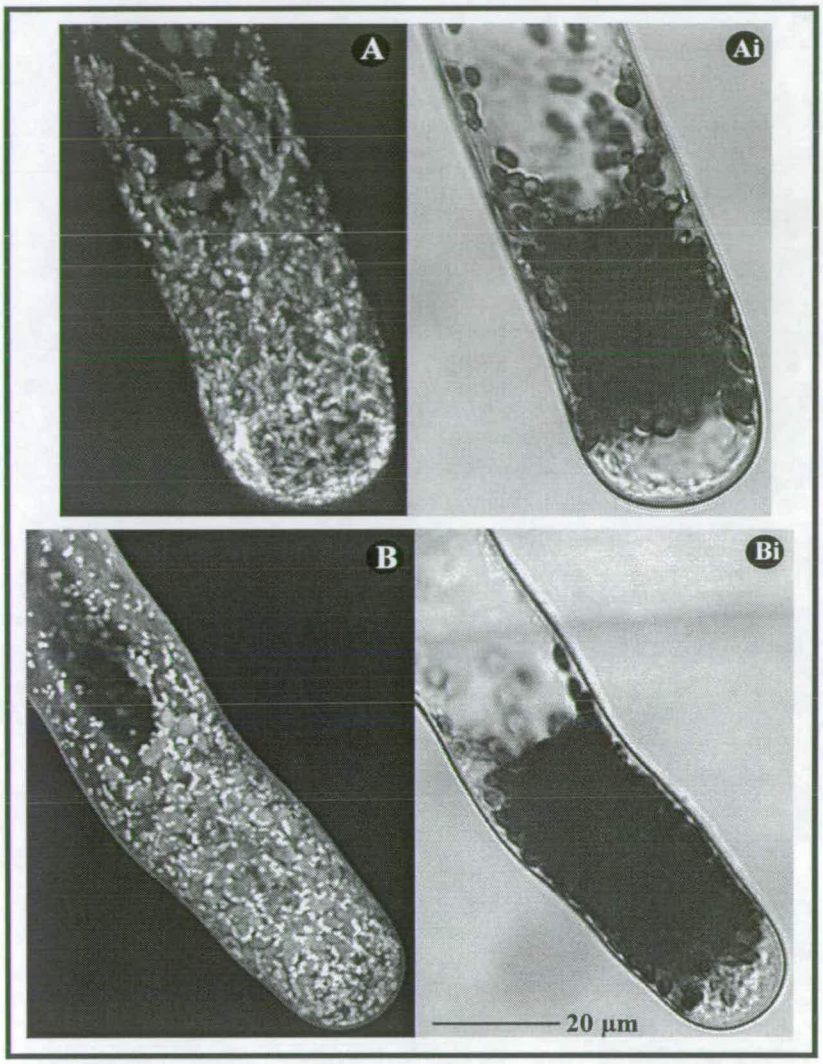

Fig. 33: Distribution of mitochondria in a rhizoid. (A and B) confocal fluorescence imaging of a Rhodamine-123 stained rhizoid to reveal the distribution of mitochondria. CLSM: x40 (NA 0.95) dry objective; zoom 3; CA setting 4; Kalman filter n = 2; F1 (see Chapter 2, Table 2). Displayed fluorescence images A and B are projections of 7 optical sections taken at 1.5 μm focus steps. (Ai-Bi) Corresponding bright-field images collected with the transmission detector. (A) Apical region, the increased numbers of mitochondria probably reflect the greater depth of cytoplasm rather than increased population density. Note the small mitochondrial free zone at the very extreme apex which corresponds to the thicker region of apical cytoplasm. (B) Subapical region of the same rhizoid; the nucleus is present at the centre right of the image (arrow in Bi). Mitochondria show up clearly along cytoplasmic strands and appear to be distributed throughout the cytoplasm -. Scale bar = 15 μm.

Fig. 33: Distribution of mitochondria in a rhizoid

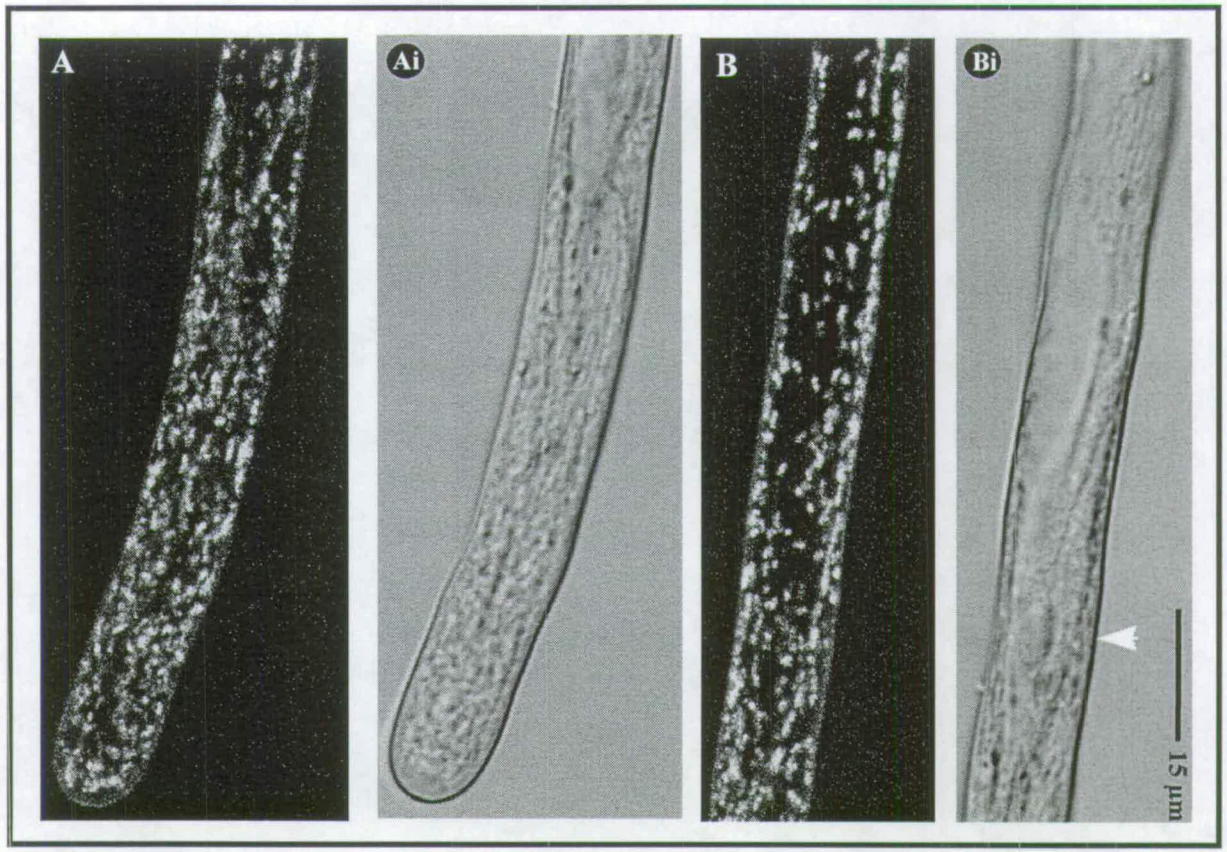

Chapter 4

Fig. 34 (A-F): Microinjection of fern protonemata with fluorescent dyes. (A-E) Ionophoretic microinjection of Calcium Green-1 into a subapical chlorocyte. (A) Bright-field image before microinjection. The injection site is marked by an arrow. (B-D) Fluorescence images showing the spread of dye from the injection site. Images were recorded at 20 sec. intervals during the injection and an extra pulse of current was applied between images. The spread of dye along cytoplasmic strands and around the cell periphery is clearly visible. The position of the nucleus (arrow) was quickly highlighted by dye fluorescence. (E) Fluorescence 20 min. after injection; after this dye rapidly sequestered within the vacuole. (F) Fluorescence image of an apical chlorocyte injected into the cytoplasm with Calcium-green-1. Note the bright fluorescence at the cell periphery and surrounding chloroplasts. Bar = 40 μm throughout.

Fig. 34 (G-J): Microinjection of fern protonemata with fluorescent dyes. (G and H) Bright field image before injection and corresponding fluorescence image after injection into the vacuole. Note the dark regions corresponding to chloroplasts masking fluorescence from the large central vacuole. (I and J) Bright field image and corresponding fluorescence image for a protonema ester-loaded with BCECF-AM. Note the loading of the nuclei (arrows) and the localisation of fluorescence to the cytoplasm around the cell periphery. Bar = 40 μm throughout.

Fig. 34 (A-F): Microinjection of fern protonemata with fluorescent dyes

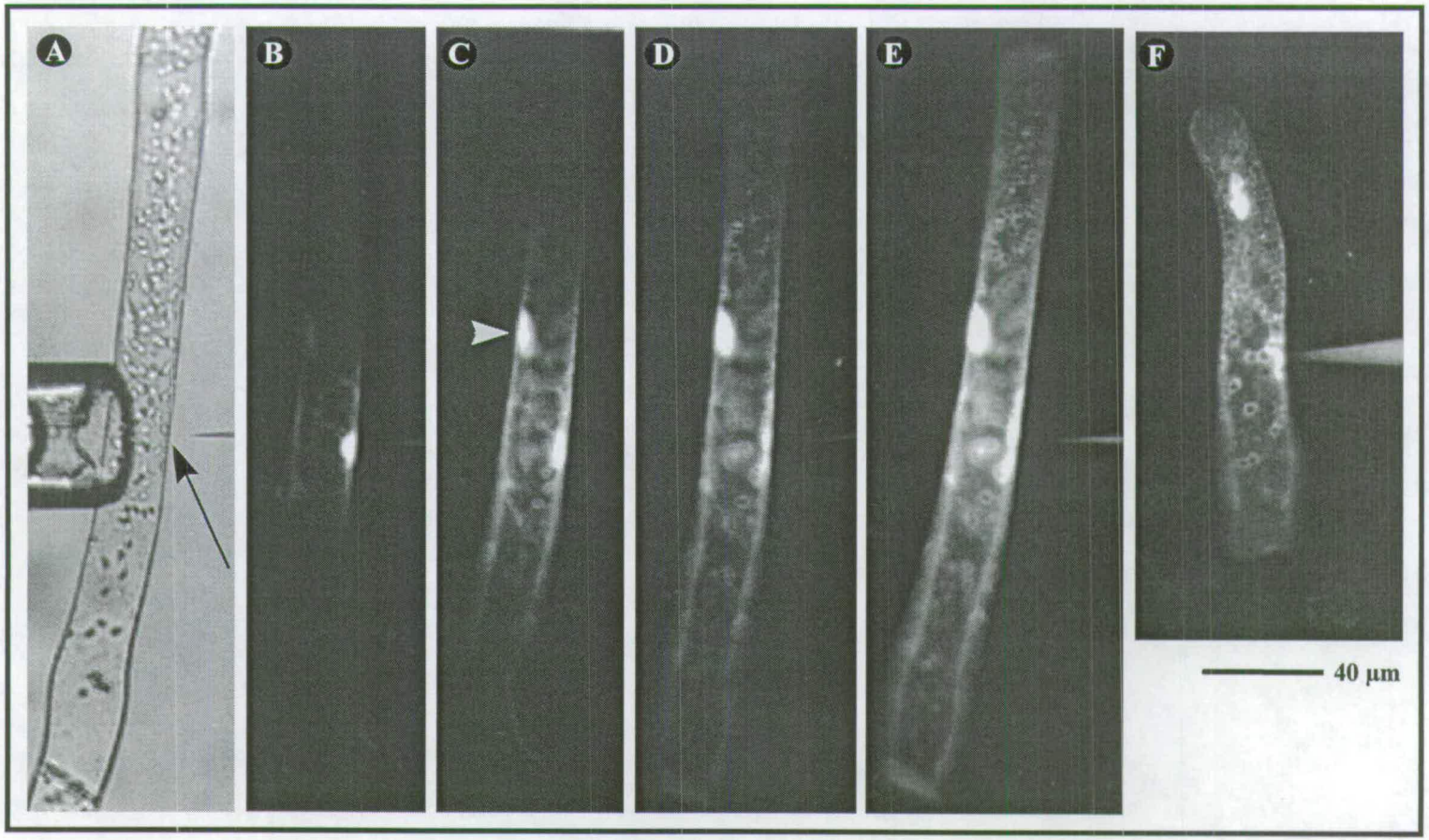

Fig. 34 (G-J): Microinjection of fern protonemata with fluorescent dyes

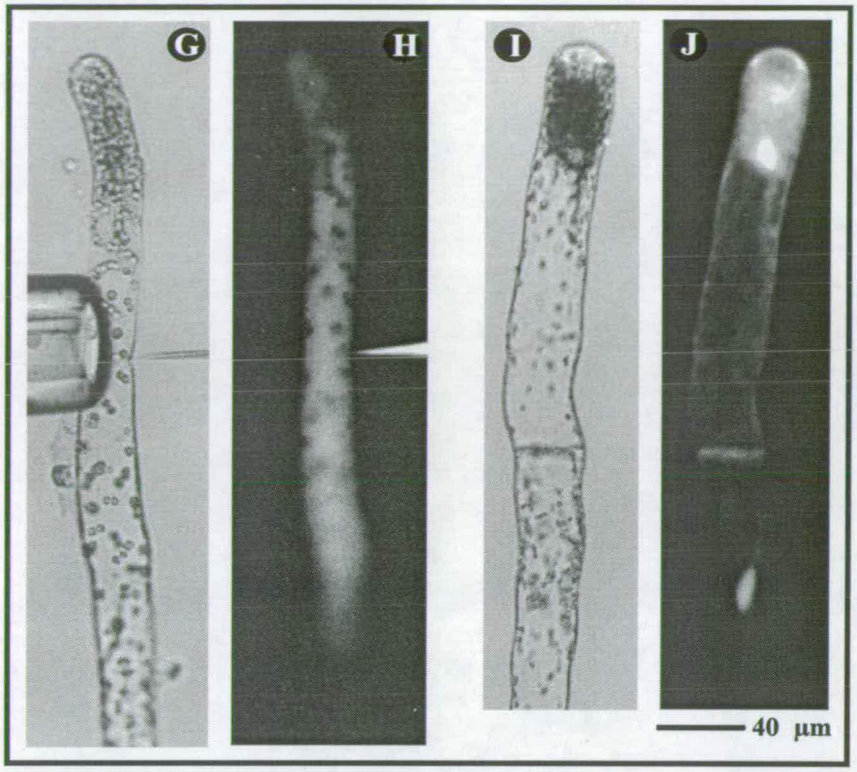

Fig. 35: Low pH loading of fern protonemata with cSNARF-1 free -acid

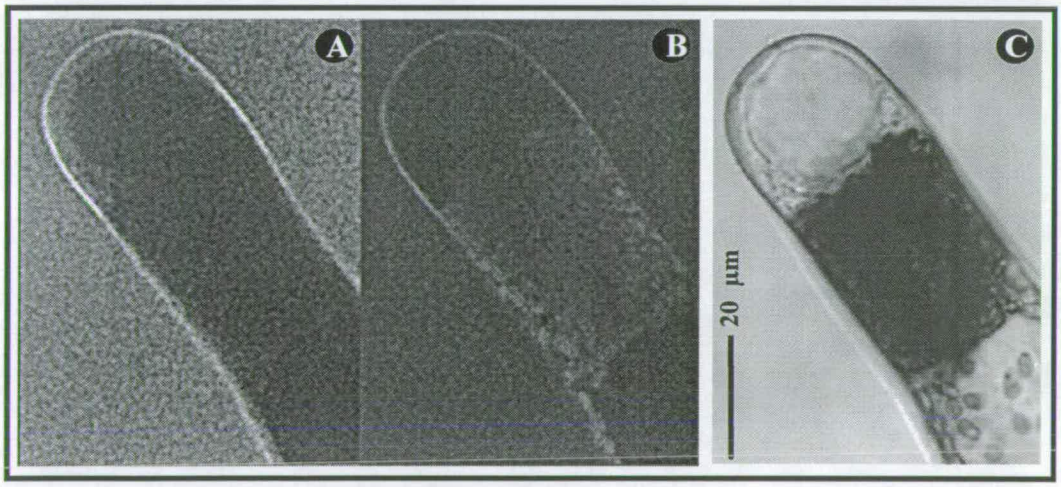

(A and B) Dual channel confocal fluorescence imaging; Ch-2 and Ch-1 images respectively after 60 min. acid-loading. The bright fluorescence at the cell periphery was shown by plasmolysis treatments to be associated with the cell wall. Some fluorescence can be seen to be associated with the apical cytoplasm; compare (A) with the bright-field image (C). The area behind the apical dome in (B) shows strong chloroplast autofluorescence. Bar = 20 µm.

Fig. 36: Ester-loading of fern protonemata with cSNARF-1 AM. All cells were examined by confocal microscopy using a x40 dry (NA = 0.95) plan apo objective. Photomultiplier gains were set below the level of detection of chloroplast autofluorescence. (A-G) Fluorescence images were projections of multiple, sequential, single channel confocal fluorescence images collected at intervals of 1.5 μM. (H and I) were single dual channel confocal fluorescence optical sections, collected for ratio analysis.

Fig. 36 (A and B): Ester-loading of fern protonemata with cSNARF-1 AM. (A and B) cSNARF-1 distribution (after AM ester-loading) in red light-grown and white light-treated protonemal apical cells. (Ai and Bi) Bright-field images corresponding to (A and B). Bar = 20 μm throughout.

Fig. 36 (A and B): Ester-loading of fern protonemata with cSNARF-1 AM

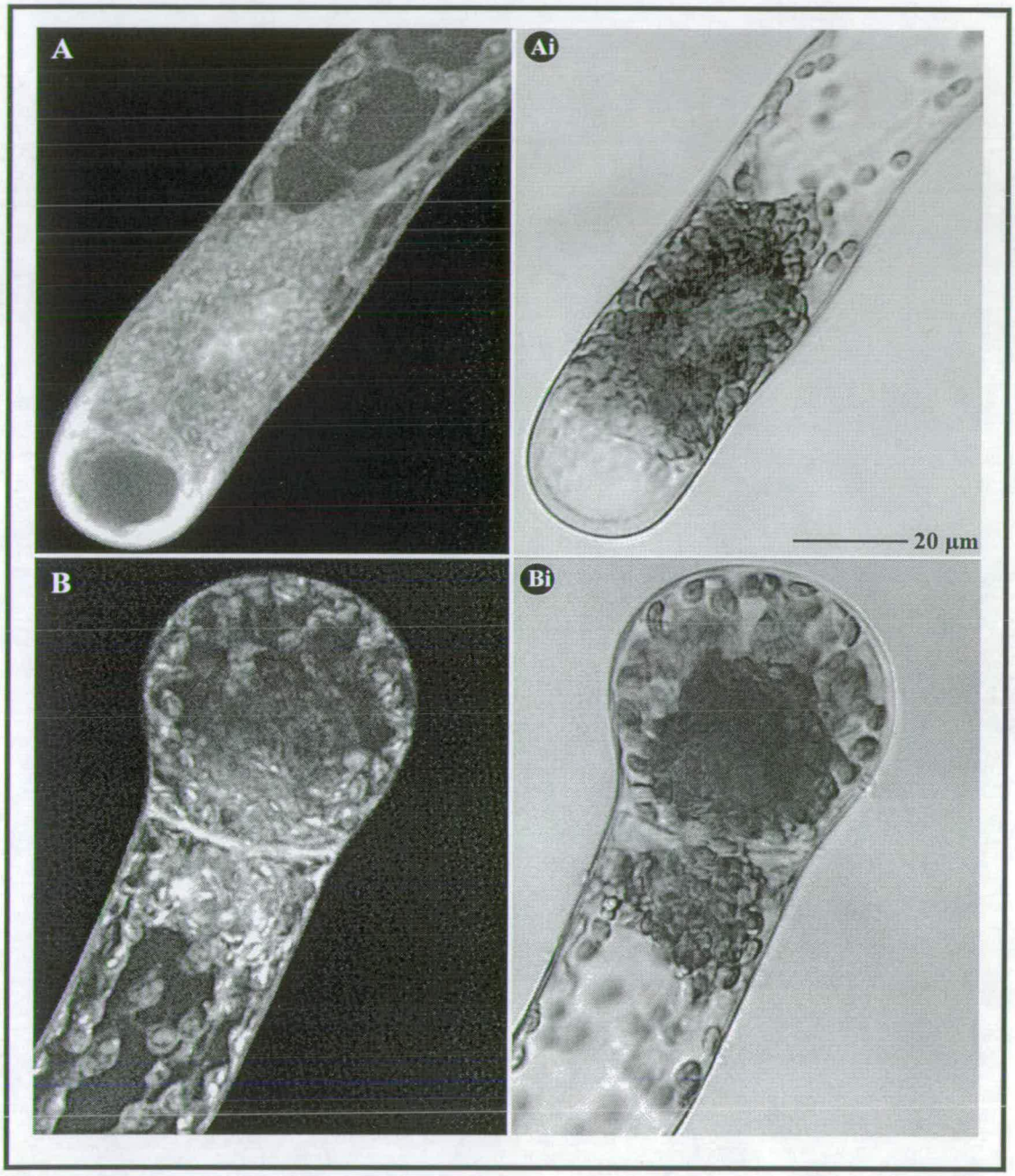

Fig. 36 (C-E): Ester-loading of fern protonemata with cSNARF-1 AM. (C-E) Examination of cSNARF-1 distribution in a red light-grown protonemal apical cell during AM ester-loading; three different focus positions are shown, from the cell periphery to the centre. In (C) Structures resembling ER can be clearly seen (arrow). In (D) the strongly fluorescent bands running perpendicular to the axis of the cell may be associated with the site of cell division. (Ei) Non-confocal, transmitted-light, bright-field image corresponding to (E). Several features are particularly clear: the subapical vacuole; peripheral and apical cytoplasm; and the nucleus with its associated cluster of chloroplasts. The position of the nucleus suggests that the cell was preparing for division. Bar = 20 μm throughout.

Fig. 36 (C-E): Ester-loading of fern protonemata with cSNARF-1 AM

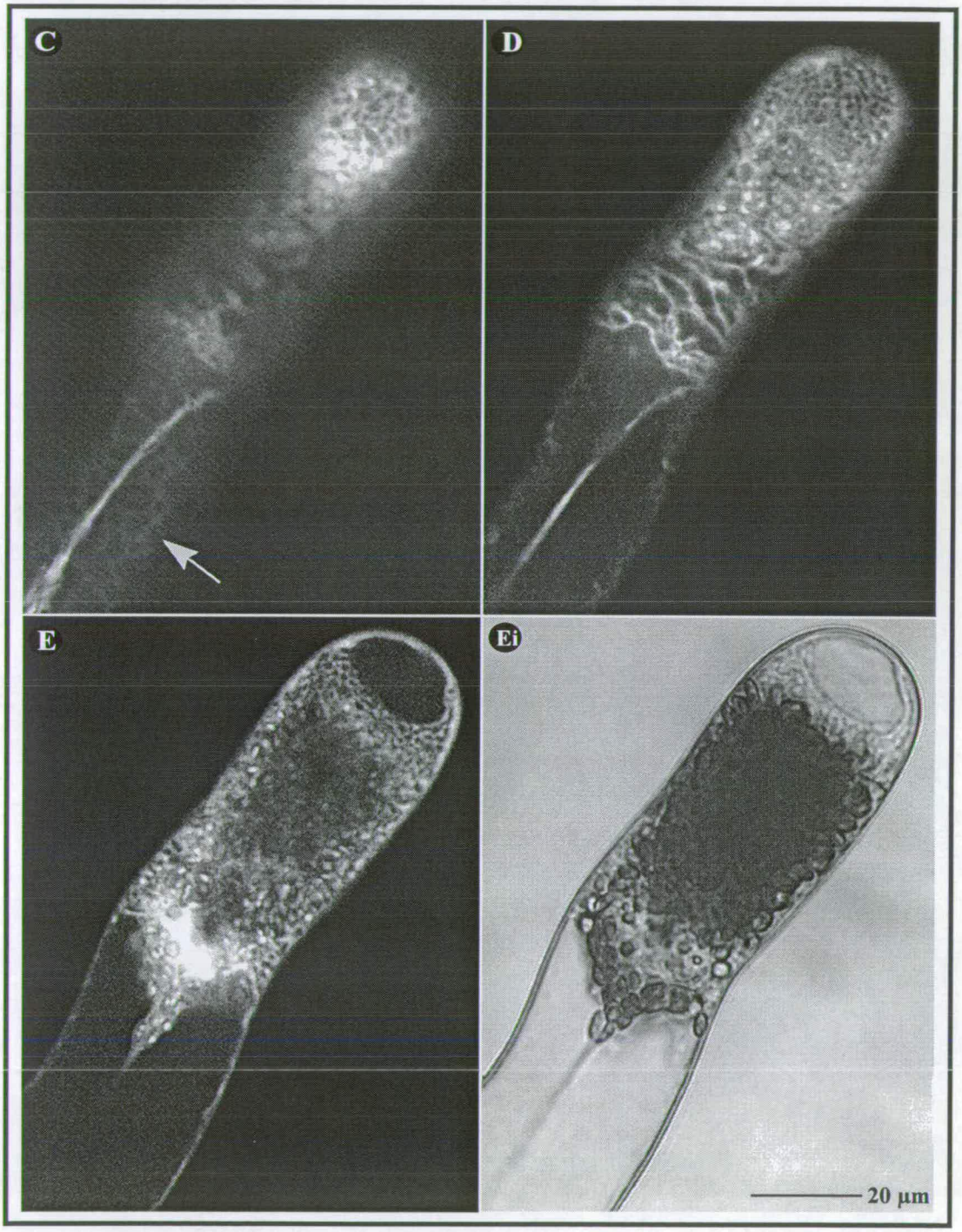

Fig. 36 (F and G): Ester-loading of fern protonemata with cSNARF-1 AM. (F) The association of cSNARF-1 fluorescence with chloroplasts. The corresponding bright-field image (Fi) shows the positions of the chloroplasts. Each chloroplast is "ringed" by fluorescence. The small central structure of each chloroplast (visible in Fi - arrows) also appears brightly fluorescent - although this structure may be an optical artefact resulting from the lens-like properties of the shape of chloroplasts or starch grains within them. Small patches of ER can be seen between the chloroplasts. (G) cSNARF-1 association with the ER during AM ester-loading of a subapical protonemal cell. A line of chloroplasts can also be seen, associated with a cytoplasmic strand. Images were only collected at the periphery of the cell as can be seen from the difference in width between the fluorescence (G) and bright-field images (Gi). Bars = 5 μm (F and Fi) and 10 μm (G and Gi).

Fig. 36 (F-G): Ester-loading of fern protonemata with cSNARF-1 AM

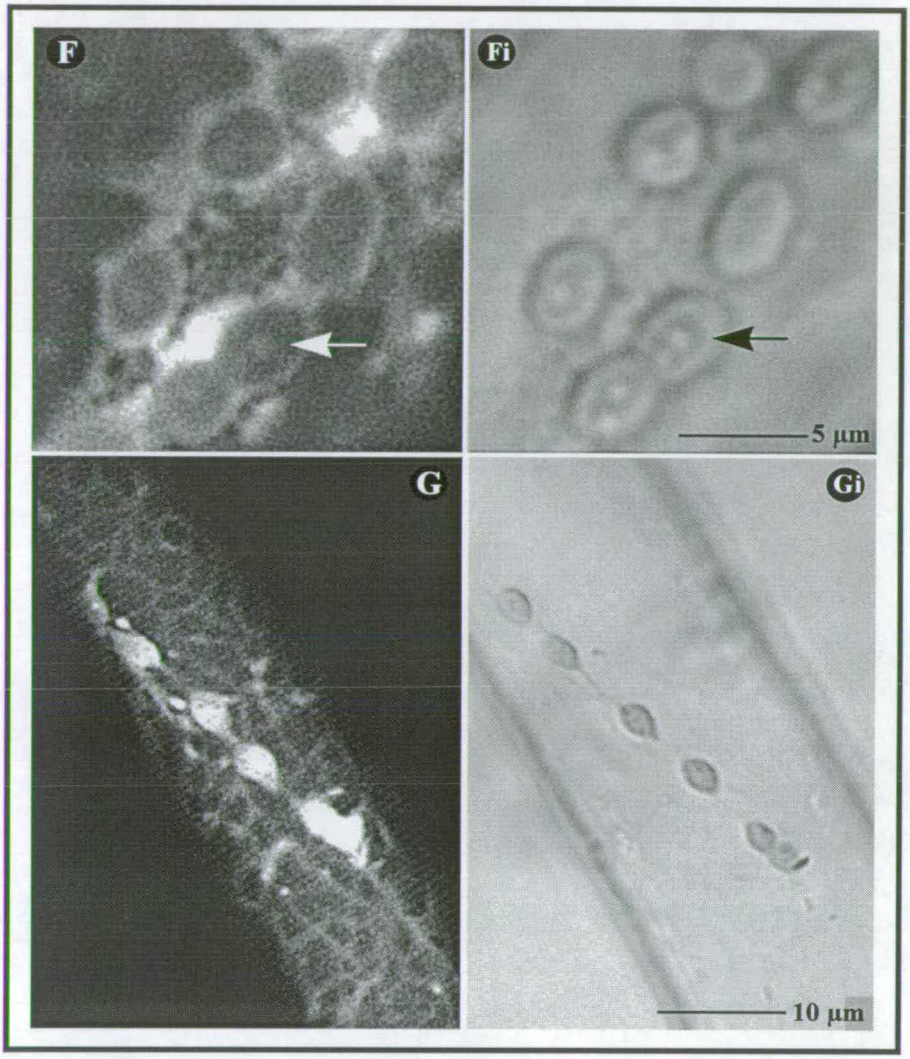

Fig. 36 (H-K): Ester-loading of fern protonemata with cSNARF-1 AM. Regions of different apparent pH in an apical chlorocyte, revealed by cSNARF-1 ratio imaging, corresponding to localisation of active dye in different subcellular compartments. (H and I) Single cSNARF-1 fluorescence confocal optical section dye distribution images for channel 2 and channel 1, respectively. (J) Corresponding bright-field image. (K) pseudocoloured cSNARF-1 ratio image (see Chapter 2; Fig. 16 for an explanation of ratioing). Regions of apparently different pH correspond to the cell wall, cytoplasm, vacuolar system and chloroplasts. Note that chloroplast autofluorescence locally affects the validity of ratioing such that the apparent alkaline pH of chloroplasts does not necessarily reflect actual pH. Bar = 20 μm.

Fig. 36 (H-K): Ester-loading of fern protonemata with cSNARF-1 AM

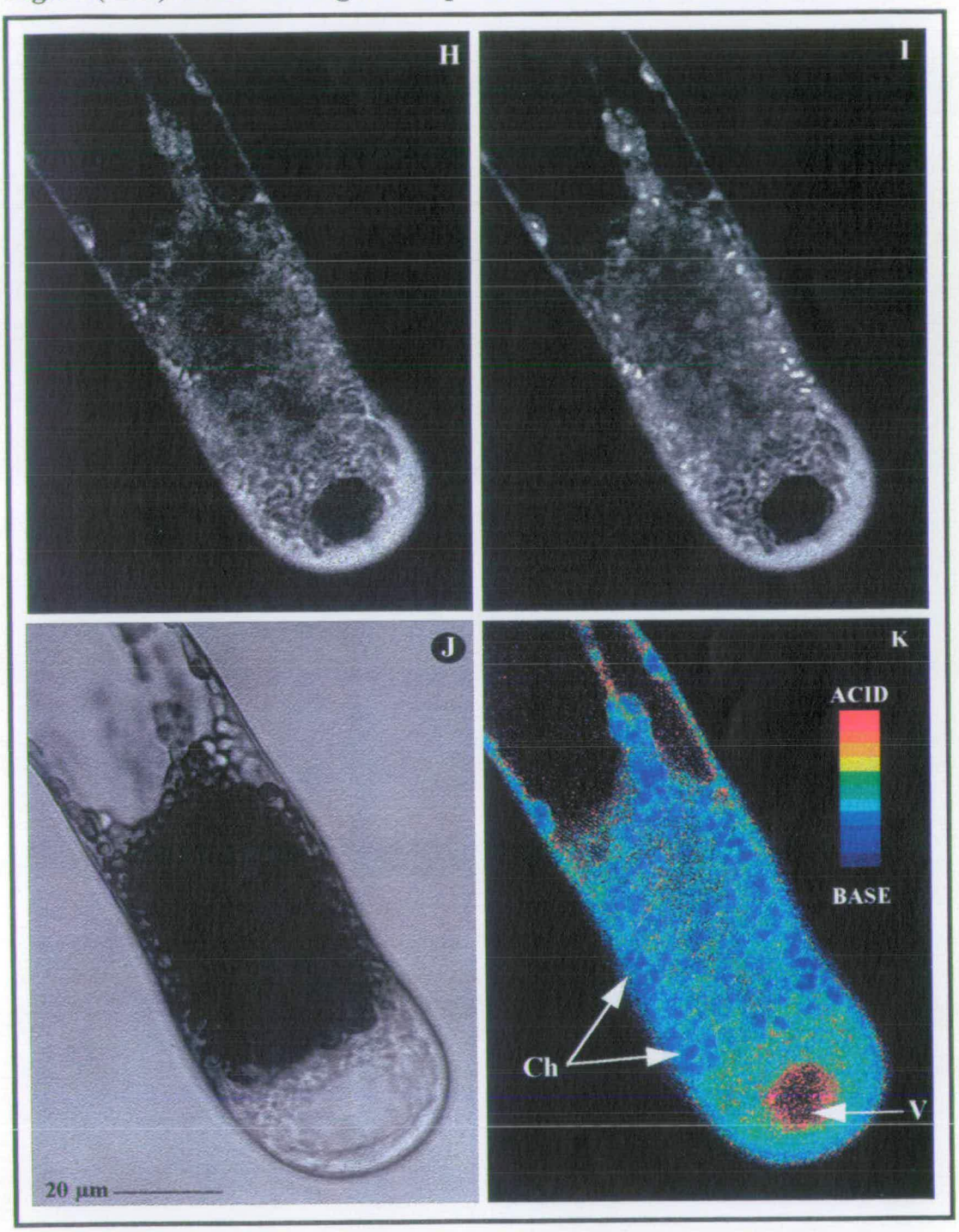

Fig. 37: cSNARF-1 imaging and chloroplast autofluorescence. (A) Bright field, non-confocal, transmitted light images showing the distribution of chloroplasts and apical cytoplasm in the apical cell of a red light-grown fern protonema. (B and Bi) Dual channel fluorescence images of the cell shown in (A), taken during ester-loading with cSNARF-1 AM (at 5μM). (B) Ch-1 images (640 nm fluorescence emission) and (Bi) Ch-2 images (580 nm fluorescence emission); time after the start of ester-loading is indicated. The first images in the sequence, at zero time, are the result of chloroplast autofluorescence. In subsequent images the accumulation of dye in the apical cytoplasm can be seen. Loading was halted after 20 min.; the cell remained viable and was able to undergo phototropic reorientation in response to laterally applied red light (C and D). In the fluorescence image (C), taken 18 h after loading, the dye can be seen to have accumulated in the central vacuole. Bar = 20 μm throughout.

Fig. 37: cSNARF-1 imaging and chloroplast autofluorescence

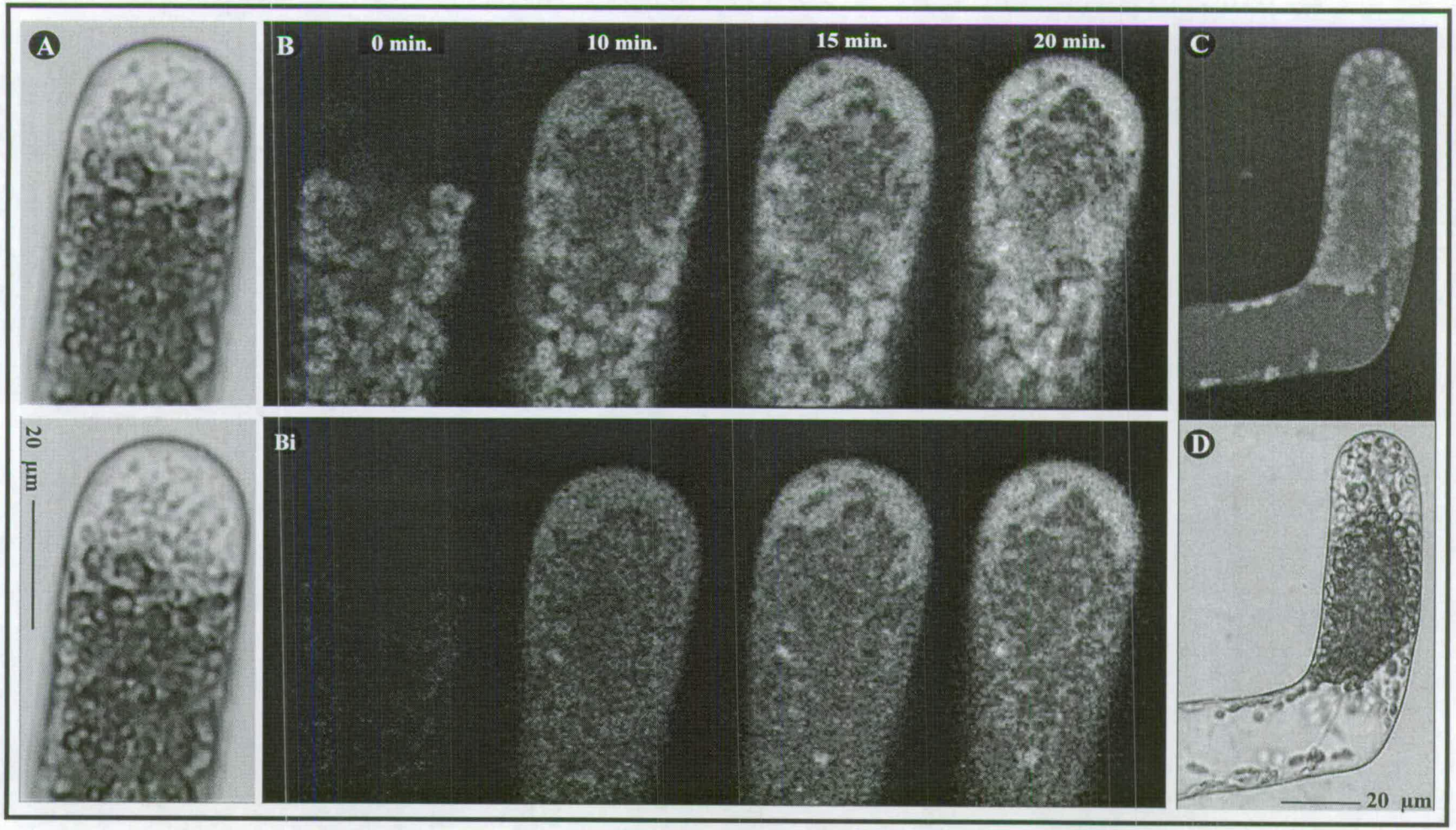

Fig. 38: Ester-loading of rhizoids with cSNARF-1 AM. (A-I) Distribution of cSNARF-1 fluorescence in the apex of a rhizoid of *D. affinis* examined, 15 min. after ester-loading (at 5 μM), by confocal microscopy. Single confocal optical sections (excitation 514 nm; emission >550 nm) were collected at 1.5 μm steps using a x60 dry (NA 0.95) plan apo objective. Dark regions within cells appear to correspond to the putative vacuolar system (described in Chapter 3; Section 3.7). (Ci, Fi and Ii) Non-confocal transmitted light images, corresponding to images C, F and I. Bar = 10 μm.

Fig. 38: Ester-loading of rhizoids with cSNARF-1 AM

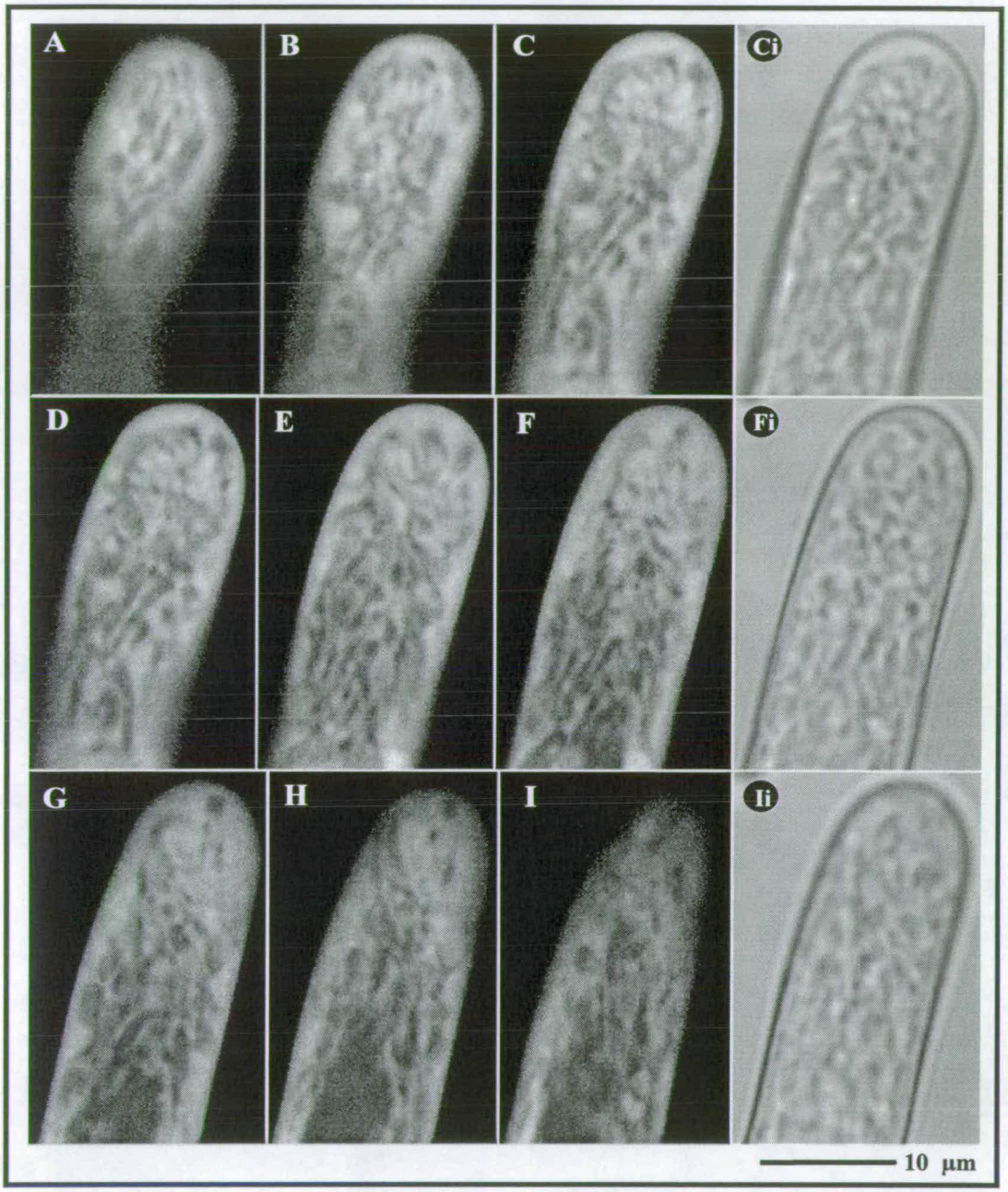

Fig. 39: Subcellular localisation of cSNARF-1 in rhizoids after AM ester-loading. (A-G) Examined by confocal microscopy using a x40 dry (NA 0.95) plan apo objective. (A) Dye distribution during loading with cSNARF-1 AM. The nucleus and cytoplasm rapidly accumulated dye whilst the vacuolar system remains unloaded. (B-E) Redistribution of cSNARF-1 with increasing time after 15 min. loading. (B) Examination immediately after loading; (C-E) 20, 30 and 40 min. after loading, respectively. Dye fluorescence, initially accumulated in the cytoplasm, was gradually "lost" while vacuolar fluorescence increased. Note the continued growth over the examination period. (F) Binding of cSNARF-1 free-acid to the cell wall after extended periods of ester-loading. (G) apparent precipitation of cSNARF-1 within putative subapical vacuoles 16 h after initial AM ester-loading. This cell had elongated by over 150 μm since being loaded. (H-J) cSNARF-1 fluorescence in an AM ester-loaded individual examined by confocal microscopy using a x60 oil (NA 1.4) plan apo objective. Images were taken: immediately after 10 min. loading and 15 min. later (H); 60 min. later (I); and finally 3 hours later (J). Small bright areas can be seen throughout the cytoplasm in (H) which may be mitochondria. Reduced cytoplasmic signal and increased signal within the putative vacuolar system can clearly be seen in (I). In (J) fluorescence in the putative vacuolar system can be seen to have exceeded that of the cytoplasm, which suggests active uptake. The putative tubular apical vacuolar network can clearly be seen converging towards the main subapical vacuole. Scale bar in (E) corresponds to (A-E); scale bar in (F) corresponds to (F and G); and scale bar in (H) corresponds to (H-J). Bars = 10 μm throughout

Fig. 39: Subcellular localisation of cSNARF-1 in rhizoids after AM ester-loading

Fig. 40: Rhizoid viability after cSNARF-1 AM ester-loading and confocal imaging

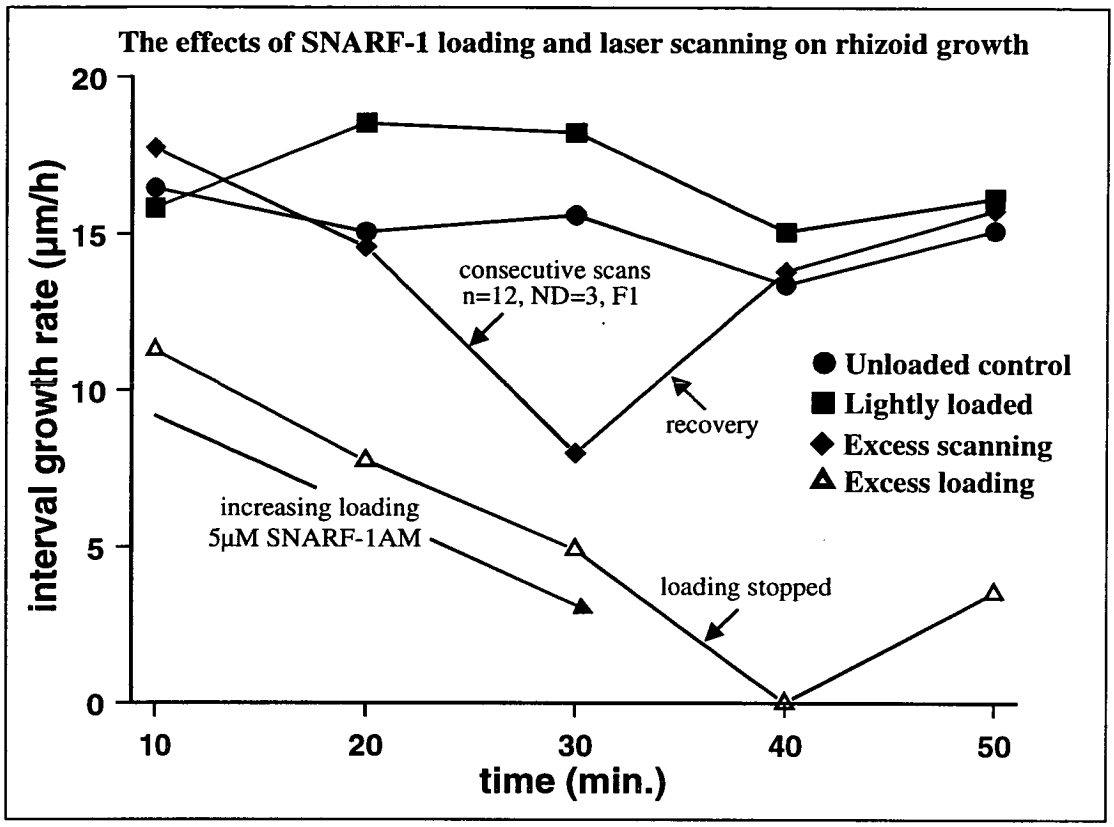

The graph shows the growth rate of individual rhizoids calculated from sequential fluorescence or bright-field images at 5 - 10 min. intervals. All imaging was performed using a x40 dry (NA 0.95) objective at zoom 4.0. The detrimental effects of "overloading" with dye and "over scanning" with the excitation laser beam are illustrated. (Δ) "Overloading" to ~ 5 times the fluorescence of standard loading. (◆) "Over scanning" with 12 consecutive scans. (■) Standard, light loading (average pixel intensity ~ 100) and imaging conditions (see Table 3). (●) Unloaded control (imaged: ND = 3; 3 sec./scan; Kalman n = 2).

Fig. 41: Confocal optical sectioning. (A) Compares the regions of a cell examined by using confocal and non-confocal microscopy. The circle represents a cross-sectional view through a cell (for example a fern rhizoid). With confocal microscopy a thin optical section, which can be less than a μm thick, is viewed. The even sampling with confocal sectioning (shown by the arrows) becomes particularly important with quantitative fluorescence measurements. (B) The different orientations in which optical sections may be collected are shown. The X-Y and X-Z planes are longitudinal and transverse sections respectively.

Fig. 41: Confocal optical sectioning

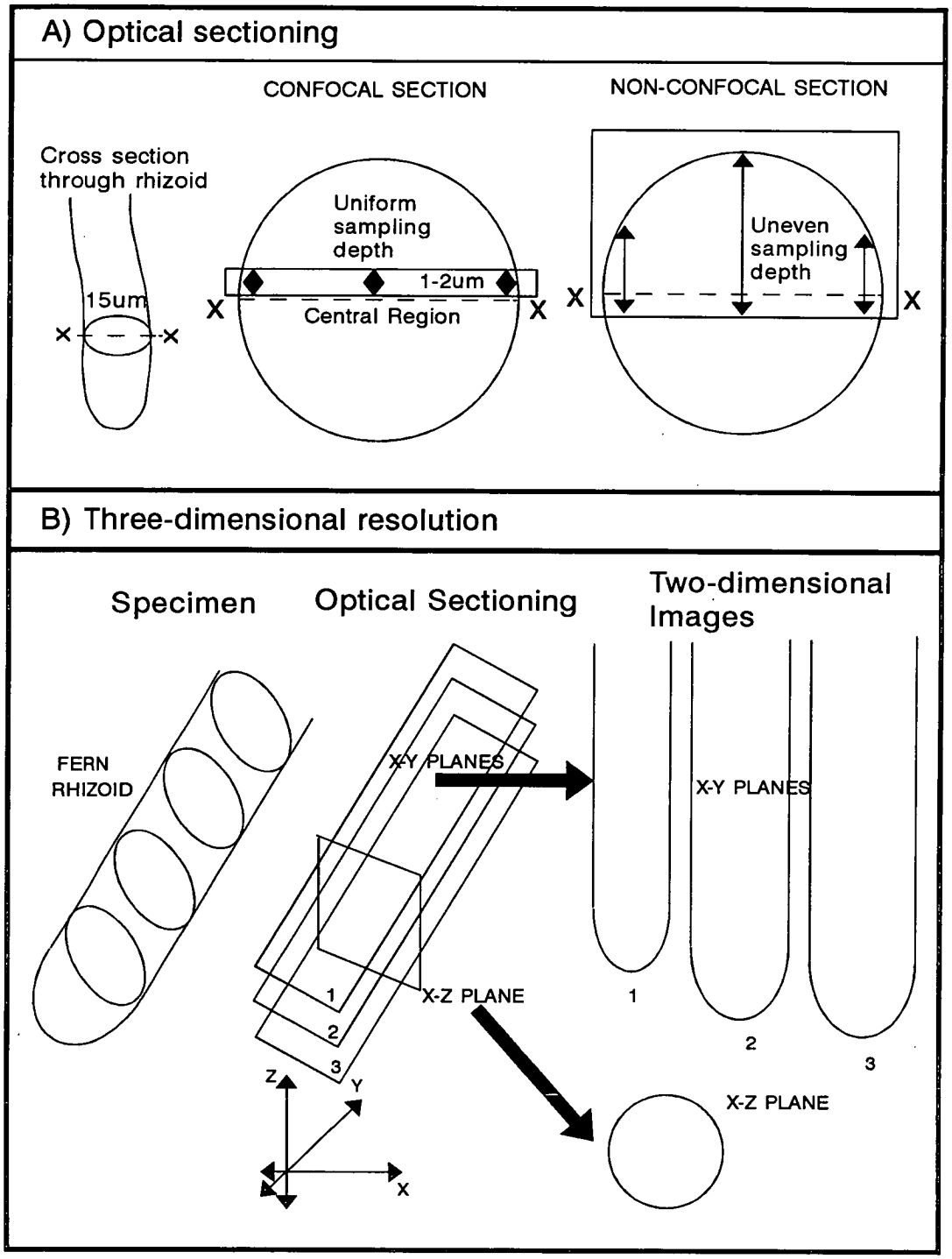

Chapter 5

Fig. 42: pH response curve of cSNARF-1 free-acid *in vitro*

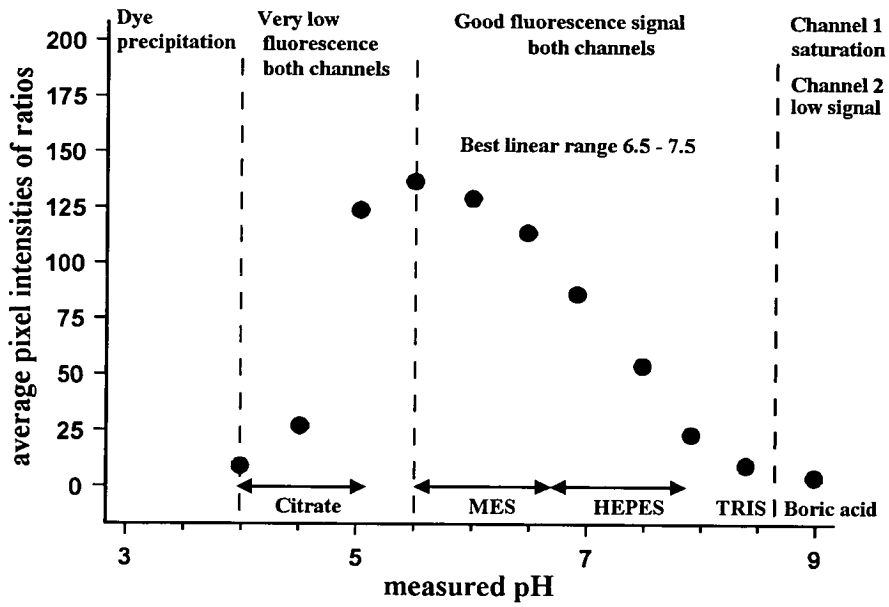

Mixtures of cSNARF-1 free-acid (400 μM) and the appropriate buffer were examined on the CLSM as described in Chapter 2. Several buffers were used to cover the pH range from 4 to 9: citrate buffer, 4.0 and 5.0; MES buffer, 5.5 - 6.5; HEPES buffer, 7.0 - 8.0; TRIS buffer, 8.5; boric acid, 9.0. Data from a single, typical experiment is shown. The ratio pixel intensity range 0 - 255 corresponds to actual ratio values of 0 - 4 (see Fig. 17; Chapter 2).

Fig. 43: Calibration curves for the pH response of cSNARF-1 free-acid *in vitro*

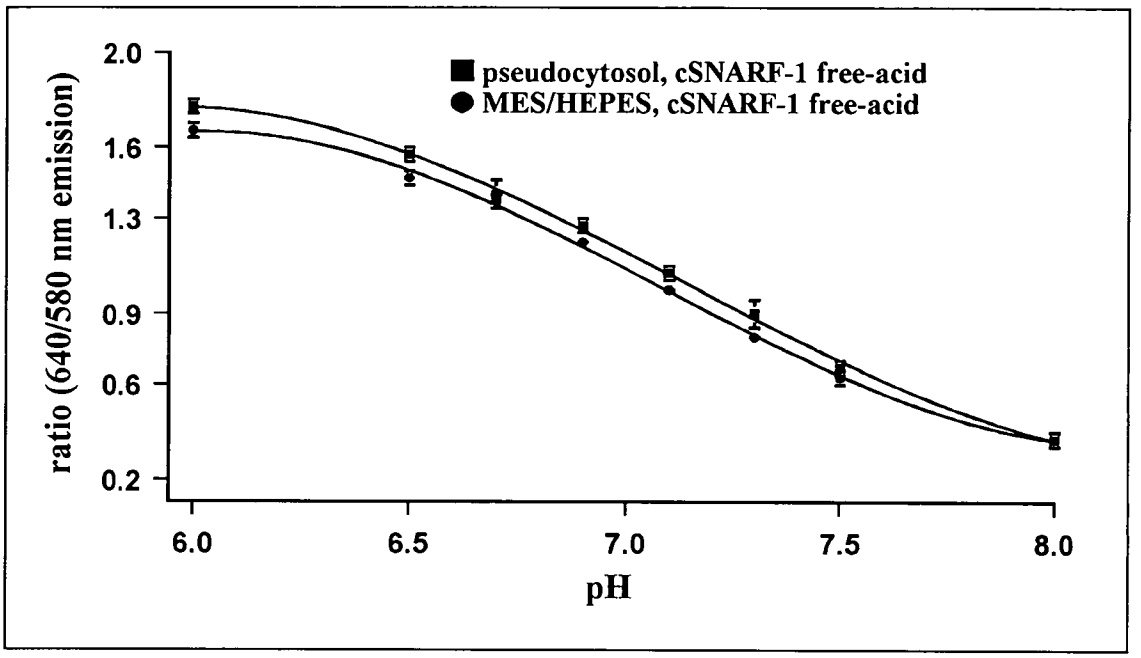

Mixtures of cSNARF-1 free-acid and either "simple buffered medium" (25 mM MES/HEPES) or "pseudocytosol" (see Section 5.3 of the main text) were examined on the CLSM as described in Chapter 2. Dye concentration was adjusted to maintain a reasonably standard fluorescence signal. Dye in "pseudocytosol" gave approximately three times the fluorescence signal of dye in "simple buffer". Error bars are s.e.m calculated from the mean fluorescence intensity of 4 repeat experiments. As the mean ratio value was determined from all pixels in the image variation between pixels within individual images was ignored.

*** Data was collected in collaboration with Dr. Till Jelitto.**

Fig. 44: Effects of environmetal conditions on the pH response of cSNARF-1 free-acid tested *in vitro*

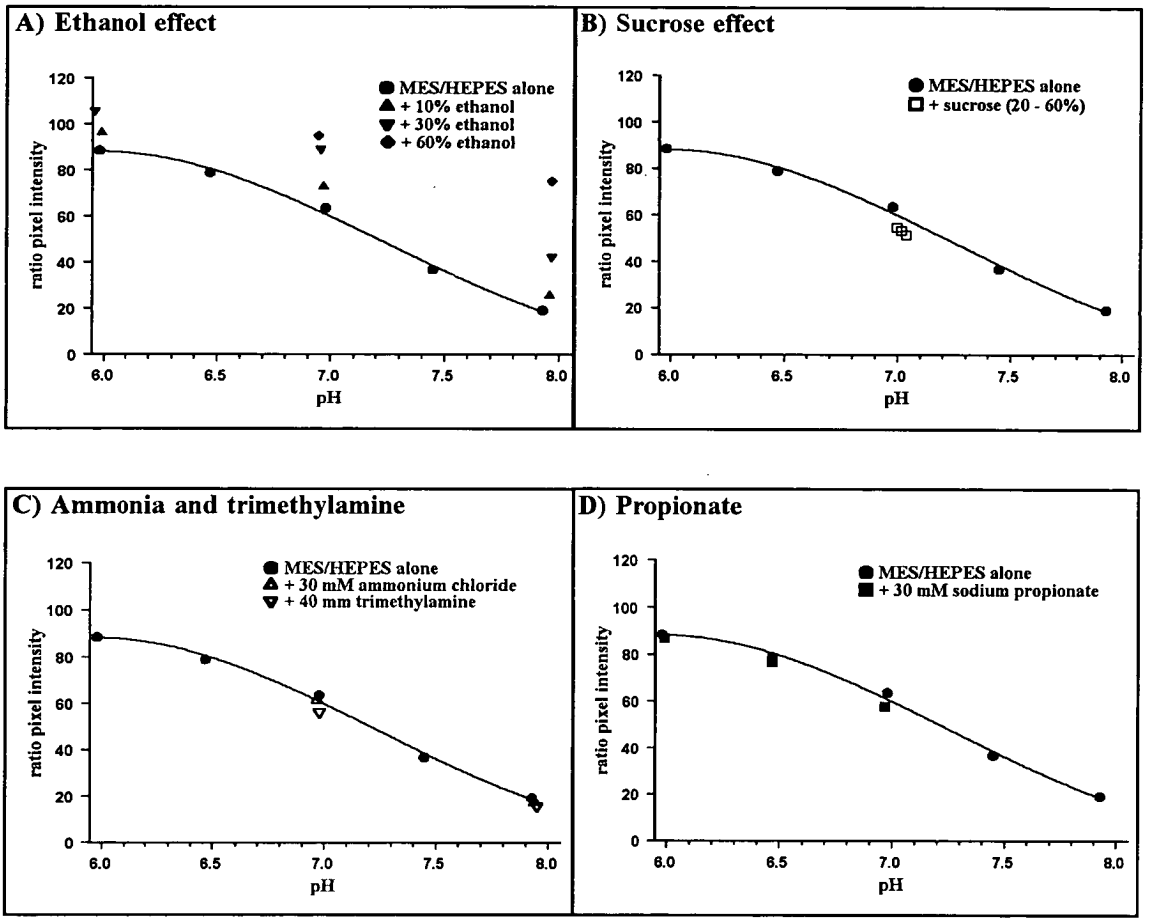

(A-D) Calibration curves were derived as described in Chapter 2; Section 2.8. The ratio pixel intensity range 0 - 255 corresponds to ratio values of 0 - 4. Simple MES/HEPES buffer was used as the standard for comparison throughout. The effects of different compounds on cSNARF-1 free-acid were assessed at known pH in simple buffer + the test compound. (A) Ethanol. (B) Sucrose. (C) Ammonia and trimethylamine. (D) Propionate. Imaging conditions were adjusted to maintain standard fluorescence intensity. Dye concentration was kept constant.

Fig. 45: Calibration of the pH response of cSNARF-1 free-acid *in situ*. The intracellular pH of cSNARF-1 AM ester-loaded rhizoids was adjusted by externally applying cell permeant weak acid and bases as buffer solutions over the pH range 6.0 - 8.0 (see Chapter 2; Section 2.8.2). (A) An example of a single calibration set. Loaded cells were ratio imaged using the CLSM and the relationship between ratio image pixel value (after 3x3 median filter) and expected internal pH was plotted. The ratio pixel intensity range 0 - 255 corresponds to ratio values of 0 - 2.5. The *in situ* calibration (■) is compared with simple MES/HEPES (●) and "clamping" buffer (O) *in vitro* calibrations over the same range. Error bars are twice the standard error in the sample mean ratio pixel value (estimated on the basis of variation in the mean pixel intensity of ten replicate 10 x 10 pixel sample areas); this is explained in Section 5.6.3 of the main text. (B-D) Images of cells treated with "clamping" buffers at pH 7.0 (propionate) pH 6.5 (propionate) and pH 7.5 (trimethylamine), respectively. Cells were imaged with a x60 NA 1.4 oil immersion objective. Bar = 10 μm.

Fig. 45: calibration of the pH response of cSNARF-1 free-acid *in situ*

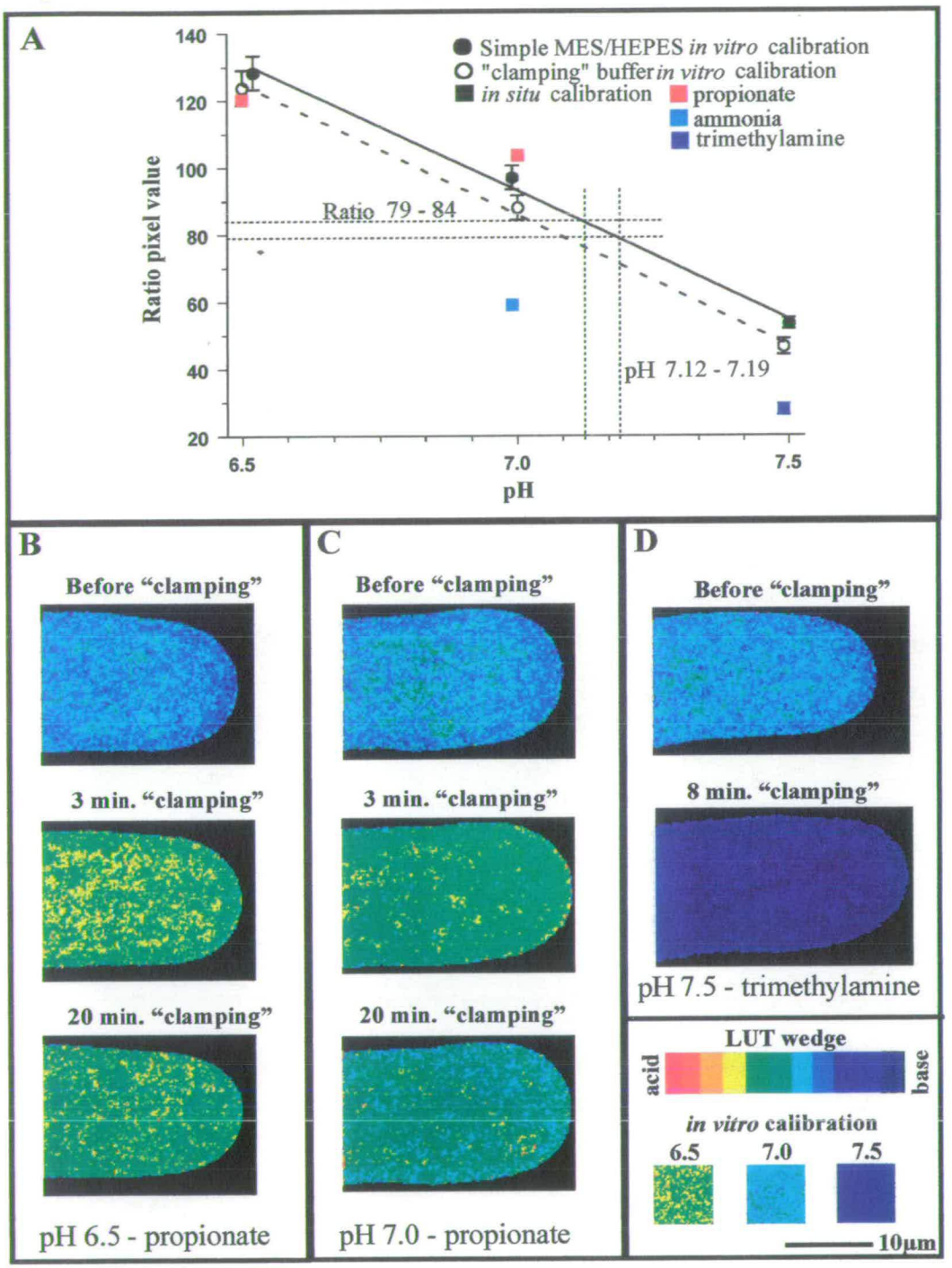

Fig. 46: Random "noise" levels in confocal fluorescence and ratio images. (A) Fluorescence image pixel intensity distributions for a typical *in vitro* cSNARF-1 free-acid calibration image at pH 7.0. 384 x 256 pixel areas were sampled in each case. In (A) the black and grey curves are frequency distributions for the pixel intensities in the channel 1 and channel 2 components of a single dual channel fluorescence image, respectively. The left hand graph relates to a direct, single scan image, while the right hand graph relates to a Kalman filtered (cumulative average n = 4) image of the same sample. (B) Ratio image pixel intensity distribution for ratio images calculated (as described in Fig. 16) from the single scan images examined in (A). 384 x 256 pixel areas were sampled in each case. The black and grey curves correspond to unfiltered and median 3x3 filtered (applied after ratioing) images, respectively. (C) Ratio image pixel intensity distribution for ratio images calculated from the Kalman filtered images examined in (A). 384 x 256 pixel areas were sampled in each case. The black and grey curves correspond to unfiltered and median 3x3 filtered images, respectively.

Fig. 46: Random "noise" levels in confocal fluorescence and ratio images

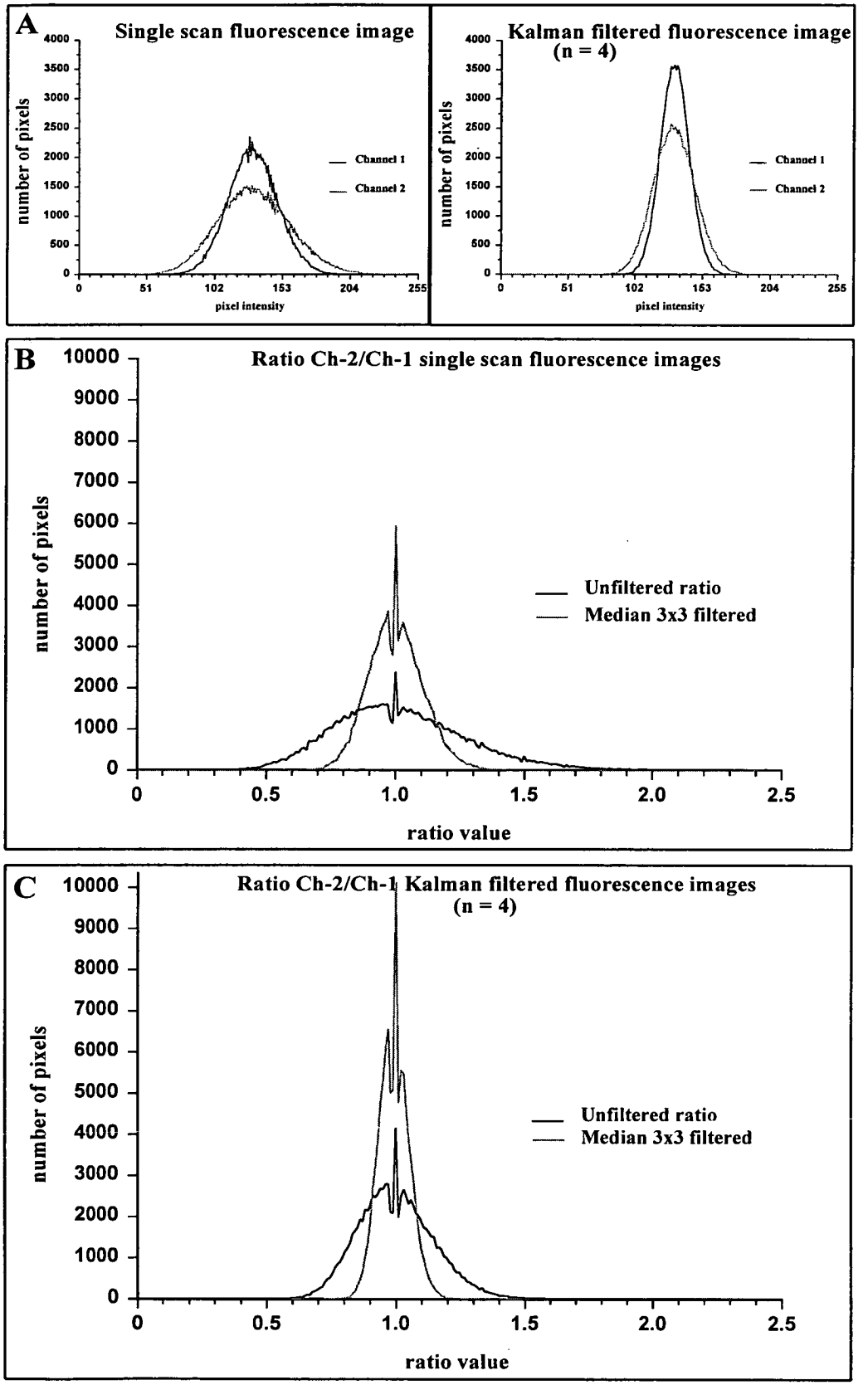

Fig. 47: The influence of fluorescence image pixel intensity on observed ratio value

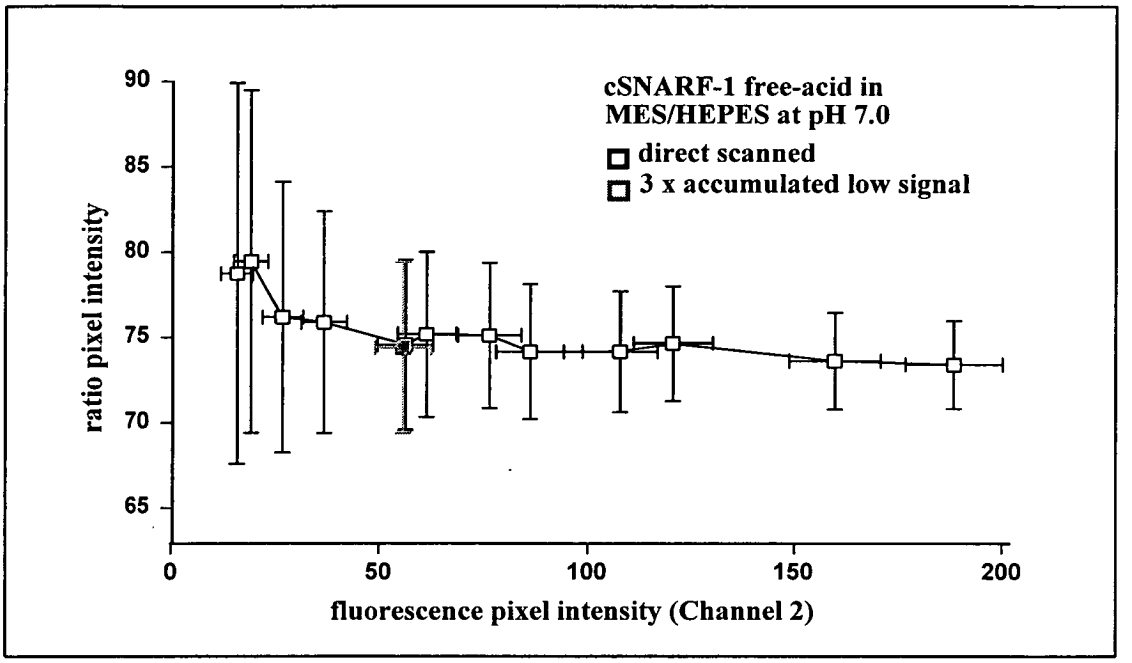

cSNARF-1 free-acid in simple MES/HEPES buffer was ratio imaged on the CLSM. Different dy concentrations and settings of ND filter and image accumulation were used to produce a series of images o different average fluorescence image intensity. Average fluorescence image intensity for the channel wit weaker fluorescence (Channel 2; 580 nm) was plotted against average ratio image pixel value. The rati pixel intensity range 0 - 255 corresponds to ratio values of 0 - 3.5. Average ratio pixel values wer determined with a 256 x 256 sample box. Error bars represent the s.d. about the mean pixel intensity for single sample area. (In the case of ratio images the s.d. is only an approximation due to the skewedness in the distribution of ratio pixel values). Ratio images were unthresholded and no median filter was applie after ratioing. The experiment was performed at pH 6.0, 7.0 and 8.0; only the results for pH 7.0 are shown.

Fig. 48: Estimation of the spatial resolution and precision of pH measurement for cSNARF-1 ratio images. cSNARF-1 free-acid in simple buffer (over the range pH 6.9 - 7.3) was confocal ratio imaged and images were processed as described in Chapter 2. The pixel intensity range 0 - 255 corresponds to ratio values of 0 - 2. The average ratio image pixel value for the image at each pH value (0.02 pH unit steps) was then determined using sample areas of varying sizes: (A) 256 x 256 pixels; (B) 14 x 14 pixels; (C) 7 x 7 pixels; (D) 3 x 3 pixels. (A) The average value for the largest sample size was assumed to be the "true" population mean. Error bars are 47.5% of the frequency distribution of ratio pixel values on either side of the mean - note that these error bars are not equal about the mean because of the skewed distribution of ratio pixel values. (B-D) For each of the small sample areas 10 repeat samples were taken per image. The mean of the results for the 10 repeat samples was plotted against pH. Error bars are 2 s.e.m for variation in the average pixel intensity of sample areas where the s.e.m is an approximated value as discussed in Chapter 5; Section 5.6.3. Each sample area size represents a different degree of spatial resolution. The 2 s.e.m. values represent an estimate of the precision to which pH can be determined with the degree of spatial resolution imposed by the sample area size.

*** Data was collected in collaboration with Sabine Fischer.**

Fig. 48: Estimation of the spatial resolution and precision of pH measurement for cSNARF-1 ratio images

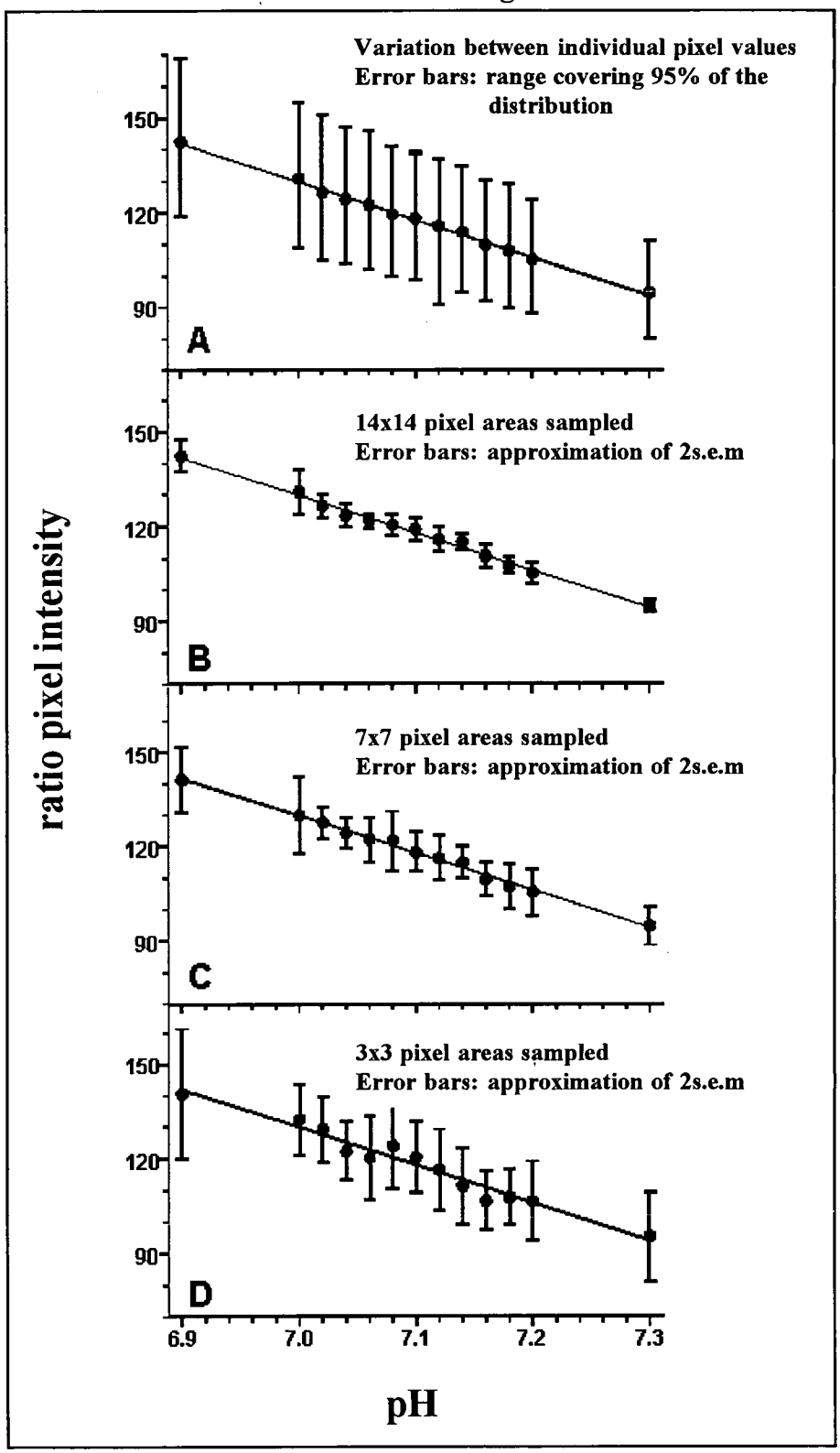

Fig. 49: Dissection of physiological cSNARF-1 fluorescence confocal images and their corresponding ratios. (A and B) Confocal fluorescence images of cSNARF-1 from Channel 2 and Channel 1, respectively, showing the fluorescence intensity distribution. Pixel intensities are displayed in three colour bands (see LUT wedge in B): background signal - blue (pixels 0 - 10); low signal - red (pixels 11 -50); good signal - green (pixels 51 - 255). Areas of low signal correspond to the cell periphery and vacuolar regions. (C) Ratio of the fluorescence images (A and B). (D) Image (C) after 3 x 3 median filtering to reduce random variation between pixels. See Chapter 2: Fig. 17 for an explanation of the relationship between the pseudocolour scale and pH. Bar = 10 μm.

Fig. 49: Dissection of physiological cSNARF-1 fluorescence confocal images and their corresponding ratios

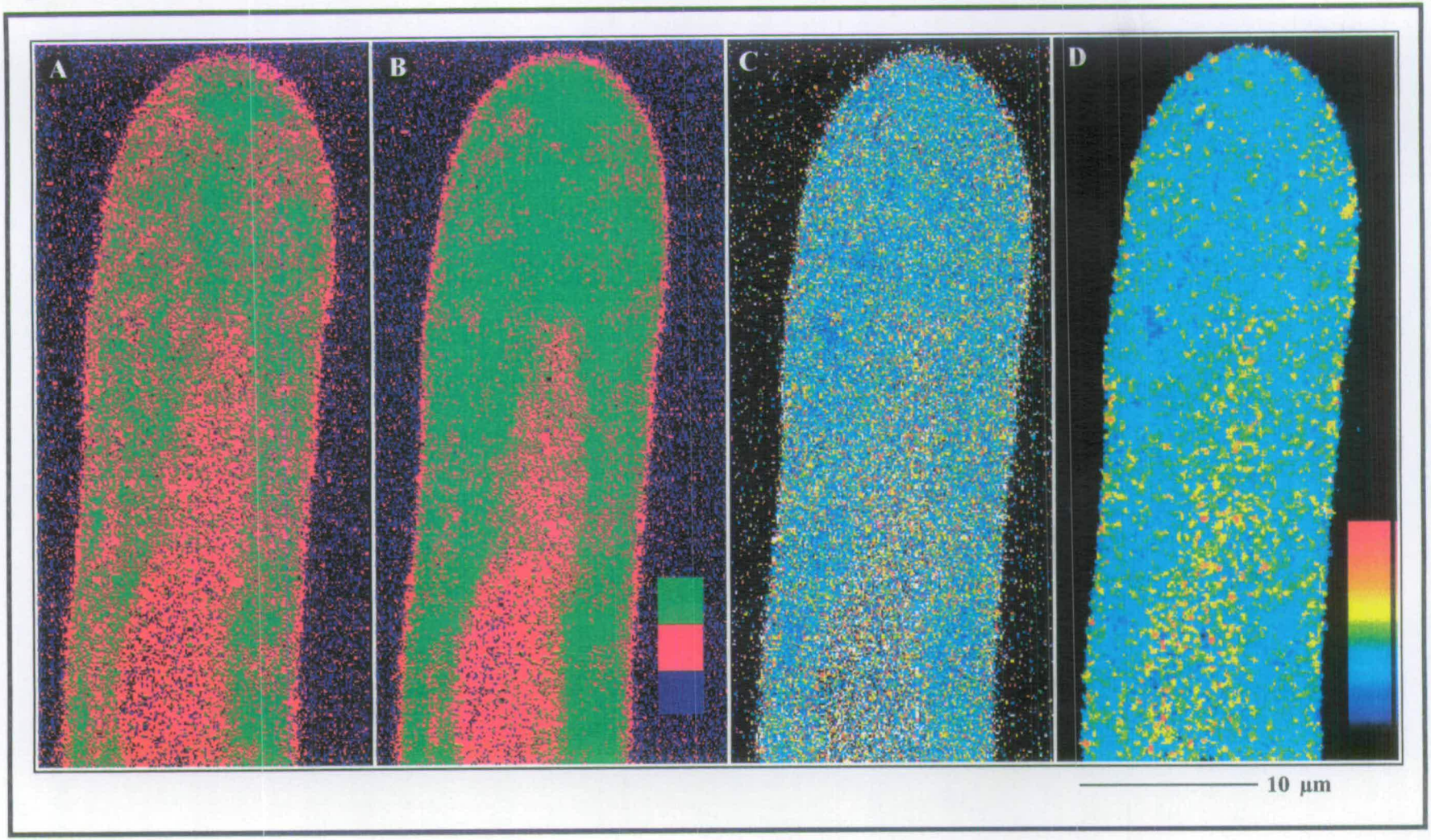

Fig. 50: Methods of extraction of numerical data from physiological images. (A) Representative diagram of a rhizoid showing the sampling zones defined (refer to Chapter 6). Zone 1 = the apical cytoplasmic "cap" confined to within 2 - 4 μm of the extreme apex; zone 2 = the subapical vacuolated region; zone 3 = peripheral cytoplasm surrounding the main vacuole, from ~ 15 μm to 50 μm behind the apex. (B) Positioning of boxed sample areas. (C-D) MPL "fat length" sampling along a median transect or round the cell periphery. (E) Image thresholding to allow an overall average to be taken in a single measurement. Filled areas represent the regions being sampled.

Fig. 50: Methods of extraction of numerical data from physiological images

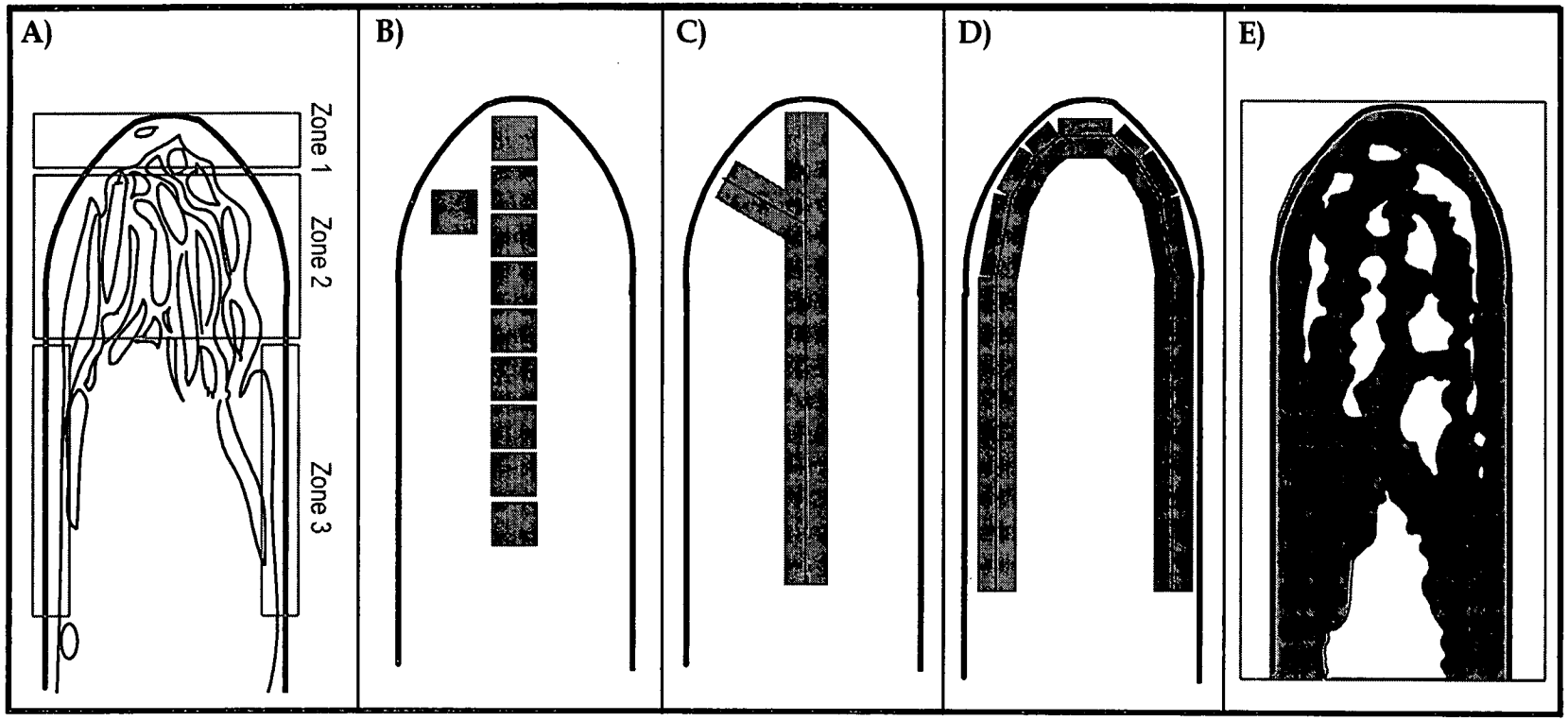

Fig. 51: Sampling cSNARF-1 confocal ratio images with a linear median transect. (A and B) Confocal cSNARF-1 ratio images of ester-loaded rhizoids immediately after and 30 min. after loading. Optical sections were taken at the central focus position within the cell. Ratioing was as described in Chapter 2 and both ratio images were median filtered. Graphs display the averaged ratio value sampled with the MPL "fat length" (averaging over 20 pixels). The sampled regions correspond to the lines shown on the ratio images. (A) Immediately after cSNARF-1 AM ester-loading the rhizoid exhibits a predominantly cytoplasmic dye distribution. Black regions correspond to areas where fluorescence was insufficient to give a reliable ratio (baseline values on the graph), this is clearly seen in the main central vacuole. Intracellular pH is relatively even throughout the apical region. pH in the cytoplasm of the extreme apex was 7.18. (B) The same rhizoid after significant vacuolar accumulation of dye. Apparent acidification of the subapical region is due to the increased contribution of vacuole sequestered dye to the ratio. This gives an artefactual tip to base gradient of decreasing pH. The acidic spike at the extreme apex (higher ratio value) is the result of cSNARF-1 free-acid binding to the cell wall. pH in the cytoplasm of the extreme apex was still 7.18, based on *in vitro* calibration. Scale is indicated by the graph axis. Images were taken with a x60 (NA 0.95) dry objective.

Fig. 51: Sampling cSNARF-1 confocal ratio images with a linear median transect

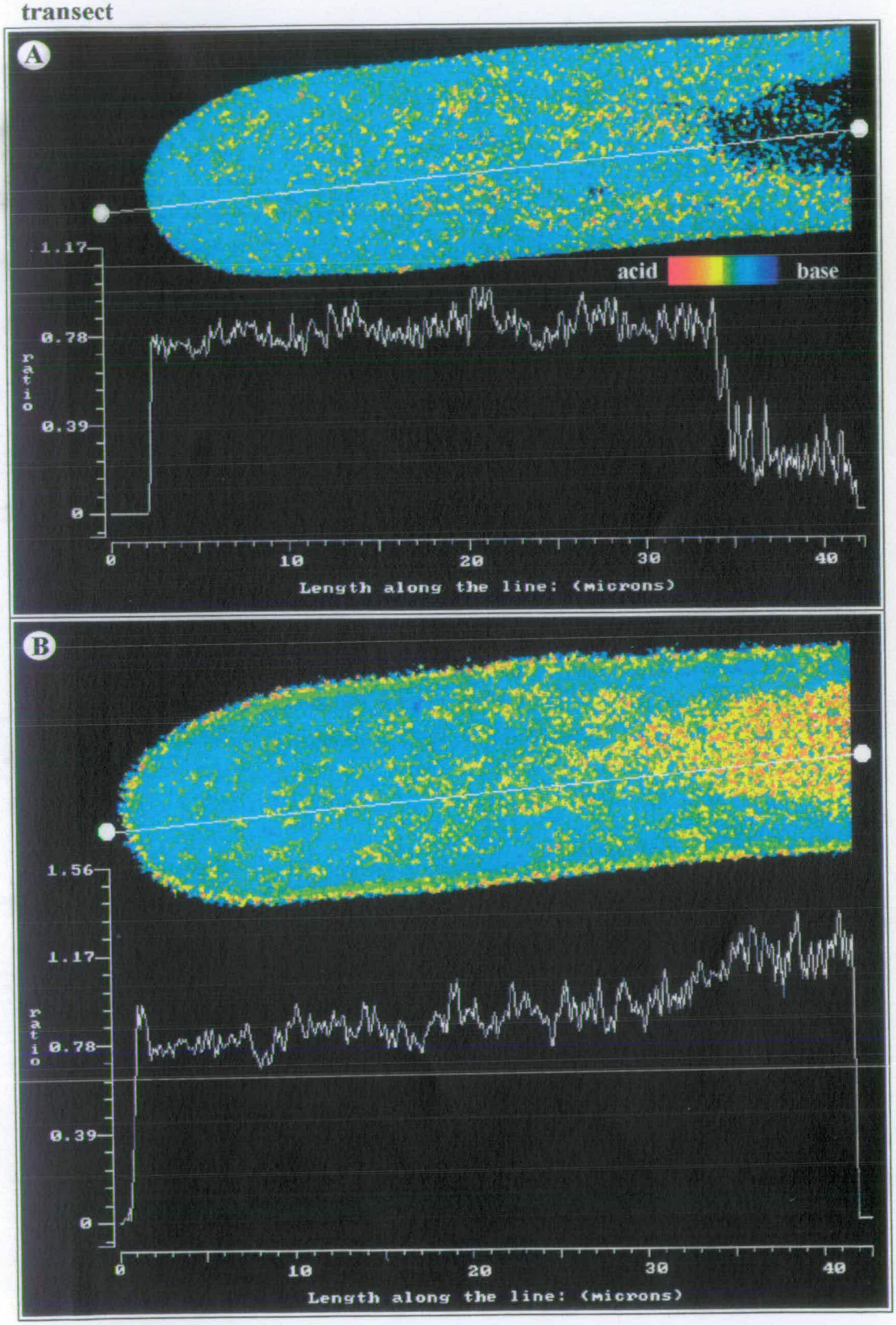

Fig. 52: Image thresholding to eliminate low signal and vacuolar signal contributions from ratio images. (A and B) Fluorescence images of a cSNARF-1 AM ester-loaded rhizoid (10 min. after loading) corresponding to channel 2 and channel 1 respectively. (C) Ratio image produced with thresholding at 6 (both channels). (D) Ratio image produced with thresholding at 135 (both channels). Bar = 10 μm.

Fig. 52: Image thresholding to eliminate low signal and vacuolar signal contributions from ratio images

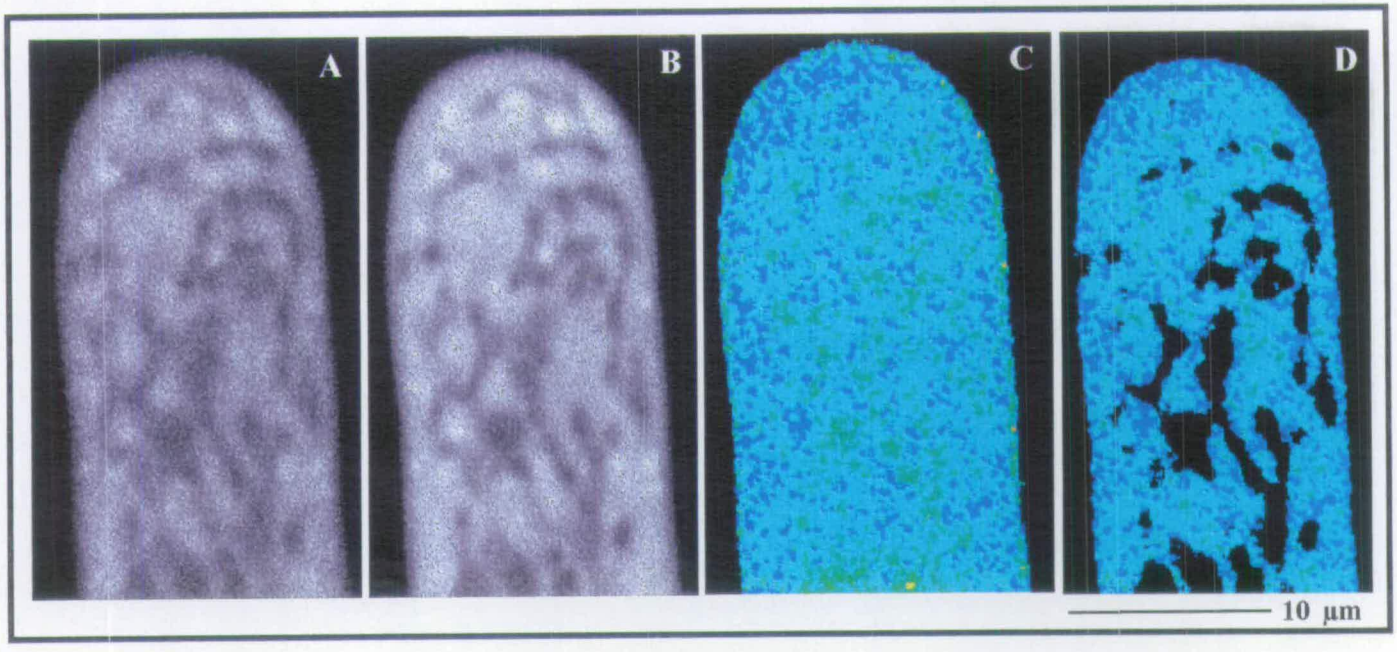

Fig. 53: Ratio image of a vegetative hypha of *Neurospora crassa* loaded with cSNARF-1 10 kDa dextran conjugate

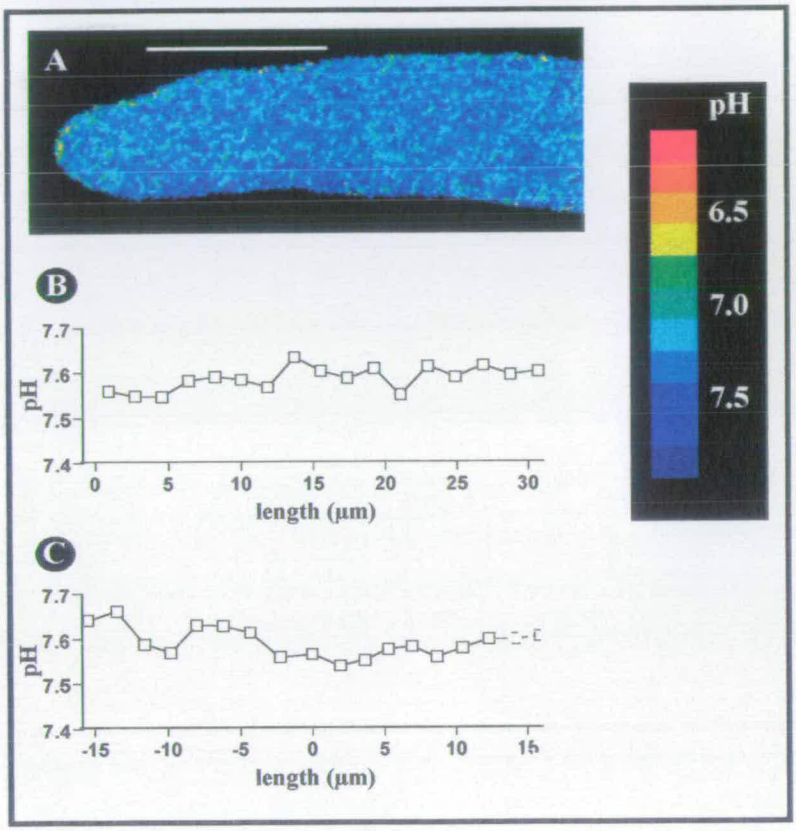

(A) *Neurospora* hypha loaded with cSNARF-1 10 Kda dextran conjugate by pressure microinjection and imaged under similar conditions as for *D. affinis* rhizoids (x40 NA 0.95 dry objective; zoom 4.0; direct scanning). (B and C) graphs of pH along a median transect (B) and round the periphery (C) of the image shown in (A) - see Fig. 50 C and D. Bar = 10 μm. (Figure reproduced courtesy of S. Fischer).

Fig. 54: cSNARF-1 dual emission ratio image misalignment artefact. (A and B) Misalignment can be seen as the red and blue edges on either side of the image. (B) The extent of misalignment is shown more clearly by increasing the magnification of the region indicated in (A). (C and D) The misalignment could be eliminated by shifting the Ch-2 image by one pixel to the left before ratioing. See Fig. 55 for the pseudocolour LUT. Bar: 10 μm for (A and C) and 2.5 μm for (B and D).

Fig. 55: Confocal and non-confocal imaging of cSNARF-1 in a rhizoid of *D. affinis*. (A and B) Confocal cSNARF-1 ratio images taken (A) immediately after AM ester-loading and (B) 40 min. later after vacuolar uptake of dye. (C-D) Non-confocal images corresponding to (A-B). Confocality was reduced by fully opening the confocal aperture. The effects of non-confocality can be clearly seen at the edges of the image and with increased vacuolar sequestration of dye - vacuolar signal contributes more significantly to the "averaged" non-confocal ratio image. The pseudocolour scale was uncalibrated. Bar = 10 μm.

Fig. 54: cSNARF-1 dual emission ratio image misalignment artefact

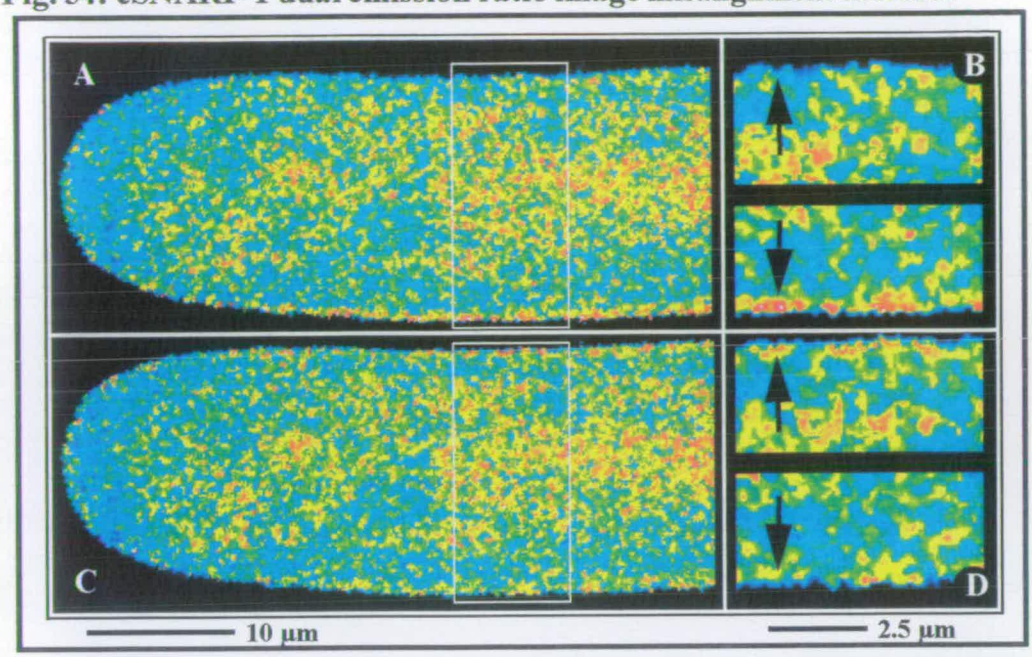

Fig. 55: Confocal and non-confocal imaging of cSNARF-1 in a rhizoid of *D. affinis*

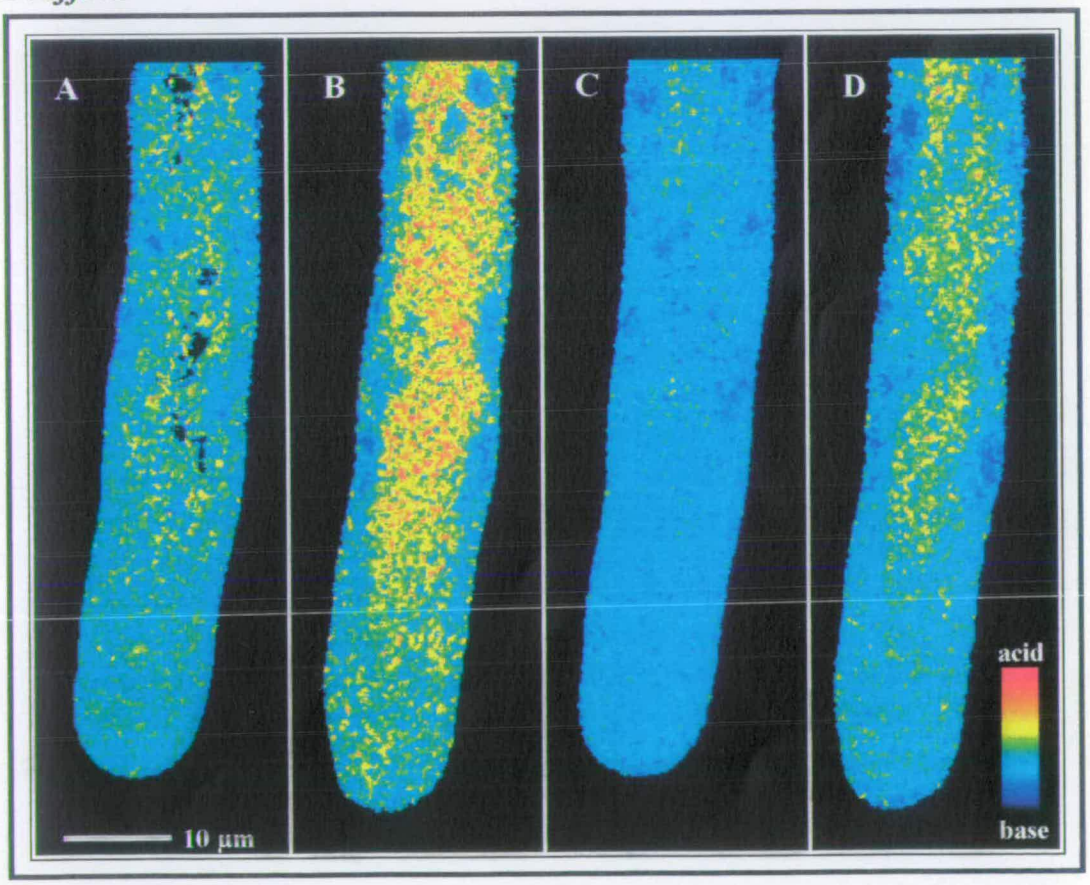

Fig. 56: cSNARF-1 confocal ratio imaging at different depths within a rhizoid

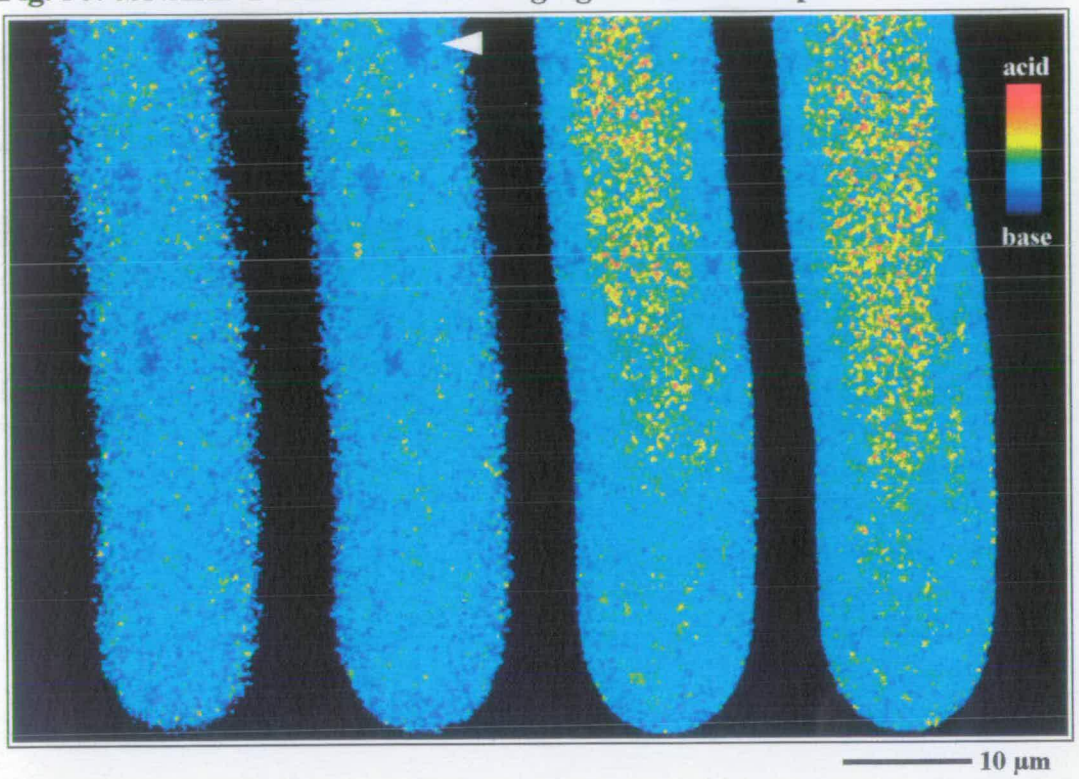

cSNARF-1 ratio images produced from fluorescence confocal optical sections collected at 2.0 µm focus position increments from the lower side to the centre of a rhizoid (ratio images from left to right). Optical section thickness was approximately 2 µm. Note the increasing contribution of the acidic central vacuole to ratio images at increasing depth. Plastids appear as dark blue regions (arrow) Bar = 10 µm.

Chapter 6

Fig. 57: Typical cSNARF-1 confocal ratio images of growing *D. affinis* rhizoids. (A) Typical ratio image of a rhizoid produced from dual channel fluorescence confocal images taken with a x60 (NA 0.95) dry plan apo objective immediately after AM ester-loading. (B) A similar image for a x60 (NA 1.4) oil immersion plan apo objective, Kalman averaged over three scans. In all images the cytoplasmic pH was estimated at between pH 7.1 and 7.3 by simple *in vitro* calibration and did not differ significantly between the apex, subapical and peripheral regions. Images (Ai) and (Bi) were taken soon after loading so dye was predominantly cytoplasmic. (Ai-iii and Bi-iii) Ratio images show increasing contribution of an acidic compartment with increasing times after ester loading as dye accumulated in the putative apical vacuolar system (Ai-Aiii taken over 30 min., Bii taken 1 h and Biii 3 h after loading). The pH of this putative vacuolar compartment was estimated at around pH 6 - 6.5 on the basis of the simple *in vitro* calibration. Bars = 10 μm.

Fig. 57: Typical cSNARF-1 confocal ratio images of growing D. affinis rhizoids

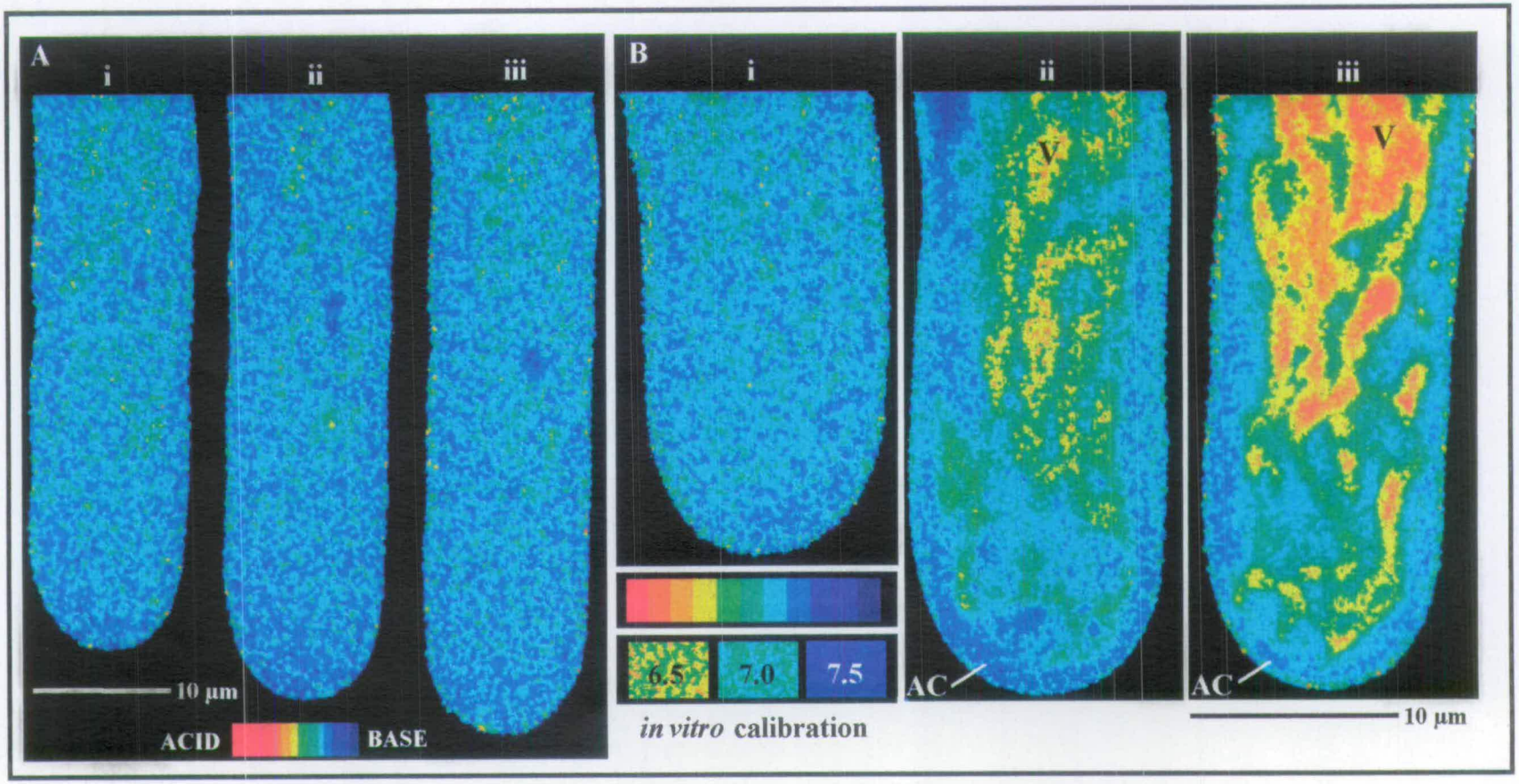

Fig. 58: Cytoplasmic pH in fern gametophyte rhizoids. (A and B) Numerical analysis of typical ratio images of growing cells immediately after AM ester-loading with cSNARF-1 (x60 (NA 1.4) oil immersion plan apo objective; Kalman n = 3). (A) Three typical examples of cytoplasmic pH along the central region through the apical 20 μm of rhizoids. Each point represents the value for a 10 x 10 pixel area (0.83 μm^2). Regions of the putative vacuolar system were avoided by reference to the dye distribution in cSNARF-1 fluorescence images. (B) Cytoplasmic pH around the periphery of a rhizoid, plotted on the same basis as in (A). pH was estimated on the basis of the simple *in vitro* calibration. Bar = 10 μm.

Fig. 58: Cytoplasmic pH in fern gametophyte rhizoids

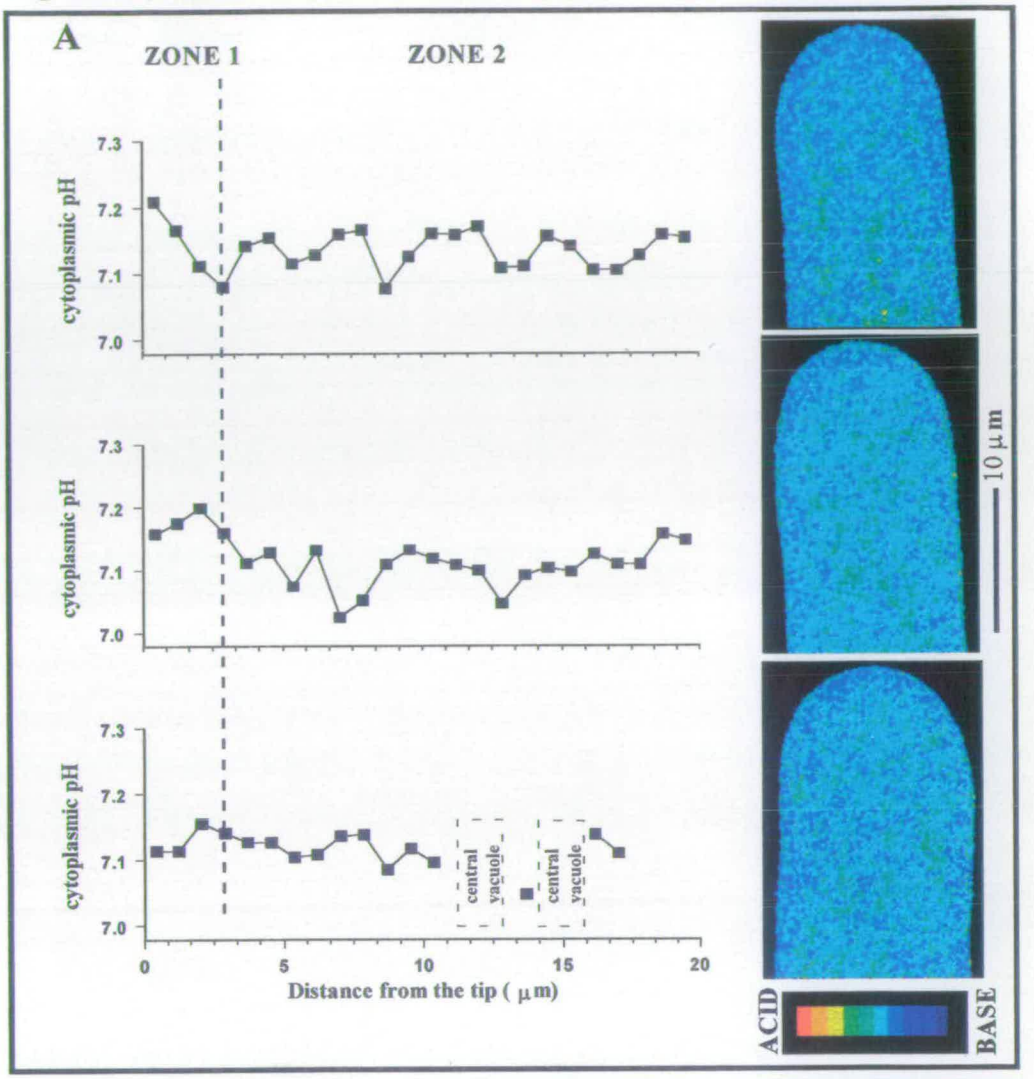

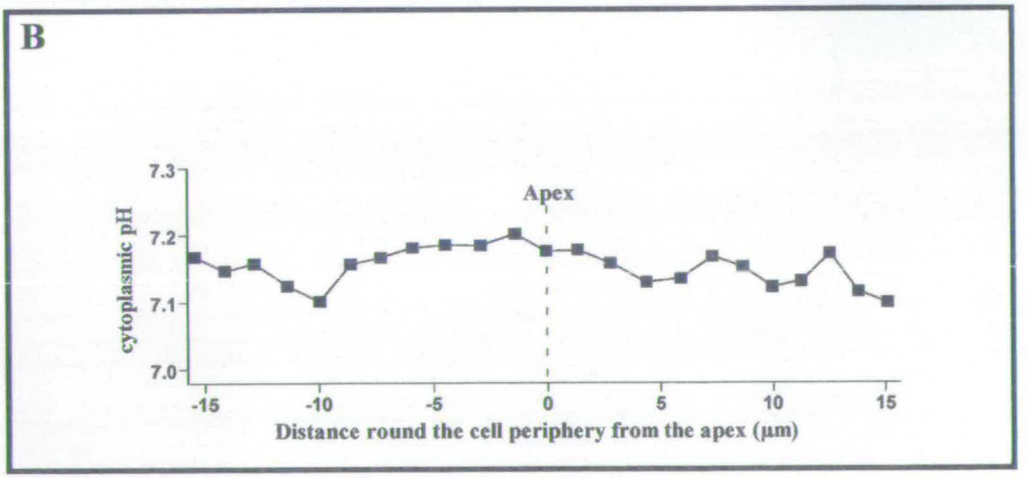

Fig. 59: Recovery of rhizoids after intracellular pH manipulation using cell permeant weak acids and bases

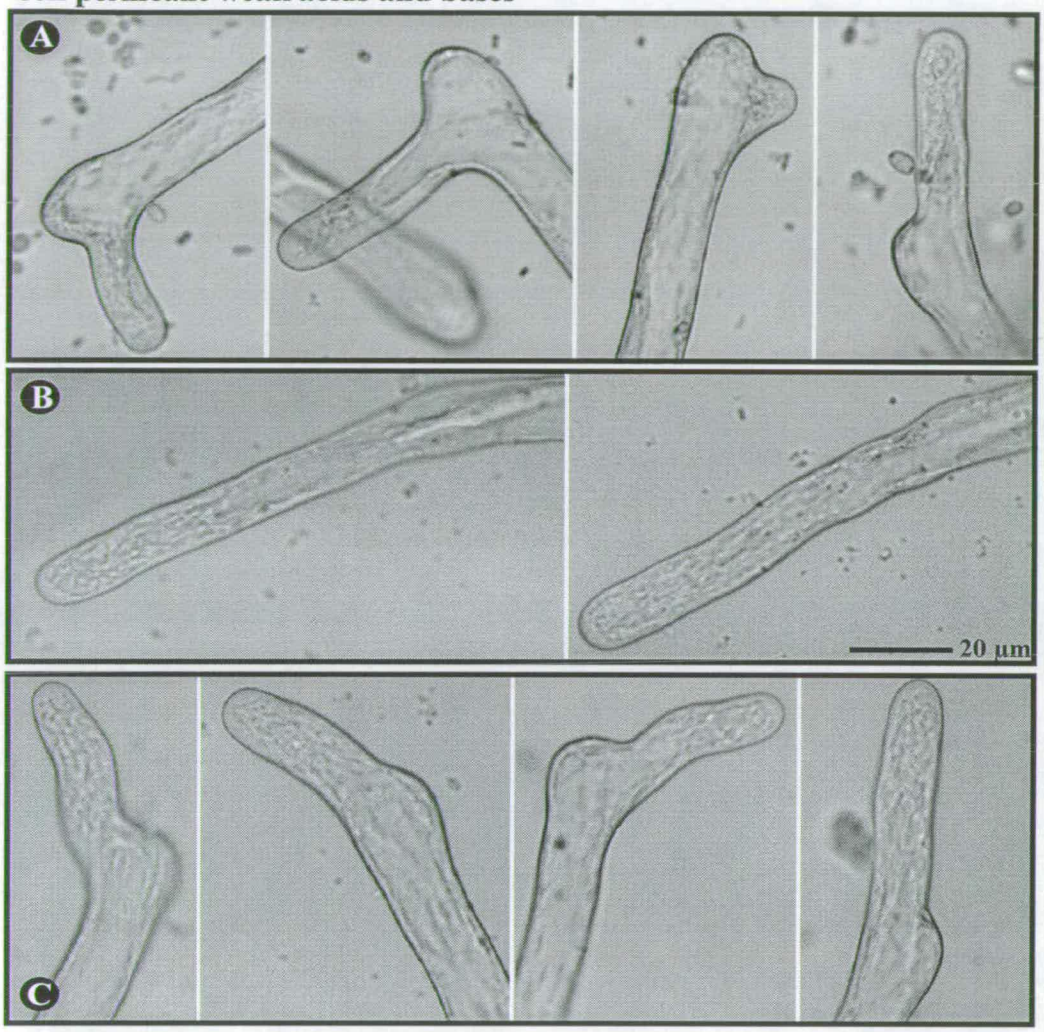

(A-C) Images of recovered rhizoids taken 24 h after exchange to normal medium (unbuffered pH 5.6) from 15 min. pH "clamping" treatments at pH 8.0 (ammonium chloride), 7.0 (ammonium chloride) and 6.0 (sodium propionate), respectively. Images were collected on the CLSM using the transmission detector. Bar = 20 µm.

Fig. 60: Effects of external buffering at pH 5.6 and 6.0 on *D. affinis* rhizoids. (A) Examination of a population of rhizoids exposed to 25 mM MES/HEPES buffer at pH 5.6 over 9 h. 100 protonemata were examined at each time point. (B) An example of an individual rhizoid transferred from normal medium to pH 6.0, 25 mM MES/HEPES buffer growing normally. (C) Transfer from normal medium (i and ii) to pH 6.0, 25 mM MES/HEPES buffer in the presence of high (45 mM) $[K^+]$. Images (i-v) collected at 40 min. intervals; (vi) was collected after a further 90 min. and (vii) after a further 6 h. Growth continued throughout. Bar = 15 μm.

Fig. 60: The effects of external buffering at pH 5.6 and 6.0 on *D. affinis* rhizoids

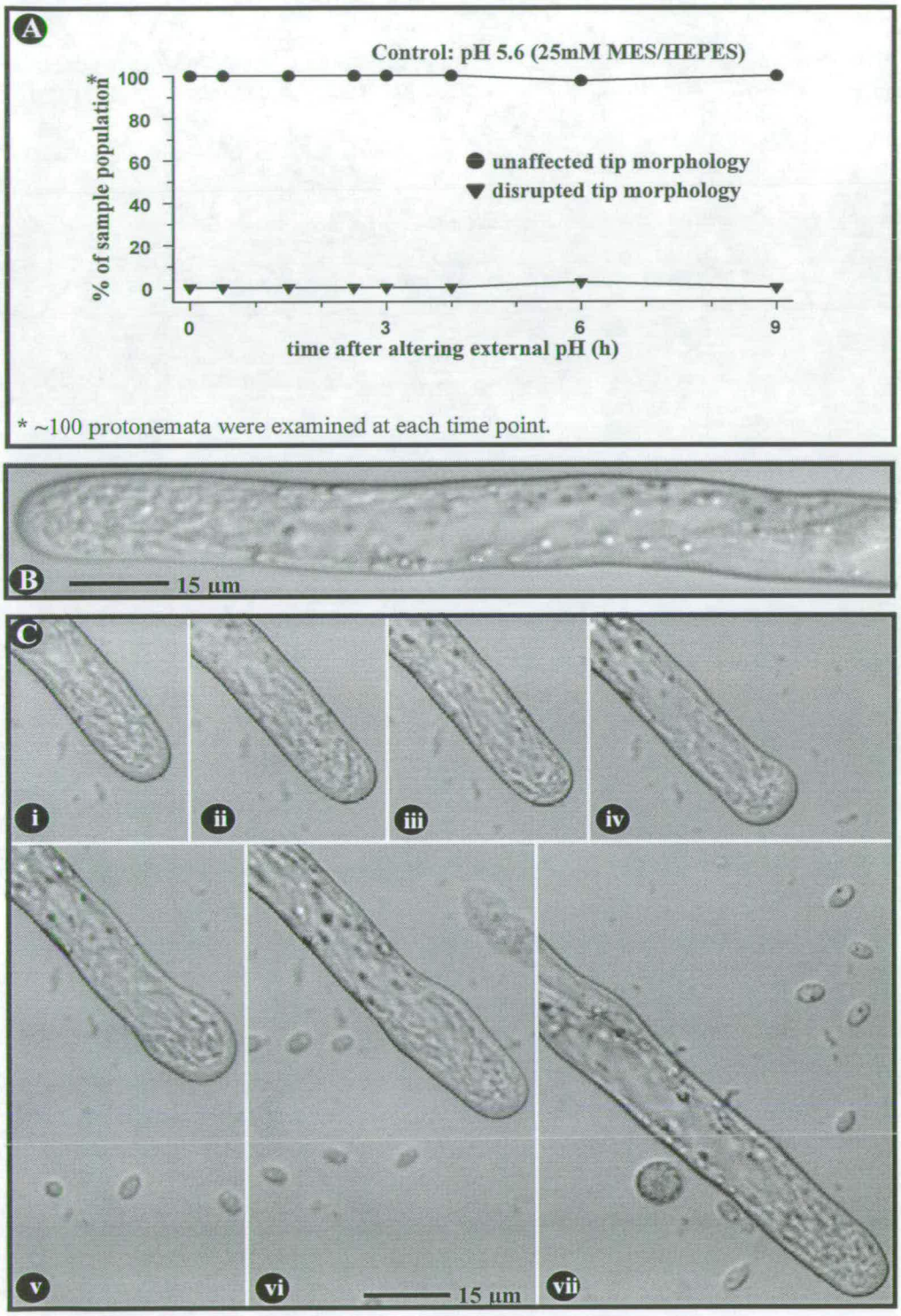

Fig. 61: The effects of external buffering at pH 7.0 on *D. affinis* rhizoids

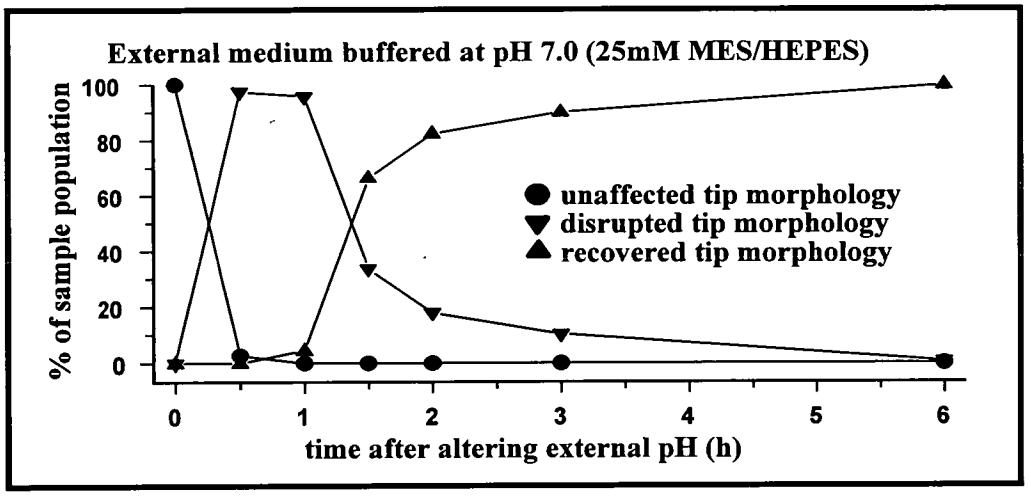

Examination of a population of rhizoids exposed to 25 mM MES/HEPES buffer at pH 7.0 over 6 h. 150 protonemata were examined at each time point. Growth and cytological organisation were only transiently disturbed. Recovery occurred spontaneously within a few hours while at the modified external pH, similar to that shown in Fig. 62(B).

Fig. 62: Effects of external buffering at pH 8.0 on *D. affinis* rhizoids. (A) Examination of a population of rhizoids exposed to 25 mM MES/HEPES buffer at pH 8.0 over 9 h. 150 protonemata were examined at each time point. (B) An example of an individual rhizoid transferred from normal medium (i-ii) to pH 8.0, 25 mM MES/HEPES buffer (iii-vi) and back to normal medium (vii). Images (i-v) were collected at 40 min. intervals; (vi) was collected after a further 2 h and (vii) after a further 6 h. This individual never recovered even after transfer to normal medium. (C) As in (B) but this time recovery occurred in normal medium (viii-ix). Images (i-iii) collected at 40 min. intervals; (iii-viii) were collected at 90 min. intervals; and (ix) after a further 6 h. (D) again as in (B) but recovery occurred spontaneously after 6 h while at pH 8.0. Bar = 20 μm.

Fig. 62: The effects of external buffering at pH 8.0 on *D. affinis* rhizoids

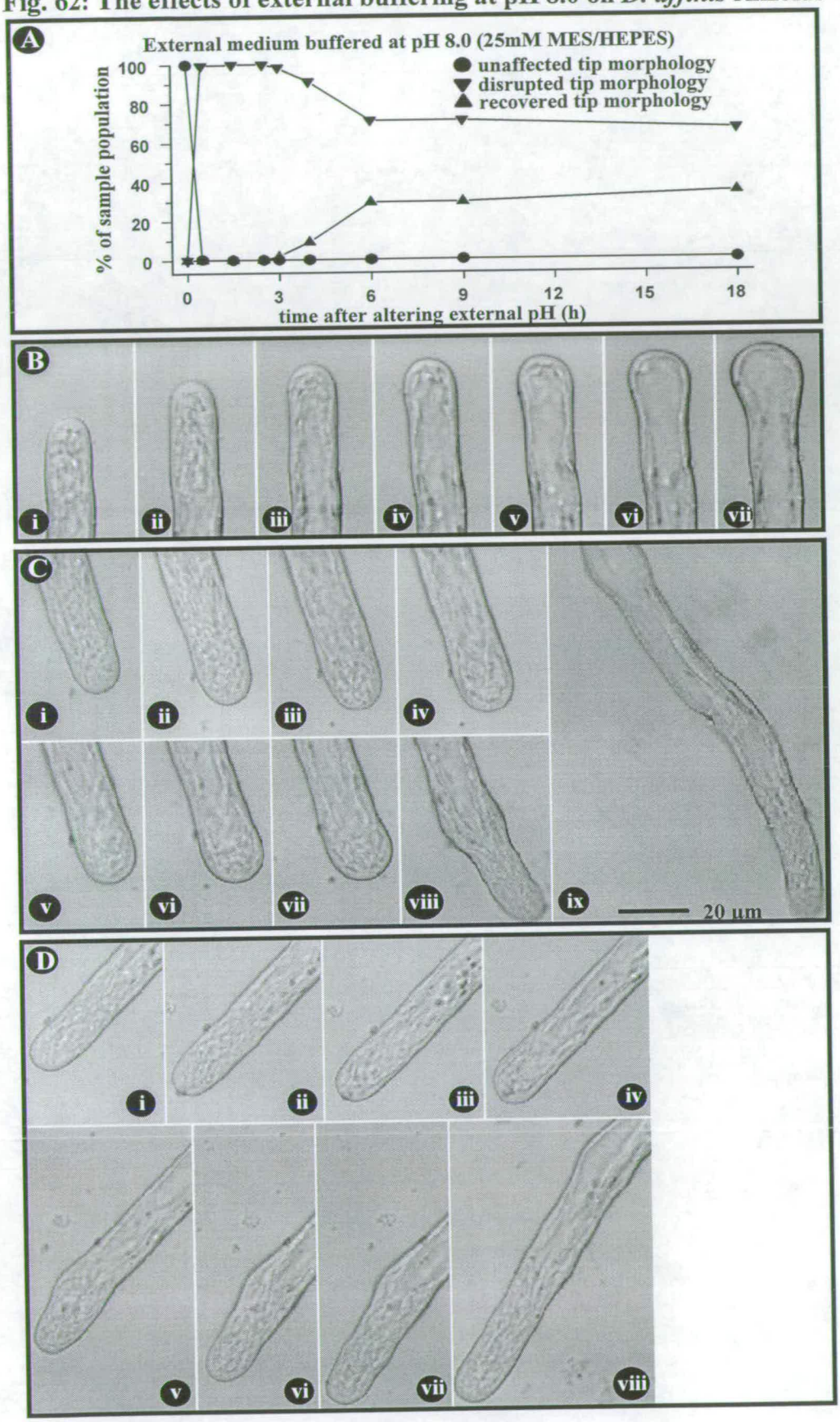

Fig. 63: Possible positions of pH gradients in a tip-growing cell

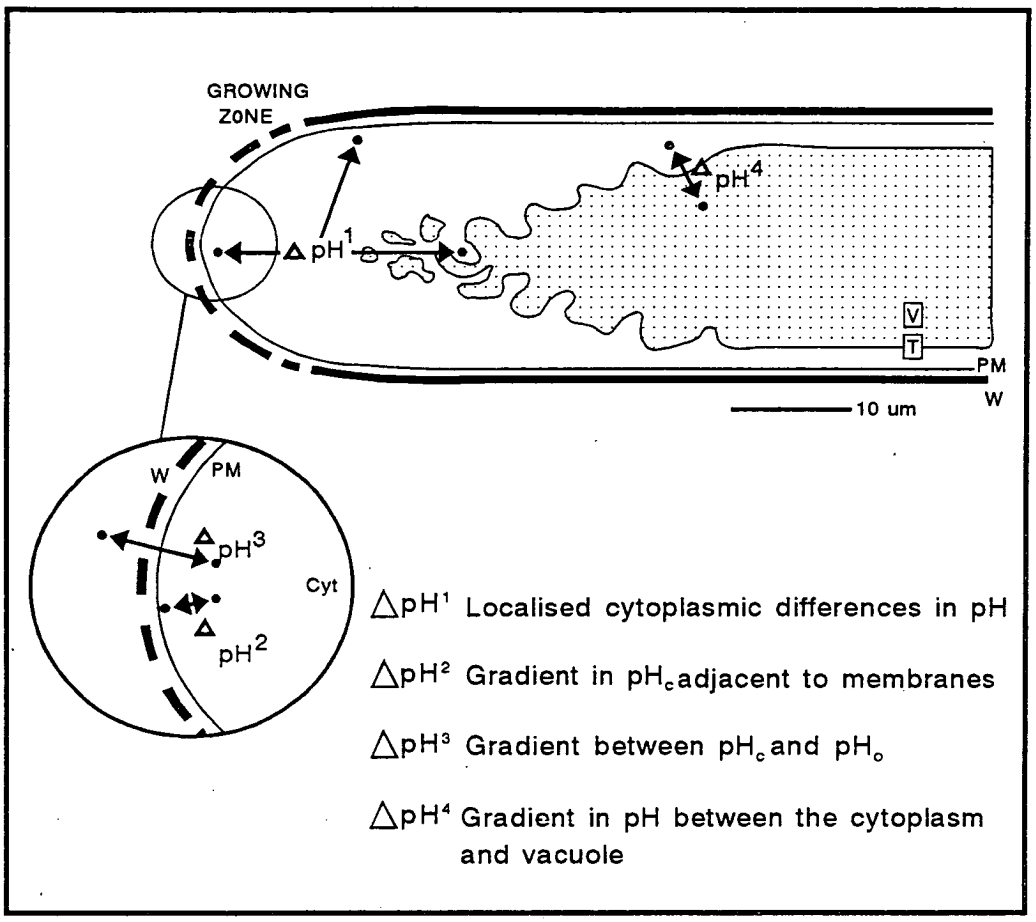

The model was based on work with a variety of cell types using different techniques (see the main text of Chapter 6 for references) and serves to illustrate where domains of different pH may occur and which may have bearing on polarity and apical growth.